Optimal management of district heating networks using different flexibility sources

Dissertation Submitted in Partial Satisfaction of the Requirements for the Degree Doctor of Philosophy in Engineering

Al Dipartimento di Ingegneria Industriale (DII) Corso di Dottorato In Ingegneria Industriale Curriculum Energetica, XXXIV Ciclo

UNIVERSITÀ DEGLI STUDI DI PADOVA

Davide Quaggiotto

Supervisor: Prof. Angelo Zarrella
Co-supervisor: Dott. Jacopo Vivian

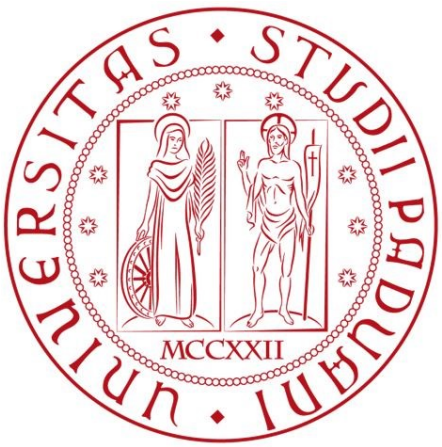

Abstract

District heating networks (DHNs) are a key infrastructure to decarbonize the heating sector, allowing cogeneration plants, renewable plants, and waste heat integration. However, there are some problems related to these integrations. Regarding the cogeneration plants, electricity production can be cost-effective at different times than the thermal energy demand, while about the renewable plants and the waste heat, there may be a mismatch between the heating demand and the heat provided by these sources. A solution can be the sources of energy flexibility in DHNs system, which can increase the efficiency of DHNs from both economic and environmental standpoints. Usually, district heating operators use centralized storage tanks to decouple the supply from the demand of the substations, but space constraints can undermine this possibility. As a result, it can be useful to exploit the sources of flexibility that are inherently part of the system and don't need to be added.

In a first step, the research aimed to assess the flexibility potential provided by the thermal capacitance of the heat carrier fluid in the network pipelines and the building structures. The case study under consideration was the district heating network of Verona Centro Città (Italy), which supplies residential, tertiary and industrial customers, operating at constant supply temperature and variable flow rate. Computer simulations were carried out to calculate the network's thermal response to circulating mass flow rate variations. The latter were designed to cause an early or late shift in the daily peak thermal load. The local temperature drop at the user's substations was used as a relative discomfort indicator compared to the current situation. The simulations were conducted using a detailed district heating network model, Nemo, based on a finite difference method. They showed that the pre-charge process achieves significant peak shaving and load shifting results. To produce the desired change in the mass flow rate, the district heating operator would need to install one or more bypass pipes. The effects of the different flow distributions on the network's dynamic behaviour, obtained with different numbers of bypasses, were investigated. About the thermal capacitance of the building structure, two representative buildings (an apartment building and a school) connected to the Verona district heating network were analyzed. Considering the related detailed Energy Plus models, modifying the setpoint and anticipating the switch on of the heating system, the heat demand pattern modification and its impact on the thermal comfort were evaluated. Furthermore, the influence of the building envelope type, the user behaviour and the weather conditions were analyzed. Energy flexibility was

assessed using mainly two indicators: the available thermal storage capacity and the Active Demand Response event efficiency.

As a second step, the objective of the research work was to exploit these sources of flexibility with two different types of control. These are the supply station control (SSC), which considers centralized thermal storage and the thermal capacitance of the water in the network pipelines, and the demand side control (DSC), which exploits the building thermal capacitance. The SSC is based on a MILP optimization problem to schedule the heat supply units of the district heating network of Verona based on heat demand, waste heat availability and electricity price forecasts. Coupling the optimization problem to the model NeMo, allowed to repeat the scheduling with a rolling horizon scheme. So, it was possible to determine the optimal energy management at the supply stations from the environmental and economic points of view. About the demand side control, the concept was to consider the substations as virtual storage tanks. From the ADR simulation results obtained in the first step, it was possible to define the virtual storage tanks' volume and heat transfer coefficient. Then, considering the thermal energy price and the external temperature forecasts, the optimization was performed at the district level, determining the optimized energy demand and the average indoor temperature of some substations connected to Verona DHN.

As a final step, the integration of renewable energy sources to a new generation district heating network was studied, considering a novel technical solution for heating, cooling, domestic hot water and electricity production to a small residential district in cold regions. Simulations were performed at the building and the supply station level to analyze the novel solution. The core of the energy system was a low-temperature district heating network supplied by a high-efficiency ground source heat pump. The source-side of the booster heat pumps installed in the buildings was connected to the district heating network. Rooftop photovoltaic thermal panels (PVT) partially met the electrical demand of the district. Moreover, they contributed to the production of domestic hot water and, when their thermal energy production exceeded the demand, the heat was injected into the ground to reduce the thermal unbalance, which typically affects the performance of the ground source heat pump systems in cold climates. Finally, using the network heat carrier fluid to decrease the average temperature of the PVT panels further enhanced their electrical efficiency. So, the proposed multi-energy system reached an electrical self-consumption of 70% in the coldest locality and efficiently combined different renewable energy sources at the district level.

Riassunto

Le reti di teleriscaldamento sono un'infrastruttura chiave per decarbonizzare il settore del riscaldamento urbano, permettendo l'integrazione di impianti di cogenerazione, impianti rinnovabili e calore di scarto. Tuttavia, ci sono alcuni problemi. Per quanto riguarda gli impianti di cogenerazione, la produzione di elettricità può essere conveniente in momenti diversi rispetto alla domanda di energia termica, mentre per quanto riguarda gli impianti rinnovabili e il calore di scarto, ci può essere uno scostamento tra la domanda di riscaldamento e il calore fornito da queste fonti. Una soluzione è rappresentata dalle fonti di flessibilità energetica nel sistema rete di teleriscaldamento, che possono aumentare l'efficienza sia dal punto di vista economico che ambientale. Di solito, i gestori del teleriscaldamento usano serbatoi di accumulo centralizzati per disaccoppiare la produzione dalla domanda delle sottostazioni, ma i vincoli di spazio possono minare questa possibilità. Di conseguenza, può essere utile sfruttare le fonti di flessibilità energetica che sono intrinsecamente parte del sistema e non hanno bisogno di essere aggiunte.

In una prima fase, la ricerca ha avuto lo scopo di valutare il potenziale di flessibilità fornito dalla capacità termica del fluido termovettore nelle tubazioni della rete e nelle strutture degli edifici connessi. Il caso studio preso in considerazione è stata la rete di teleriscaldamento di Verona Centro Città (Italia), che fornisce calore ad utenze residenziali, terziarie e industriali, operando a temperatura di mandata costante e portata variabile. Sono state effettuate simulazioni al computer per calcolare la risposta termica della rete alle variazioni della portata circolante. Queste ultime sono state determinate per causare un spostamento del carico termico in anticipato o ritardato rispetto al picco giornaliero. Il calo di temperatura locale nelle sottostazioni è stato utilizzato come indicatore di discomfort relativo rispetto alla situazione attuale. Le simulazioni sono state condotte utilizzando un modello dettagliato della rete di teleriscaldamento, Nemo, basato su un metodo alle differenze finite. Tali simulazioni hanno mostrato che il processo di precarica raggiunge risultati significativi nella riduzione dei picchi e nello spostamento del carico. Per produrre la variazione desiderata della portata di massa, il gestore dell'impianto di teleriscaldamento dovrebbe installare uno o più tubi di bypass. Sono stati studiati gli effetti delle diverse distribuzioni e del diverso numero di bypass sul comportamento dinamico della rete. Per quanto riguarda invece la capacità termica dell'involucro degli edifici, sono stati analizzati due edifici rappresentativi (un condominio e una scuola) collegati alla rete di teleriscaldamento di Verona.

Considerando i relativi modelli dettagliati, sviluppati in Energy Plus, modificando il setpoint e anticipando l'accensione dell'impianto di riscaldamento, è stata valutata la variazione della domanda di calore e il suo impatto sul comfort termico con simulazioni di Active Demand Response (ADR). Inoltre, è stata analizzata l'influenza del tipo di involucro dell'edificio, il comportamento dell'utente e le condizioni meteorologiche. La flessibilità energetica è stata valutata utilizzando principalmente due indicatori: la capacità di accumulo termico disponibile e l'efficienza dell'evento ADR.

In una seconda fase, l'obiettivo del lavoro di ricerca è stato quello di sfruttare queste fonti di flessibilità con due diversi tipi di controllo. Questi sono il controllo della centrale termica (SSC), che considera l'accumulo termico di serbatoi centralizzati e la capacità termica dell'acqua nelle tubazioni della rete, e il controllo delle sottostazioni (DSC), che sfrutta la capacità termica dell'edificio. L'SSC si basa su un problema di ottimizzazione MILP per programmare lo scheduling degli impianti di generazione del calore in base alla domanda di calore delle sottostazioni, alla disponibilità di calore di scarto e alle previsioni del prezzo dell'elettricità. L'accoppiamento del problema di ottimizzazione al modello NeMo, ha permesso di eseguire simulazioni settimanali della rete di teleriscaldamento. Così, è stato possibile determinare la gestione ottimale dell'energia nelle centrali termiche dal punto di vista economico. Per quanto riguarda il controllo delle sottostazioni, l'idea è stata di considerarle come serbatoi virtuali di accumulo termico. Dai risultati delle simulazioni ADR ottenuti nella prima fase, è stato possibile definire il volume dei serbatoi di accumulo virtuali e il coefficiente di scambio termico. Poi, considerando il prezzo dell'energia termica e le previsioni di temperatura esterna, l'ottimizzazione è stata eseguita a livello di distretto, determinando la domanda di energia ottimizzata e la temperatura media interna di alcune sottostazioni collegate alla rete di Verona.

In un'ultima fase, è stata studiata l'integrazione delle fonti di energia rinnovabile in una rete di teleriscaldamento di nuova generazione. E' stata quindi analizzata una nuova soluzione tecnica per il riscaldamento, il raffreddamento, l'acqua calda sanitaria e la produzione di elettricità in un piccolo distretto residenziale in regioni fredde. Sono state eseguite simulazioni a livello di edificio e di centrale di produzione. Il cuore del sistema energetico è una rete di teleriscaldamento a bassa temperatura alimentata da una pompa di calore geotermica ad alta efficienza. Il lato sorgente delle pompe di calore booster installate negli edifici è collegato alla rete di teleriscaldamento. I pannelli termici-fotovoltaici (PVT),

installati sui tetti delle sottostazioni, soddisfano parzialmente la domanda elettrica del quartiere. Inoltre, contribuiscono alla produzione di acqua calda sanitaria e, quando generano più energia termica di quella richiesta, il calore è immesso nel terreno per ridurre lo squilibrio termico, che tipicamente influisce sul rendimento dei sistemi a pompa di calore geotermica nei climi freddi. Infine, l'uso dell'acqua di rete per diminuire la temperatura media dei pannelli PVT migliora ulteriormente la loro efficienza elettrica. Così, il sistema multi-energia proposto ha raggiunto un autoconsumo elettrico del 70% nella località più fredda e ha combinato in modo efficiente diverse fonti di energia rinnovabile a livello di distretto.

Contents

List of figures

List of tables

CHAPTER 1 INTRODUCTION

According to Eurostat data, in 2019, the final energy consumption in households has reached 26 % of the total final energy in the European Union. A high rate, equal to 64 %, of the final energy in the residential sector has been used for space heating [1]. So the energy efficiency measures related to heating services are part of the European energy policy [2].

In this context, district heating networks (DHN) play a key role in the transition towards sustainable cities, thanks to their ability to efficiently provide space heating and domestic hot water to buildings through renewable sources (such as geothermal and solar energy), waste heat sources and cogeneration plants. So, the construction and the expansion of efficient district heating (DH) systems, according to the principles of fourth-generation [3] and fifth-generation [4], are some of the key points of the European energy policy [2]. In particular, the DHN construction is advantageous where different types of energy demand are simultaneously present and when, at the district level, a sufficient spatial energy intensity justifies investments in smart grids [5]. This typically occurs in cities and in general in the urban context, where there is an increasing demand for energy services.

At the same time, improving the operational aspects of the existing district heating networks can increase their efficiency from both economic and environmental standpoints. These improvements consist of increasing the energy flexibility of the DH system and integrating renewable energy sources (RES).

The present Thesis is focused on the improvement of the operational conditions and, in a first step, tried to answer the following question:

"What is the flexibility potential of the main sources of energy flexibility that are inherently part of the DH system?"

District heating operators usually use centralised storage tanks to decouple the supply from the demand of the substations, but space constraints can undermine this possibility. Alternatively, the thermal capacitance of the heat carrier fluid in the network pipelines and the building structures can be exploited. These sources are characterised by a high thermal mass and don't need to be added.

The case study under consideration was the district heating network of Verona Centro Città (Italy). This network extends for 25 km, providing heat for space heating and, in some cases, domestic hot water to 247 users, operating at constant supply temperature and variable flow

rate. The generation plants in the supply stations are cogeneration units, heat pumps and gas boilers. Furthermore, waste heat is recovered from a foundry.

Regarding the source of flexibility represented by the heat carrier fluid enclosed in the network pipelines, computer simulations were carried out to calculate the network's thermal response to circulating mass flow rate variations. The latter was designed to cause an early or late shift in the daily peak thermal load. Therefore, to charge or discharge the network, the mass flow rate was respectively increased or decreased compared to the current pumping strategy, where heat generators strictly follow the demand of the district heating customers. The idea was to regulate the mass flow rate based on the heat load predictions for the following hours. Two representative weeks were chosen to study the load shifting strategies: a cold winter week and a week during the midseason. The load-shifting results obtained with different mass flow adjustment strategies were evaluated considering some performance indicators, which quantify the cost of the flexibility in terms of energy consumption at the supply stations and thermal comfort at the user substations. The simulations were conducted using the detailed district heating network model NeMo, based on a finite difference method. This model describes the topology of the network using graph theory. So, the network is represented by a set of nodes and oriented branches, and an adjacency matrix determines their mutual connections. A plug flow is assumed, which implies that the velocity of the heat carrier fluid is uniform in the radial direction (one-dimensional model).

From a practical point of view, the district heating operator cannot directly set the mass flow rate circulating in the network, which depends on the opening degree of the valves in the user substations. The greater the demand for thermal power by the user substations, the greater the opening of the valves and, therefore, the total flow rate circulating. The operator must only guarantee a minimum pressure difference on all customers' substations. So, this study tried to address a further research question:

"How can the network manager adjust the circulating mass flow rate in the network?"

A possible solution is to install some bypasses between the supply and return lines. The district heating network operator may perform daily planning of the flow rate based on heat load forecasts. Then, the desired change compared to the current situation would be achieved by a proportional opening of the bypass valves when the mass flow rate must be increased and by a proportional decrease of the pump head when the mass flow rate must be reduced.

Therefore, another set of simulations was carried out to show how the number and position of the bypasses affect the thermal load profile at the supply station.

About the thermal capacitance of the building structure, two representative buildings (an apartment building and a school) connected to the Verona district heating network were analysed. Considering the related detailed Energy Plus models, modifying the set-point and anticipating the switch on of the heating system, the heat demand pattern modification and its impact on the thermal comfort were evaluated in Active Demand Response simulations. Furthermore, the influence of the building envelope type, the user behaviour and the weather conditions were analysed. Energy flexibility was assessed using mainly two indicators: the available thermal storage capacity and the Active Demand Response event efficiency.

Once the flexibility potential of the considered sources has been assessed, the question that the present Thesis tried to answer is:

"How can these sources of energy flexibility be exploited in a useful way?"

Two different controls were developed. These are the Supply Station Control (SSC), which considers centralised thermal storage and the thermal capacitance of the water in the network pipelines, and the Demand Side Control (DSC), which exploits the building thermal capacitance. The SSC is a model predictive control (MPC), characterised by a MILP optimisation problem to schedule the heat supply units of the district heating network of Verona based on heat demand, waste heat availability and electricity price forecasts. Coupling the optimisation problem to the model NeMo, allowed to repeat the scheduling with a rolling horizon scheme. The objective of the proposed control strategy was to minimise the operational costs for the DH operator using only the thermal capacitance of the water enclosed in the network pipelines as a thermal buffer in a first phase, and also a thermal storage tank installed in the main supply station, in a second phase.

Regarding the Demand Side Control, the substations connected to the DHN have been considered virtual storage tanks to exploit the buildings envelope's thermal capacitance and modify their heat demand pattern. In accordance with the typology of the substation, the virtual storage tank is characterised by different values for the volume and the heat transmission coefficient. These parameters have been evaluated thanks to Active Demand Response simulations of the residential and a tertiary building (the apartment building and the school). Considering the monitoring of nine residential and seven tertiary buildings of Verona DHN, thanks to the DSC, it was possible to minimise the costs related to the heating

demand, modifying their thermal load profiles. Furthermore, at this point, it was possible to answer the question:

"What is characterised by a higher flexibility potential between the two considered sources of energy flexibility?"

The comparison was assessed on a representative day considering the results of load shifting and peak shaving obtained by exploiting the thermal capacitance of a certain number of substations and the water in the network pipelines, respectively.

As a final step, the Thesis tried to answer the following question:

"How can RES be integrated efficiently into district heating networks?"

A novel technical solution has been studied to provide heating, cooling, domestic hot water and electricity to a small residential district in cold regions. The core of the energy system is an ultra low-temperature district heating network (ULTDHN) supplied by a high-efficiency ground source heat pump (GSHP). The booster heat pumps' source-side in the buildings is connected to the DHN. Rooftop photovoltaic thermal panels (PVT) partially meet the electrical demand of the district. Moreover, they contribute to the production of domestic hot water. When their thermal energy production exceeds the demand, the heat is injected into the ground to reduce the thermal unbalance, which typically affects the performance of the GSHP systems in cold climates. During the cooling season, the GSHP is bypassed, and the heat is directly released into the ground through the borehole heat exchangers. Furthermore, using the network heat carrier fluid to decrease the average temperature of the PVT panels further enhances their electrical efficiency. Three reference climates have been considered: Helsinki, Berlin and Strasbourg. Simulations were performed at the building and the supply station level to analyse the novel solution.

Concerning the current state-of-the-art research, the study's novelty is determined by comparing the sources of energy flexibility in a real case study and the method used to exploit the thermal capacitance of the heat carrier fluid in the network pipelines. Unlike several studies, where the supply temperature set-point is adjusted, the circulating mass flow rate is the control variable. In addition, the concept of considering the substations as virtual storage tanks to assess the flexibility potential of the buildings' envelope connected to the DHN, and modify their heat demand pattern, is new in the current state-of-the-art research. Finally, the study's novelty also lies in the considered technical solution for integrating RES into DH systems.

The Thesis is structured as follows. Chapter 2 provides a framework on the evolution and the last trends of district heating networks, as well as on the sources of energy flexibility used in the DH system. Chapter 3 describes the case studies, and Chapter 4 describes the models used to analyse the sources of energy flexibility. Chapter 5 presents the flexibility potential results of the two considered energy flexibility sources (thermal capacitance of the water in the network pipelines and buildings envelope), Chapter 6 those of the two system controls developed to exploit these flexibility sources. Chapter 7 presents a novel technical solution to efficiently integrate RES in the DH system. Finally, some conclusions and prospects for future work are outlined in Chapter 8.

CHAPTER 2 LITERATURE REVIEW

The present chapter aims at giving an updated overview on the current status of district heating (DHN) systems, the employed heat sources and the heat distribution system. Before that, the fundamental idea of the DHN and some historical notes on its development are given. Then, in section 2.5, the main measures studied to improve the operational conditions are described. These aim to improve the DHN system's energy flexibility and integrate renewable energy sources.

2.1 The fundamental idea of district heating

A district heating network is an energy service based on moving heat from available heat sources to immediate use directly by customers. It was introduced commercially in the United States in the late nineteenth century and in Europe in the early twentieth century. Similar district cooling systems emerged in 1960 in both the United States and Europe [6]. The English expression *district heating* underscores the large-scale nature of the consumer base of this sort of energy service. In the name, it is assumed that the network must serve a city or at least a neighbourhood, with a minimum of hundreds or even thousands of users. Therefore, the plant that produces the heat shall be much larger than any household boiler. Between the plant and the households, a network of pipes transports the heat. The network is easier to build and operate if the users are concentrated in a small area. In Italian, district heating is called *teleriscaldamento*: the emphasis is on the *distance* between producer and user. Today, the fundamental idea of DH is to use local fuel or heat resources that would otherwise be wasted to satisfy local customer demands for heating by using a heat distribution network of pipes as a local marketplace. This idea encompasses the three obligatory elements of a competitive DH system: a suitable heat source that is cheap, demands from the heat market, and pipes that connect the demands and the sources. These three elements must all be local to minimise the capital investment in the distribution network through the use of short pipes.

The fundamental goals of DH engineering will then be to maximise the advantages while mitigating the drawbacks. Which are these advantages and drawbacks? Which conditions are more conducive to the deployment?

The main advantages of district heating are:

- *Economy of size*: denotes technologies, which have lower costs at higher product volumes. Larger generators can be built and operated at a smaller cost per unit of energy delivered. This is due, among other reasons, to lower staffing per unit of installed power, smaller use of land and space (in an urban setting, space savings on the consumer side can be particularly important). These savings result in manifold advantages that can be described from other points of view. For example, in a large machine, it can be cheap enough to install a more efficient pollution control system, or a different boiler can be used that can withstand "difficult" fuels such as wood or municipal waste.
- *Economy of scope*: multiple services can be produced at once in a centralised system. Typically, low-grade civil heat production is associated with the delivery of electric power or with an industrial process that requires high-grade heat. But not only energy services are tied together: the incineration of waste with heat recovery for the city is an example of hybrid public service.
- *Flexible energy sourcing*: multiple sources of energy can be integrated into a DH system, especially those that would be too expensive, or dangerous, or polluting for an individual generation. The operating company can increase or decrease the relative importance of each energy source in response to market conditions or environmental concerns. The heat supply source of an entire city can be changed by modifying a central plant, which is not necessarily simple but, on the other hand, can be quicker than involving the entire citizenry.
- *Smaller local environmental impact*: the environmental impact from residential heat generation is moved away from the customer households. It should be noted that this sometimes encourages the use of "dirtier" fuels like coal, biomass and municipal waste, but larger plants, as mentioned above, can allow more significant pollution control systems to be installed.
- *Benefits on the user side*: generally speaking, the consumers of district heat obtain the final product by using a water-to-water heat exchanger. A water heat exchanger takes little space, is cheaper to install and maintain, and does not use a chemical reaction to heat the cold side fluid. So, there are no combustible materials to store and transport, which is a public safety benefit. Moreover, heat delivery can be more reliable, and contracts can be signed where only the heat is purchased, and not, for example, a boiler.

On the other hand, the DH service is characterised by some disadvantages:

- *Inequality* between the individual customer and the monopolistic heat provider.

- *Inflexible planning and implementation*: the infrastructure has a long lifetime, which can make it complex to correct mistakes made, for example, in the prediction of consumption patterns. Such a system might involve stakeholders that could develop different interests and no longer want or be able to participate after a while (for example, the owners of an industrial activity that provides waste heat).
- *Complexity and high investment costs:* on the operator's side, that has to build a network of pipes to connect all the users without dissipating too much heat and keeping them in good condition. This can result in DH being viable only in areas with strong heat demand during the year and per unit of area: i. e., for practical purposes, a densely populated city where the weather is consistently cold during a large portion of the year. The parameter of linear heat density (LHD) is sometimes used to evaluate the economic feasibility of DH. It is the ratio between the energy delivered yearly and the length of the supply pipes. It has been estimated that the minimum LHD that allows DH is around 3 MWh/(yr m) [7].

In Figure 2.1, the share of the population served by DH in EU countries in 2013 is shown.

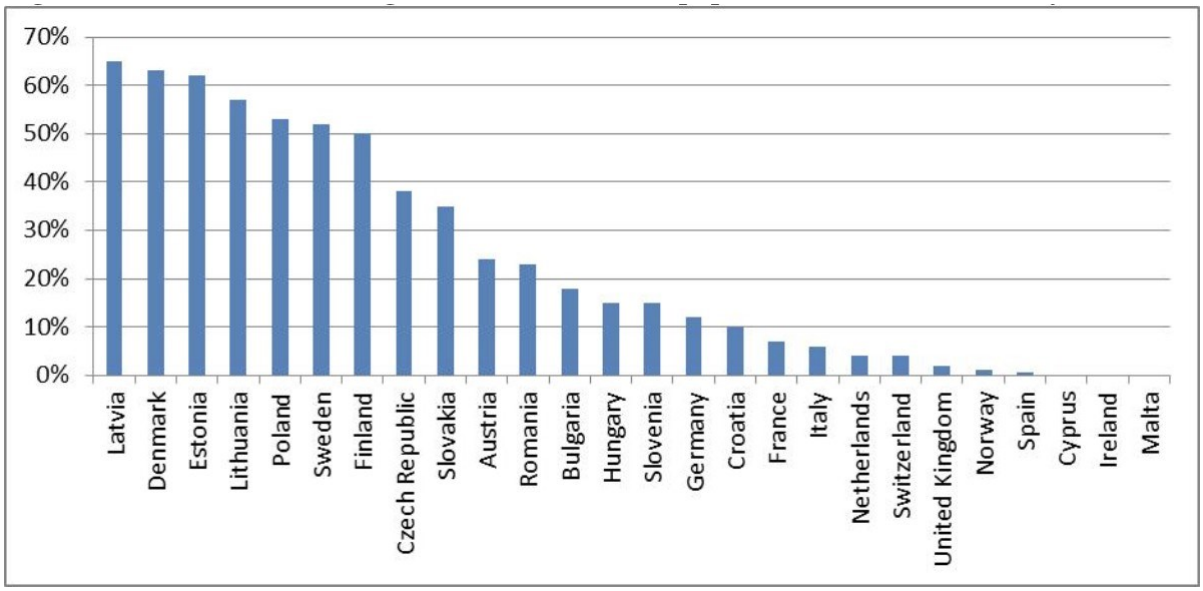

Figure 2.1 The share of the population served by DH in EU countries in 2013. (Euroheat and Power).

2.2 District heating and cooling development

An overview of the history of district heating can be found in several works, such as [3]. Generally, four or five successive *generations* are identified. Every generation is characterised by different thermodynamical parameters, materials, and heat sources.

Furthermore, the systems of one generation were retrofitted with the devices of the following generations, where economically feasible.

- The *first generation* of DH dates back to the second industrial revolution. In late 1800s cities, boilers supplied heat to one building each, boiling water at high pressures by burning solid fuel, typically coal. The furnaces had to be stoked manually around the clock. They were complicated to build and maintain, suffered from important heat losses at the chimney and through the walls, and were at risk of malfunction or even explosion because of the high operating pressure. It was thought simpler to build large boilers and connect them with the buildings through pipes that carried high-pressure, high-temperature steam. The water evaporated in the boilers and condensed in heat exchangers located in the served buildings. However, steam posed significant challenges in mechanical losses caused by speed and friction, heat losses due to the high temperatures and safety risks related to the high pressures. Today, of the many steam DH systems developed in northern Europe and North America, only a few are still operational in their original form, but among these are notable the Paris and New York City networks.
- The *second generation* of DH was developed starting around the year 1930. The hot water had been identified as a better alternative to steam, but it required the use of electric pumps to be moved around. In addition, water systems required smaller supply pipes but larger returns installed in concrete ducts. The supply temperatures were still high (over 100° C). The interest was to centralise production and integrate the production of electric power and heat to conserve primary energy. With combined generation and water pipes, this type of network became widely adopted in central Europe and the standard for urban space heating in the Soviet Union.
- The *third generation* started being introduced in northern European countries around 1970, marked by the use of hot water with reduced operating thermodynamic parameters. It attempted to go near atmospheric pressure and below 100 degrees Celsius. This allowed the operator to use lighter and cheaper materials such as polymers, simplify the installation of components, and integrate different heat sources, even large heat pumps. These measures resulted in a decrease in the thermal level of the heat delivered, the generation of more electric power if a combined plant was used, and smaller thermal losses.
- The *fourth generation* of DH systems was implemented in response to the need to integrate greater shares of renewable energy into heating and reduce the losses further. This concept

was developed by Lund et al. [3]. It was an evolution of the third generation in the general direction of lighter components, cheaper materials and lower pressures and temperatures (around 1 bar and 70° C). The decrease in operating temperatures requires household heating systems that accept lower temperatures (like radiant floor heating or lower-temperature radiators). With lower temperatures, the same district network is characterised by lower heat losses. This generation of DHN is also defined as low-temperature district heating network (LTDH).

- The *fifth-generation* district networks, was developed around 2010. The network temperatures, in this case, could be lowered even further, essentially to ambient levels up to 45 °C. With these temperature levels, they sometimes are called "ultra-low temperature DH", and they require the use of heat pumps by the customers and are intended to allow both extraction of heat from the network and release of heat to the network from those customers that need cooling. This new generation of DH, also defined as ultra low-temperature district heating network (ULTDH), should thus enable a higher level of decentralisation of heat and cold production and new business models in which the consumers also act as producers [4].

2.3 Sources of Heat

The large size, distance and centralisation allow choosing sources of energy that are free from the constraints imposed under modern standards upon the generation of heat in proximity to the consumer. Any heat source can be used, including challenging ones, like biomass, waste and even nuclear power. In Figure 2.2, the primary fuels amounts used in the DH sector in the world are shown for different years.

From a sustainable energy generation perspective, the interest is on reducing the primary energy consumption, which generally means reducing the amount of fuel that we need to burn. A large boiler only marginally increases the amount of thermal energy extracted from the fuel compared to a smaller one. This increase is largely outweighed by the losses caused by separating generation and use and by requiring the heat to be transported. After all, in a household boiler, even the wall losses end up inside the building and, if the goal is space heating, contribute to the useful effect. So the size of the machines does not save fuel, and obviously, neither does the distance between generator and user. What conserves primary energy is that large-scale connections allow tapping into heat that needs to be generated anyway and would otherwise be lost (dissipated into the environment).

A detailed overview of heat generation for district heating is given in [6].

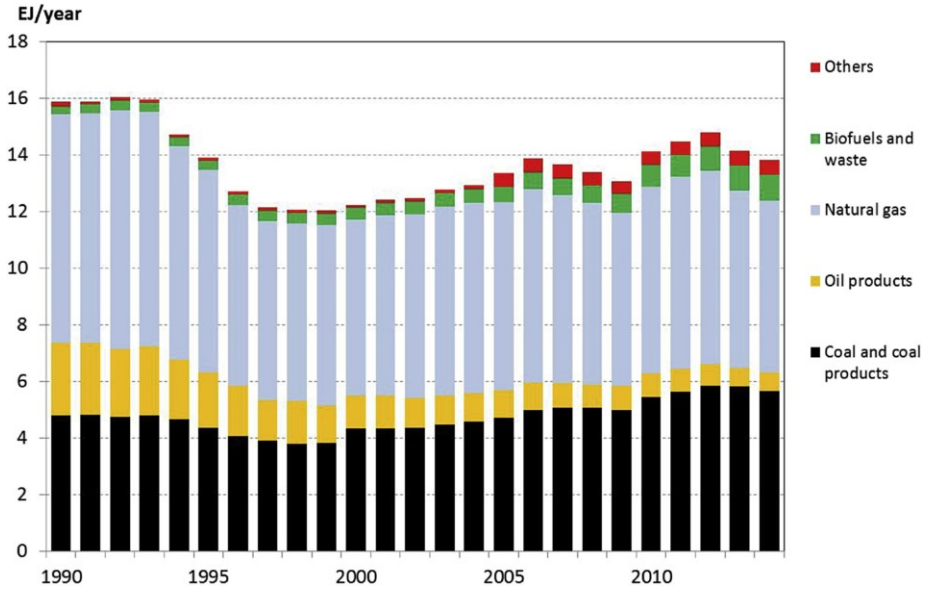

Figure 2.2 The primary fuels used in the DH sector in the world. [8]

2.3.1 Fossil fuel

Various generating plants in district heating systems, both CHP plants and heat-only boilers, handle a wide variety of fuels, even those that present difficulties in conversion efficiency, wear, fouling, and compliance with environmental regulations. Earlier, district heating plants were often employed to burn heavy fuel oil. This is no longer the case in most industrialised countries. Today the main use of oil for district heating is as light distillation oil, largely in peak and reserve boilers of a fairly simple

Design. Although natural gas is used for the thermal load peak in boilers, the major part is burnt in the combustion chambers of gas turbines or in predominantly small plants based on reciprocating engines (CHP plants).

On the other hand, the facilities that do not provide electricity or other products, commonly called Heat-Only Boilers (HOB), can consume biomass, natural gas, coal or Diesel fuel. Heat-only systems do not entail a saving in primary energy. They are often used to match the demand for heat when other sources with lower marginal costs are already exploited to their limit or are unavailable because of an extraordinary occurrence like a malfunction. There is a large variation in heat demand over the day and the year, and expensive systems per unit of power, such as CHP plants and heat pumps, cannot be sized for the highest demand. In the European Union, the direct use of fossil and renewable fuels is of lesser importance, but not negligible since, as late as 2014, it accounted for about one-fifth of the total DH production,

with fossil fuels representing more than three-quarters of the total energy supplied by direct combustion. In other contexts, direct fuel combustion is much more significant: it provides around 50% of the urban heat consumed in Russia and China, which raises its share of the world total to well over 40% [8].

2.3.2 Waste heat recovery

All industries and activities that need to cool a product, a byproduct, or an intermediate substance and do not have an immediate on-site use for the heat are potential providers of district heat.

The experience of Nordic countries and especially Sweden shows that four main industries can provide heat to DH: oil refining, paper and pulp, chemicals production and steel and metal making [6]. The city of Gothenburg[8] uses waste heat from two nearby oil refineries as its second most important energy source, essentially as important as the combustion of municipal solid waste (27% and 28% of the heat provided, respectively). According to data provided by the city utility and quoted in [6], refining waste heat is the second source in the order of merit, after waste combustion and ahead of CHP, heat pumps and finally biomass, which has a significant share of the supply, 16%, but is used as a "last resort". Steel producers use electric arc furnaces that give hot exhaust gas, often cooled in heat exchangers where water is evaporated. The steam obtained can be used for the internal needs of the facility, such as moving pumps or fans, and produce electric energy or heat for sale to a third party [9]. In Brescia, an electric arc furnace facility for steel production uses exhaust gas to boil water, which provides heat to an organic Rankine cycle. In addition, the steam can be used to heat district heating water when electricity demand is low or when, like during the winter, the DH network demands heat. In the metallurgical sector, there are waste heat streams within a broad range of temperatures, for example, from 30 to about 100 °C in copper smelting, complex to integrate into district heating: it is particularly important to reduce the network return temperature [10].

2.3.3 Renewable sources

The most important source of renewable heat for DH is, by far, the combustion of biomass and waste [8]. Another significant source of heat that can be considered renewable is geothermal power, especially in certain countries (Iceland, Turkey). Some small systems

even use solar energy. Sometimes in legislation, heat pumps are considered a renewable energy source since they bring important benefits like the reduction in primary energy use and the absence of chemical reactions that can produce dangerous effluents.

Legal considerations aside, district heating can be considered, with reasonable certainty, renewable or non-fossil whenever it relies on electricity or heat that are produced by these kinds of sources. Figure 2.3 shows the sources of heat used for DH in Gothenburg during a mid-season week. Waste heat is used as much as possible, and HOBs meet demand peaks, prioritising those fuelled by biomass.

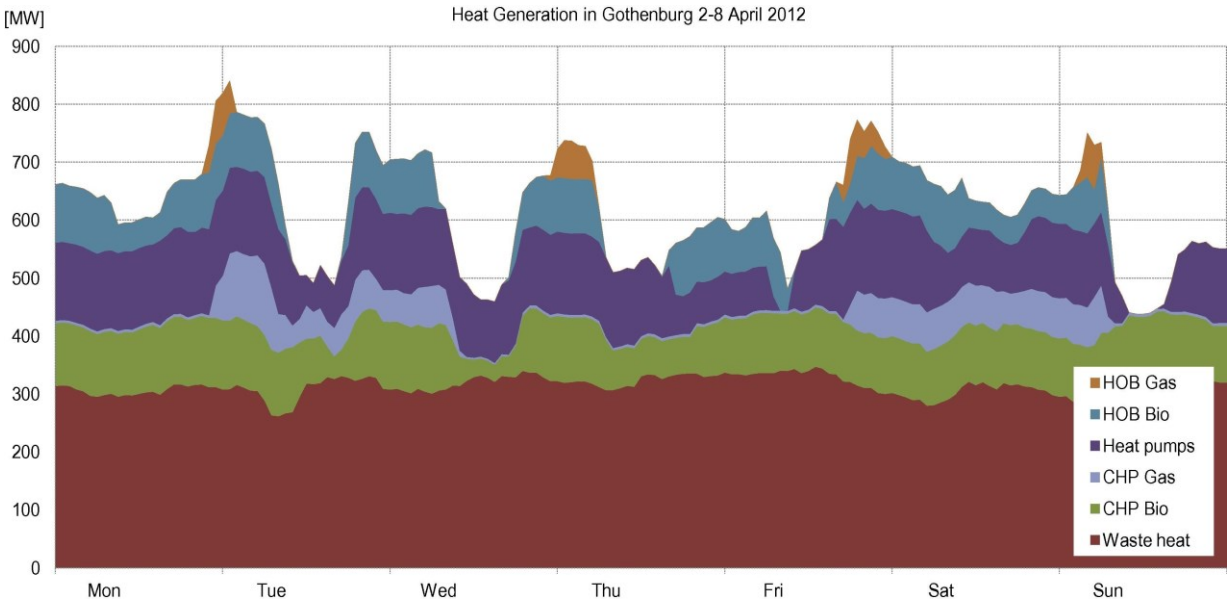

Figure 2.3 The heat sources used for DH in Gothenburg during a mid-season week. (Courtesy of [11]).

2.3.4 Combustion of biomass and waste

Biomass and municipal waste are generally consumed in Rankine cycle power stations, requiring special boilers to handle these fuels in pure form; alternatively, they can be mixed with conventional fuels (typically coal) in more conventional steam plants. It can be necessary to lower the operating temperature to preserve the boiler's components from corrosion. Particularly challenging are those fuels whose ashes melt at relatively low temperatures.

The most common biomass burners are of the *fixed-bed* type, where there is a grate on which combustion takes place that often moves horizontally to remove the ashes and receives air from beneath. In larger machines, the airflow from the bottom to the top is strong enough

that the fuel burns while suspended and mixed with minerals like dolomite or limestone, called a *fluidised bed*. The bed acts as a thermal reservoir which "protects" the boiler operation from inhomogeneous fuels and controls certain pollutants, especially by reacting with sulphur oxides. If the airflow is even faster and the size of the fuel bits is reduced further, the bed leaves the combustion chamber together with the fumes. It is retrieved with a cyclone separator located downstream before being sent back: a *circulating fluidised bed* or *CFB* combustor is obtained [6].

Other biomass burners use gaseous fuels, directly obtained by biochemical reaction (biogas) or by gasification of solid biomass, which is still a nascent technology.

Waste incineration as a heat source, particularly its environmental impact, is the subject of numerous research studies since it can reduce carbon emissions and produce significant pollutants [12]. With biomass, the reduction in carbon emissions is more pronounced but so can be the production of particulate and NOx.

A significant barrier to the use of biomass for DH is the low density of the energy source, which makes it complicated to collect in sufficient amounts for plants that serve entire cities. As a result, Italian biomass DH facilities have an average power rating of about 6 MW and are generally located in small municipalities [13]. Municipal waste combustion is often preferred in urban settings as the resource is more abundant. Furthermore, its disposal is a service for which the heat producer can be paid.

In northern Italy, a famous example of a waste CHP plant is the one in Brescia, which has a thermal power of 160 MW and an electrical capacity of 84 MW [14].

2.3.5 Geothermal district heating

District networks can provide an opportunity to exploit geothermal resources, which are often concentrated and far away from cities. We shall discuss the cases in which the geothermal resource is available at a significantly higher temperature than the environment; otherwise, its exploitation falls into the *heat pump* category.

An example of geothermal district heating is the Hellisheiði power station in Iceland. A mixture of water and steam is extracted from about 30 production wells, then flashed at a pressure of 10 bar; the steam is directly expanded in a turbine until the pressure of 2 bar, where it exists in two-phase form, which is flashed again to extract new power, until a pressure of approximately 0.22 bar. The fluid is finally condensed, which provides heat to the district

network at about 57° C temperatures. More heat at higher temperature levels is taken from the separated water; the total electrical power from seven production units is 303 MW, while the thermal power is about 400 MW [15].

Reykjavik also relies on heating supplied by heat-only geothermal plants drawing power from several different hydro-thermal fields at different temperature levels. Water is heated in boilers, mixed with cold water and finally brought to a common level of about 80° C on a standard day before being directly sent to the users. After passing through heating and DHW heat exchangers, it is at a temperature of about 35° C and can be used to melt snow on the roads. It is interesting to remark that the geothermal production is very constant, and therefore tanks with a capacity of tens of thousands of cubic metres have been installed to meet the needs of the coldest days [16].

2.3.6 Solar district heating

Generally, solar thermal energy is integrated into small DH networks. It usually covers from 10 to 50% of the total heat demand. It is provided by large installations of solar thermal collectors, with ratings of up to 50 MW. The most commonly used technology is the flat-plate collector, which suits the low temperature of third and fourth generation DH [17].

Historically, one of the world's largest solar DH systems has been the one serving the town of Marstal in Denmark. With an installed power of 13 MW, it provides about 30% of the total demand, with the help of several hot water tanks, the largest of which has a volume of 10 000 cubic metres [6].

The experience of Danish district heating networks has shown that, without thermal storage, the contribution of solar energy cannot go beyond 5 to 8% of the total annual energy demand. With diurnal storage, this can be raised to about 20%. To exceed this threshold and to obtain a solar penetration of 40%, it requires seasonal storage with a volume of about 1.2 m^3 for every square metre of solar collectors [18].

2.4 Heat distribution

This section describes a brief overview of the major network components' historical advancements and the current situation.

2.4.1 Transmission pipelines

First-generation DH used steam, which is transported inside steel pipes contained inside tunnels called ducts, originally made of masonry and then of concrete slabs. Still today, steam is sometimes delivered at pressures of 20 bar, with a temperature that can reach 300° C. This makes the heat quite expensive to produce but allows the survival of complex steam systems since high-pressure steam is useful for many applications beyond space heating. In the first generation configuration, in addition to a steam supply pipe, there is a smaller pipe for the return of the condensate formed when the steam has released heat energy at the customer sites. Some systems lack a return line, and all the condensate ends in the sewers. The lack of a return represents a simplification that avoids several problems and initial costs, but on the other hand, quite a lot of energy in the steam is lost. One of the problems with condensate is that the condensate readily absorbs oxygen and carbon dioxide, which makes it highly corrosive. Therefore, the pipes always have a mildly sloping configuration and compensate for the fall with a short vertical stretch every 30 to 50 metres called a *condensate trap* that collects the liquid water formed in the pipelines whenever there is a heat loss.

The hot water pipelines of the second generation are housed in concrete ducts as well, which are also sloped to make possible the extraction of leaked water. Another reason for the slope is so that, during repairs and the like, pipes can be emptied at low points, while at high points, valves can be opened to vent any gases from the network that, when present, will tend to accumulate at such high points. Around the water pipes, there is a layer of mineral wool which considerably reduces heat losses. In addition, there are thermal expansion compensators in the ducts, structural supports, and guiding elements to prevent excessive stresses and contacts between components. However, large ducts with chambers and vaults to contain the valves and joints are prone to flooding, producing heat losses and corroding the pipes, especially if there are contaminants such as salt.

The established technology for the third generation of heating networks is the all-bonded directly buried pipe. It generally consists of a carbon steel carrier pipe surrounded by cellular polyurethane, which is encased in a "jacket pipe" made of high-density polyethene. Expansion is dealt with by supporting the pipes with elastic materials like polymeric foams, lighter beds like gravel, or shapes like Z and U curves. The water flow is directed with the ball and plug valves in small-to-medium diameter pipes and butterfly valves in large-diameter pipes.

The tendency of the fourth and fifth generations of DH is towards the reduction of the need for insulation, with essentially uninsulated polymer pipes in the newest systems. Furthermore, particularly in the fifth generation, the small temperature difference between supply and return can cause large amounts of water to be moved, resulting in large pipe sizes [4].

Different configurations can be employed to connect the network. The most common are:

- Single-pipe networks only have a supply line that provides water to the hot side of the heat exchangers for space heating and DHW, or sometimes only DHW. In this way, a part of the energy is lost, but it makes the installation of long-distance pipes significantly cheaper.
- Double-pipe networks have supply and return lines that go through customer heat exchangers. Sometimes, an entirely separate network for DHW diverges from the larger network for space heating. In some systems, the return lines supply energy to customers who require low-temperature heat (like greenhouses and swimming pools).
- Triple-pipe networks have two different supply pipes for space heating and hot water and a single return.
- Four-pipe systems have two independent networks with supply and return for both heating and DHW.

2.4.2 Substations

The term substation indicates the facilities that combine all the devices needed to interconnect the network to the customer building and the building itself.

The main devices which characterise a substation are:

- heat exchangers to transfer the heat;
- valves, to regulate the flow of water on both sides of the heat exchangers and to reduce the network pressure so that it is compatible with the consumer heat exchangers;
- meters, to measure the amount of energy delivered.

As shown in Figure 2.4, there are different hydraulic connections at the substation level [6]:

A) Network water directly delivered for DHW and space heating, with no hydraulic separation. This is a very cheap solution since neither heat exchangers nor returns are required. On the other hand, much water and energy are wasted, especially when radiator water is rejected to the environment after a small temperature decrease. Moreover, the

oxygen typically dissolved in water for domestic uses can corrode the network and user infrastructure.

B) It is possible to use DHN water for DHW directly and a heat exchanger to extract energy for space heating. This option eliminates the waste of water but is vulnerable to corrosion.

C) DHN water circulates in radiators and heats DHW through a heat exchanger. This is a common configuration as it represents a good compromise of low cost and infrastructural protection.

D) DHN water passe through heat exchangers of both the space heating and DHW circuits. This indirect connection configuration allows the maximum protection of consumer devices from corrosion and pressure transients. It is generally found in the Nordic countries and the Verona network introduced in chapter 3.

E) Sometimes, the DHN warms an intermediate circuit that releases heat to the indoor air for the space heating and, using a heat exchanger, to the DHW circuit. Scale formation is thus reduced, but the network is forced to provide water at a relatively high temperature.

F) Finally, it is possible to have an indirect connection in which an intermediate circuit is dedicated to DHW exclusively. This configuration is expensive but allows a great degree of drinking water protection from the DH heat carrier fluid leaks.

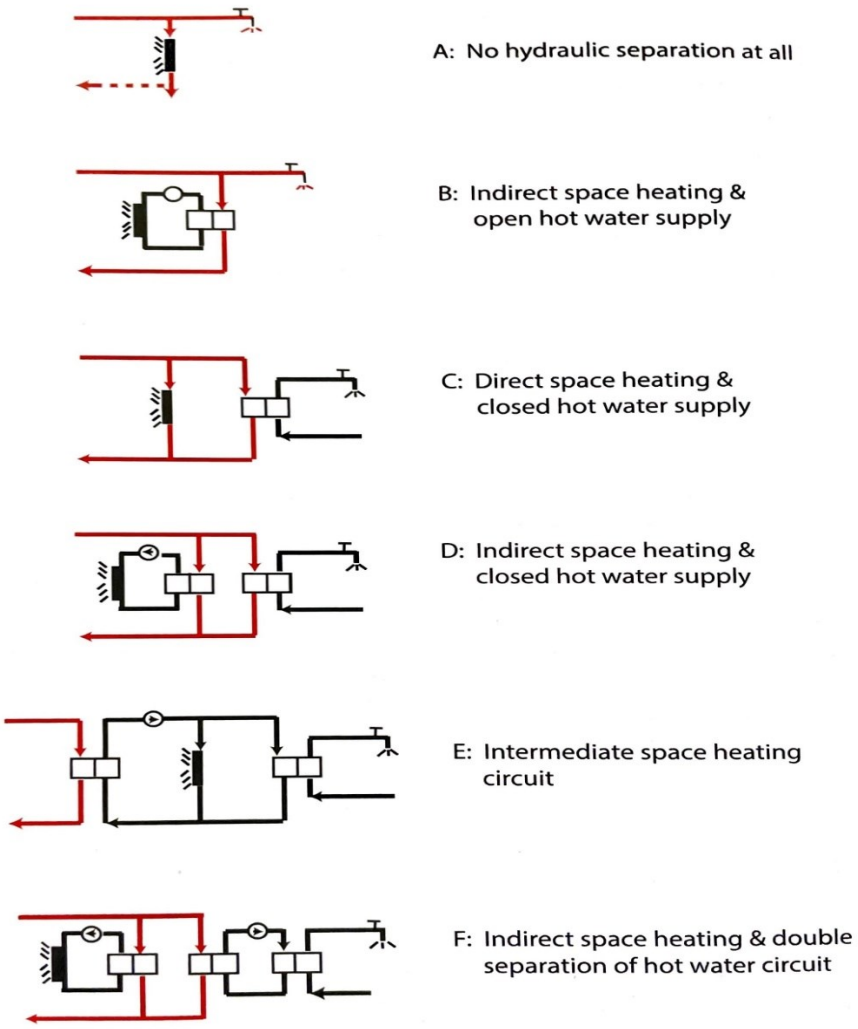

Figure 2.4 Various modes of hydraulic separation in substations. (Courtesy of [6])

Today the heat exchangers instaled in substations are usually of the brazed plate heat exchanger type. Once the brazing process is complete, the structure cannot be disassembled for cleaning. So Cleaning-In-Place systems are used, in which water of a suitable (acidulous) chemical composition is circulated through the plates.

The valves of DH substations are either self-operated valves or motorised valves, driven by electrical power supplied at low voltage. The mechanical type provides simple proportional control. Some static deviation from the set-point (control error), typically amounting to a maximum of a few degrees in the case of thermostatic control, cannot be avoided. Controls for motorised valves are usually of the PID-type control (Proportional with added Integration and Derivation), which can avoid static errors.

Finally, all substations have meters that evaluate the amount of heat transferred: they typically consist of temperature sensors upstream and downstream of the heat exchanger and a mass flow rate sensor.

2.5 Improvement of existing district heating network

In addition to the construction of district heating networks and the expansion of existing ones, improving the operational aspects of the existing DHNs is an important issue because it can increase the efficiency of the networks from both economic and environmental standpoints.

2.5.1 Energy flexibility: needs and possible sources

In Section 2.3 a portrait of the diversity and complexity of heat sources has been given. From the characteristics of heat sources, it becomes clear that it can be interesting to store heat produced in one moment for later usage. It is possible to provide some examples of the situations in which it can be advantageous to decouple heat production from the user's consumption.

A common heat supply structure is where CHP plants provide the base heat load and heat only boilers are used to match demand peaks. However, HOBs consume more primary energy per unit of useful heat. Therefore it can be beneficial to limit their use by responding to peaks in consumption with stored CHP heat. Furthermore, the electricity production of cogeneration plants can be cost-effective at different times than the thermal energy demand. Therefore, it can be profitable to store some heat when the electricity production is convenient as an alternative to only following the heat demand.

Another critical point is to improve the integration of renewable plants and waste heat in DHNs. These sources are usually intermittent, so there may be a mismatch between the heating demand and the heat they provide. Finally, exploiting the sources of energy flexibility of existing DH systems allows increasing the number of customers that can be connected once the peak load approaches the nominal power of the network, thus increasing revenues for the DH operator.

For all these reasons, usually, district heating operators use centralised storage tanks to decouple the supply from the demand of the substations, but space constraints can undermine

this possibility. As a result, it can be useful to exploit the sources of flexibility that are inherently part of the system and don't need to be added. These are mainly two:
- the heat carrier fluid enclosed in the network pipelines;
- the thermal capacitance of the building's envelope.

2.5.2 Energy flexibility in DHN pipes: network models

As mentioned, one of the main thermal masses to be exploited as a source of energy flexibility is the network itself, which contains a large amount of water. The evolution of DH networks in non-steady-state conditions has been studied quite extensively. In particular, the modelling of DH systems represents a key phase to understand the thermal and hydraulic behaviour in different operating conditions and to assess the potential of the source of energy flexibility represented by the water circulating in the network**.** Several district heating network models have been presented. In literature, two types of models for the simulation of the transient thermal behaviour in district heating systems can be found, namely the element-method and the node-method [19]. The element method solves the transient heat balance equation using different possible finite difference schemes. It was shown that low-order schemes suffer from artificial numerical diffusion, thus resulting in abnormal smoothing of sharp temperature profiles [20]. Higher-order schemes may instead bring overshooting [21]. In the element method, the temperature at each time–step is determined only from the time step before. Instead, the node method uses temperature values at different time–steps to determine the current temperature situation [20]. Pálsson et al. [19] implemented and tested two models based on the two different methods. The comparison revealed that, unless higher-order schemes are used, the node method is superior to the element method at low Courant numbers, which corresponds to a situation with long district heating pipes and sharp temperature gradients that require small time-steps. Furthermore, the computational effort seems to be also lower for the node method. However, the application of the node method is limited to tree-shaped networks [22]. A new numerical approach to model the heat transmission over long pipes has been presented by Dènariè et al. [23]. The model is based on the method of characteristics, and it splits the water thermal capacitance between the turbulent core and the boundary layer. Further modelling studies have been conducted on the temperature dynamics in variable flow DHN.

Duquette et al. [24] have constructed a pipe model using a steady-state heat transfer model combined with a variable transport delay. Gabrielaitiene et al. [25] have developed a model of the Naestved DHN in Denmark to investigate temperature variations in the system in case large and sudden changes in supply temperature were present. Stevanovic et al. [26] have presented a model of the Zemun district heating network in Serbia to analyse thermal transients and fluid propagation time delays from source to consumers in the whole system. Hassine and Eicker [27] have realised a model of the Sonnenberg solar-assisted DHN in Germany to assess the temperature and pressure variations in the network using two different pump control systems. Wang et al. [28] have investigated the optimal scales of time and spatial steps used in DHN models to realise fast and accurate calculation.

A stationary hydraulic and transient thermal model has been developed by a research group of the University of Padua, to which the author of this thesis work belongs. This model aims to reproduce the hydraulic and thermal behaviour of district heating and cooling networks. The model's accuracy has been investigated in reproducing the heat waves along a single pipe. The results proved that the heat propagation through the network can be accurately reproduced, provided that the network is correctly discretised [29]. The model, called *NeMo*, is similar to that developed at Polytechnic of Turin, which was used for studying both thermal [30] and hydraulic [31] behaviour of complex thermal networks. These physical simulation tools allow assessing different DHN management strategies to exploit network flexibility by shifting the thermal loads over time and shaving thermal load peaks.

A possible strategy is the increase in water temperature before the demand peak. This can be done by having the heat generators work at a higher power rating and provide warmer carrier fluid [32].

Other researchers have tried to exploit the flexibility source represented by the network with Model Predictive Controllers (MPC), determining the optimal energy management at the supply stations with different objective functions, such as minimising the operational costs, the primary energy consumption or the carbon emissions. In MPC, all the information about the network's current thermal and hydraulic situation, heat demand, and operating conditions forecasts are input for an optimisation problem. The objective function's solution indicates to the operator the optimal way of running the system in the following period.

A typical objective function is the minimisation of the operating cost. After finding the optimal scheduling of heat generators, the mass flow rates and temperatures, and more

generally the hydro-thermal parameters that reflect the optimal operation, are given as input to a physical system model (e.g. the DHN model). The system's physical model, which includes its ability to store thermal energy, allows predicting the evolution of the network parameters of interest. The parameters (e.g. the return temperatures) are used as new inputs for the optimisation problem in the following time interval.

Regarding the optimisation of the heat generators, Bavière and Vallée [33] focused on the design of a model predictive controller that optimises the heat distribution by appropriate scheduling of supply temperatures and differential pressure at the production level. In the early work by Benonysson et al. [20], the supply temperature was optimised to minimise the operational costs. Vesterlund et al. [34] developed a hybrid evolutionary-MILP optimisation algorithm. They coupled it to thermal network model simulations to achieve optimal control of heat generators in a complex DH network with multiple heat sources. Fink et al. [35] proposed two control methods based on mixed-integer linear programming (named global MILP and time-scale MILP) to flatten the power consumption profile of a group of heat pumps supplied by a biogas-fired CHP that also supplies heat to a district heating network. Both methods showed promising performance in flattening the power demand of the heat pumps compared to a standard PI on-off control.

Including complex thermal networks in the constraints of the optimisation problem introduces non-linear phenomena such as mass and heat propagation that are governed by the advection equation. Recently, non-linear optimisation approaches have been proposed by Krug et al. [36] and by Rein et al.[37]. In contrast, other researchers preferred to approximate non-linear phenomena through piecewise linearization techniques [38].

Thus, it is clear that the network has been considered as a source of energy flexibility in numerous research works to meet the needs of the DHN operator.

2.5.3 Demand-side management: energy flexibility of the building's envelope

The highest peak in heat demand occurs at the district level when domestic hot water is consumed, especially in the morning. For example, in the Turin DH system, the demand around 6 AM can be twice the average during daytime and four times (sometimes six times) the average during the night [30]. Therefore, it is important that a significant source of flexibility can be found on the customer's substations, allowing to act on the dynamics of heat withdrawal from the network.

The flexibility solutions involving the customers are part of the Demand Side Management (DSM). DSM, which is the modification of consumer energy demand, often requires finding a balance between the needs of the heat provider and those of the consumers. The end users can help smooth peaks in demand by using energy more constantly, resulting in an energy demand shift towards periods in which the producer finds it less expensive to provide. Sometimes the nature of the heat demand helps the generators. For example, industrial consumption is much more constant. Therefore, a user base with a large proportion of industries will improve the capacity factor of the DH plants.

On the other hand, if the customers are mostly residential, the network operator could encourage them to store energy by charging tariffs proportional to the production cost of energy or include a component based on the installed power. However, pricing heat at different rates could create other demand peaks in the hours with the lowest rates. Therefore, it is important to maintain real-time communication between user substations and the network operators.

All buildings, especially those with a large mass per unit of floor area and good insulation, accumulate heat and can act as a storage medium without dedicated facilities. The knowledge of this property can help in the operation management of a district heating network. The use of building masses is the object of significant research interest because the cost of this storage is zero, and no space needs to be reserved. Therefore, many researchers have studied Demand Response (DR) control methods to decouple the thermal needs from the energy supply. For example, a building can be heated and then be tolerant to interruptions in heat supply for a relatively long time. A residential building with a wall U-value of about 0.1 W/(m K) can remain unheated for about 24 hours with 0 °C external temperature, without a considerable loss of thermal comfort. Vivian et al. [39] demonstrated that building thermal capacitance has great potential in modifying building heat demand patterns, and it can be exploited to reduce building peak loads and operational costs. According to Vandermeulen et al. [40], the contribution of the network pipes is limited compared to that of the buildings' thermal capacitance. Le Dreau and Heiselberg [41] found that different buildings (level of insulation, type of emitter, etc.) need different control strategies to balance flexibility, energy demand, and indoor thermal comfort. So, the model-based predictive optimal control approach has mostly been used to efficiently manage the building heating and cooling plants, exploiting the building's thermal mass. Reynders et al. [42] showed that the building thermal

storage capacity, exploited through intelligent control logic, has strong potential in demand-side management. Oevelen et al. [43] demonstrated that this is true, especially in district heating networks. Aoun et al. [44] used reduced-order models to predict the space heating needs of buildings connected to a DHN and shift their consumption towards off-peak hours maintaining thermal comfort in the indoor environment.

It is possible also to add thermal mass to a building to increase the heat demand, which can be shifted. However, this can be counterproductive from an environmental and energy consumption standpoint because of the high energy and carbon footprint of concrete per unit of mass. Therefore, it is advisable only to use the mass of the building that has already been provided for structural reasons [45].

Sometimes, the structural and plant design of the building, and not just the envelope conception, can be a resource to achieve a greater degree of independence. It is possible to speak about Thermal Mass Activation (TMA) in this case. Thermo-Activated Building System (TABS) is a relatively widespread TMA strategy. In TABS, the concrete structure (especially the floor slabs) is cooled during the summer nights with cold water pipes, and then it absorbs the thermal load of the daytime, slowing down the rate at which the rooms heat up. In winter, the heating load is less irregular, but the mass of a building can still be heated at night to a certain extent and rely mostly on the solar and activity gains during the day.

2.5.4 Dedicated thermal energy storage systems

Thermal energy storage (TES) systems used in DHN can be classified based on different criteria. According to Guelpa et al. [46], a criterion is the physical phenomenon used for storing heat, as shown in Figure 2.5. So, there are:

- *Sensible heat storage*, whose temperature increases and decreases when charged or discharged with energy. This is a mature technology that has been installed in various DH networks.
- *Latent heat storage*, which undergoes a phase change. They are currently tested in experimental field installation.
- *Thermo-chemical storage* in which a chemical reaction occurs. They are currently tested in laboratory installation.

Furthermore, sensible TES can be further classified by duration in long-term and short-term storage. In the first case, the time passing between the loading and unloading of energy can vary from several weeks to months. On the other hand, short-term storage usually has a duration varying from some hours to a day. Figure 2.5 also gives an idea of the Technology Readiness Level (TRL) to show the maturity of each TES system.

A low TRL still characterises latent heat and thermochemical storage, so they are not investigated in this research work. As a result, the following description is focused on sensible heat storage.

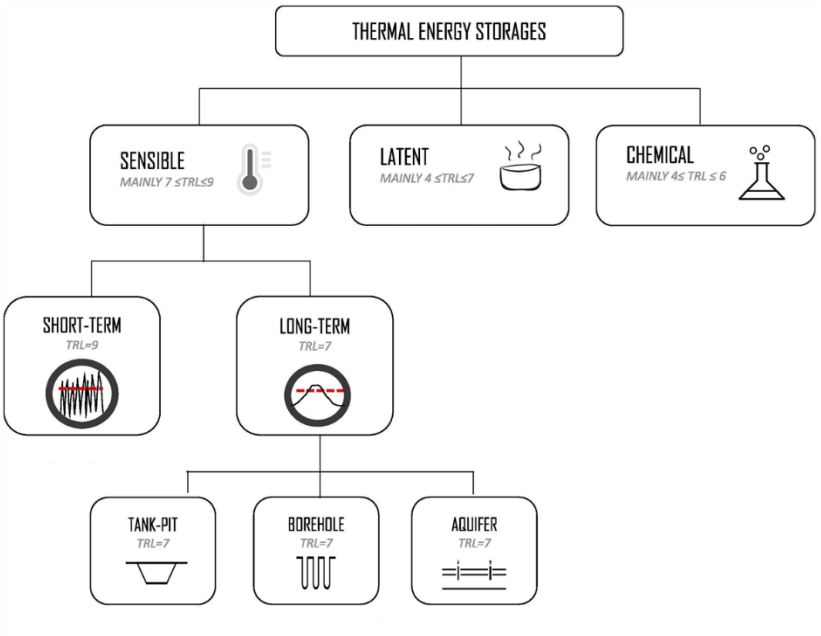

Figure 2.5 TES classification based on the physical phenomenon used for storing heat and TRL. [46]

2.5.5 Sensible heat storage system

The most common sensible systems are based on liquid water, accumulated in tanks that range in size from hundreds of litres in households to hundreds of cubic metres in tanks for daily and hourly balancing in DH networks, and up to hundreds of thousands of cubic metres in large reservoirs sometimes used for seasonal energy storage [46].

Water has relatively high thermal conductivity and density and the highest sensible heat capacity per unit of mass of all naturally occurring substances. It is liquid and therefore easy to move and use as a heat transfer fluid as well, has low viscosity, is chemically inert, non-toxic, inexpensive and widely available. The main constraint on water use is the need to increase its pressure beyond equilibrium with the atmosphere to heat it above 100 °C. So,

water is an optimal medium for energy stocks since at least the third generation district heat developed in the 1970s, characterised by temperatures below 100 °C.

Other important sensible media are thermal oils and molten salts, which present the advantage of remaining liquid at high temperatures without pressurisation. Molten salts can conserve heat at temperatures above 400 °C [47]. On the other hand, these substances can present fire and corrosion hazards and are significantly more expensive than water. Other common sensible storage materials are solid, like sand, gravel, rocks, minerals or concrete. They are generally used in packed-bed structures, with a liquid or gaseous heat transfer fluid adding or removing the heat. Solid materials also have temperature limits beyond which chemical degradation and erosion can occur.

2.5.5.1 Short-term TES

A remarkable analysis reported in [48] shows that most of the TES installed in DH systems are short-term storage. Most of them are tanks filled with water. These have a TRL of 9. S-TES can be divided into two main categories [49]:

- *Pressurised TES*: DH systems working with superheated water are currently quite widespread, and they are typically used in large DH systems. Pressurised TES are usually directly connected to the DH network. As a result, storage and pipeline operate at the same pressure level. An advantage of pressurised TES systems is that, when directly connected, they can operate as a pressurisation vessel. This is an essential component in DH networks. In the case of direct connection, the installation of a dedicated pressurised vessel can be avoided by exploiting the TES.
- *Atmospheric TES*: This is mainly used with low-temperature DH, where the maximum temperature in the storage does not exceed 100 °C. They are connected indirectly to the DH network because of the pressure difference compared to the pipeline.

2.5.5.2 Long-term TES

- *Tanks for seasonal heat storage* (T-TES) consist of concrete or steel containers filled with the storage medium. They are built in large part above ground. The storage medium is usually water. This type of reservoir is thought to have the highest energy density, typically around 60-80 kWh per cubic metre. The important height of such structures allows the greatest degree of thermal stratification, and they can be built in such a way as to extract or

inject large amounts of energy per unit of time. It is insulated at least on the top and the side walls by a layer made of glass wool or polyurethane, foam glass or fibreglass to minimise the thermal losses [50]. At least 1 m thickness insulation should be used when long term storage is considered [51]. Furthermore, inspection and maintenance are greatly simplified.
- *Pit storage* (P-TES) is built by excavating the ground to form a large space with the shape of a truncated inverted cone or inverted pyramid. Then it is lined with a waterproof material like polymers, cement, or bentonite, and covered with an insulated vaulted surface, that either floats or is supported by pillars or a solid filler material like gravel [52]. The sheer volume of these chambers is in the order of hundreds of thousands of cubic metres. The storage medium is typically not pure water but a mixture of water and sand or gravel, introduced for structural reasons. Therefore, the higher the share of solid materials, the smaller the energy density, which is about 30-50 kWh per cubic metre. The maintenance is quite challenging.

- *Borehole Thermal Energy Storage (BTES)* is a technology that requires the drilling of deep boreholes, in which polymer water pipes are placed, along with a filling material. When the reservoir is filled with thermal energy, warm water from a solar plant or a heat pump condenser circulates in the ground's boreholes. The reservoir's energy is discharged by heating cold water, typically during the winter. An important advantage of BTES is the minimal amount of civil engineering works, the small occupation of space above ground and the relative simplicity when it comes to expansion of the reservoir. On the other hand, ground energy storage suffers from low energy densities, in the order of 15 to 30 kWh per cubic metre, and is difficult to insulate, with the possible exception of the upper boundary surface. Heat exchangers can be designed with a horizontal rather than vertical geometry to reduce costs. However, this solution keeps the boreholes closer to the ground, resulting in greater space occupation and increased energy losses due to the larger surface-to-volume ratio. What is more, maintenance can be difficult or impossible once the system is built [53].

- *Aquifer Thermal Energy Storage (ATES):* The water table can be used for thermal energy storage. In this case, warm water can be injected in the summer and then replaced during the winter with cold water in the systems that rely on ATES. Extraction wells are typically located at a distance in the order of magnitude of 100 m from the injection. The temperature

difference between cold and warm water is relatively small. As a result, these systems often work together with reversible heat pumps that extract heat in the winter.

2.5.6 Integration of RES in DHN

Another aspect that can improve the operational conditions of the DHNs is the integration of renewable energy sources. At the building level, multi-source energy systems (MSES) are rising interest as they can increase the exploitation of renewable energy sources, reduce the environmental impact related to the use of fossil fuels, and enhance the efficiency of heating and cooling systems. Emmi et al. [54] investigated a solar assisted ground source heat pump system in six cold locations. The results showed that when solar thermal collectors are not used, the seasonal energy performance of the heat pump decreases by about 10% over ten years. Instead, when solar energy was used, the seasonal energy performance was constant and above 4.5 over time. Significant research efforts combine photovoltaic thermal (PVT) panels with heat pumps for space heating and cooling application. A previous study[55] analysed the energy performance of different multi-source energy system combinations coupled with PVT collectors and a heat pump. The investigated multi-source energy systems increased the energy efficiency by up to 25% over a conventional air-to-water heat pump system. Sommerfeld and Madani [56] studied a solar-assisted ground source heat pump system to describe its technical and economic potential for Swedish multi-family houses. The results showed that the PVT can reduce borehole length by 18% or spacing by 50% while maintaining an equivalent seasonal performance factor to systems without PVT. Bellos et al. [57] performed a techno-economic assessment of a PVT assisted heat pump for space heating in the building sector. A simulation model of a PVT assisted heat pump system for space heating and cooling was developed by Calise et al. [58]. Dannemand et al. [59] conducted an experimental analysis on a solar PVT assisted-heat pump system with a cold buffer storage tank and a domestic hot water storage tank. Focusing on the interplay between the different components, the analysis indicated that the PVT collector helped the two-tank heat pump system.

The possibility of interconnecting these solutions fosters the development of sustainable energy districts. This is possible thanks to district heating and cooling (DHC) networks, essential urban infrastructures to enable the flexible integration of renewable energy and distributed generation systems. A prerequisite to their deployment is the reduction in the

supply temperature of District Heating Networks (DHN) [60]. In the last decade, around 40 DHC systems of the so-called 5th generation, or ultra-low-temperature district heating, were put in operation [4]. These networks' heat carrier fluid temperatures are closer to the ambient temperature. They can fulfil buildings' heating and cooling demands through distributed heat pumps installed at the customer substations [61]. Despite the extra investment for the booster heat pumps, they can save the distribution heat loss and utilise low-grade energy sources. Examples of ultra-low-temperature thermal grids coupled to borehole thermal energy storage with decentralised solar supply have been reported in a few projects, such as the well-known Solar Drake Landing Community in Canada and the Suurstoffi district in Switzerland [62]. In Østergaard and Andersen [63], the performance of ULTDH is significantly better, compared to LTDH, in terms of both costs and primary energy demand for a theoretical case representing a typical small Danish DH network. An innovative ultra-low-temperature heating and cooling network, the district "Suurstoffi", in Central Switzerland, was monitored by Vetterli et al. [64]. This case study is characterised by a large geothermal field, functioning as seasonal storage, with warm and cold ducts and PVT systems to operate the heat pumps. Chen et al. [65] evaluated the sustainability of a district heating system integrated with solar and geothermal sources, employing both vapour-compressor and absorption cycles through a GSHP and an AHP subsystem. A previous study conducted by Vivian et al. [66] investigated the advantages of ULTDH networks with booster heat pumps at the customers' substations and their sensitivity to the main design parameters for a heating-only case study. Also Ommen et al. [67] conducted a theoretical investigation on the optimal use of booster HPs in ULTDH for new buildings. They found that the booster heat pumps can improve the system performance if a central HP is used for the heat supply of the network. Behzadi and Arabkoohsar [68] modelled and studied a novel solar-based building energy system on different district heating integration scenarios (existing, LTDH and ULTDH). In this case, the solar system, which uses PVT panels and has neither a battery nor a heat pump, is integrated in the best way with ULTDH. In Garcia et al. [69], a hybrid system including PVT panels and a heat pump is proposed to provide domestic hot water (DHW), heating and electricity to a house located in central Europe. They demonstrated that the interaction of the proposed renewable-based system with the local DH system results in higher energy efficiency and reduced CO_2 emissions. Rosato et al. [70] investigated a centralised hybrid renewable district heating system based on the exploitation of solar energy

and integrated with a seasonal borehole thermal energy storage. Pakere et al. [71] studied the optimal integration of PVT technology in district heating systems by covering industrial power consumption and heat demand of buildings in the Northern European climate.

2.6 Discussion

The literature review shows that significant research efforts are aimed at improving the energy flexibility of district heating systems. Different thermal energy storage systems available in DHNs, each with its own characteristics and dynamics, have been studied as sources of energy flexibility by researchers with different methodologies. On the other hand, the literature review uncovered a lack of an accurate assessment and comparison between the flexibility potentials of the two main sources that are inherently part of the DH system (the thermal capacitance of the heat carrier fluid enclosed in the network pipelines and of the building's envelope). Vandermeulen et al. [40] used transfer functions through optimal control problems to quantify and compare the energy flexibility of the thermal capacitance of buildings and network pipes. This analysis showed that the flexibility that the network pipes can deliver is limited compared to the flexibility delivered by the buildings' thermal capacitance. On the other hand, concerning the methodology to determine and compare energy flexibility through transfer functions, an important limitation of the methodology became apparent. For example, in the case of congestion determined by mass flow rate limits, the behaviour of the subsystems changes. These changes imply that the separate step responses can no longer be summed up together to determine the overall system response, limiting the applicability of the flexibility function methodology. Therefore, an interesting research issue is to investigate and compare these sources of energy flexibility considering a methodology that doesn't present these limitations, also analysing the economic and environmental benefits.

CHAPTER 3 REAL CASE STUDY

3.1 District heating network of Verona Centro Città

Verona is the largest city municipality in the Veneto region, with 259,610 inhabitants. The climatic characteristics of Verona, obtained from the UNI 10349-1:2016 [72], are the following:

- Degree-days: 2,469
- Climatic zone: E
- External design temperature: -5 °C
- Annual heating period: 183 days.

Figure 3.1 is a satellite photograph that provides a view of Verona's district heating networks. Overall there are five district heating networks, 1318 user substations with a total length of network pipelines equal to 220 km and a thermal load peak of 170 MW. Two of them, Forte Procollo and Borgo Trento, are connected by a heat exchanger. So they are not hydraulically connected but can exchange heat.

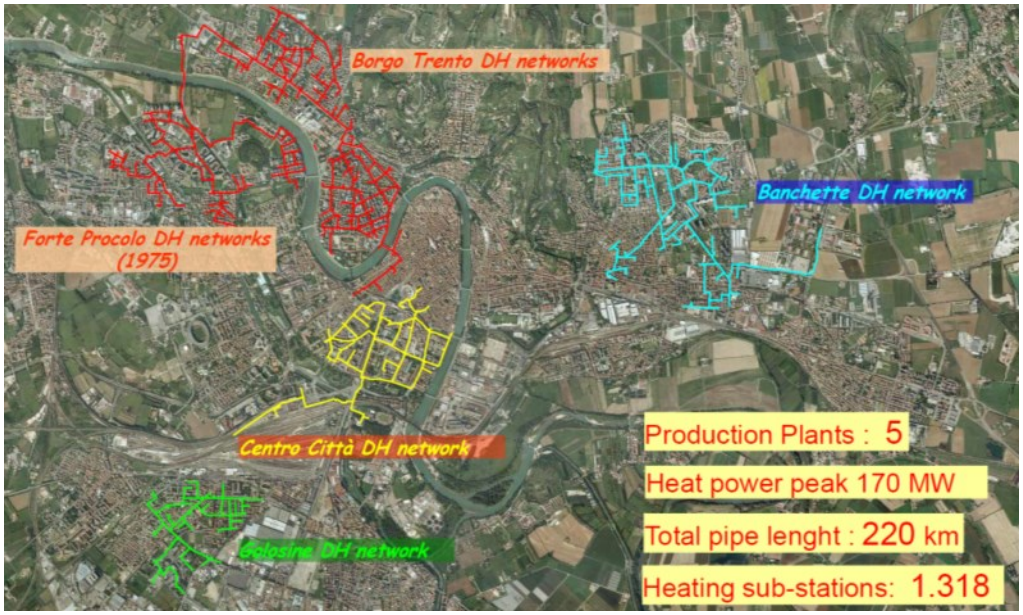

Figure 3.1 Satellite photo of Verona's district heating networks. (Courtesy of AGSM).

3.1.1 The DH network and the supply stations

The case study under consideration is the district heating network of Verona Centro Città (Italy), shown in Figure 3.2. This DHN operates at constant supply temperature and variable flow rate. Furthermore, the network extends for a length of about 25 km with a volume of

652 m^3, providing heat for space heating and -in some cases- domestic hot water to 247 users. The substations connected to the network have a total volume of about 3.2 $Mm^{3,}$ and they need about 70 GWh/year of heat, with a load peak of approximately 38 MW.

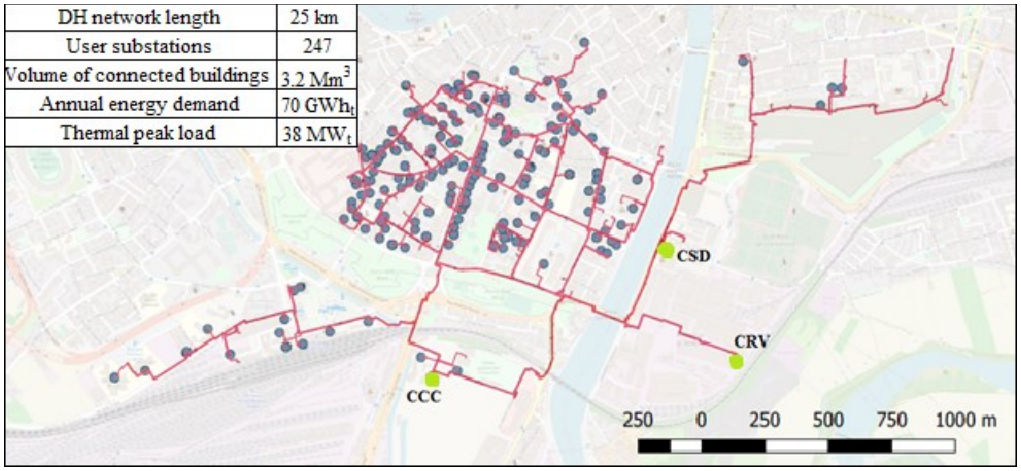

Figure 3.2 Plan of the district heating network of Verona Centro Città obtained with QGis [73] (the blue dots represent the substations and the green dots represent the supply stations).

The blue dots in Figure 3.2 represent the user substations, while the three green dots correspond to the supply stations. The main one is CCC, which supplies heat produced by five CHP units, heat pumps (supplied by the cooling circuit of the CHP) and three auxiliary gas boilers; CRV recovers heat from a foundry, and CSD has other three auxiliary and reserve gas boilers. Table 3.1 summarizes the characteristics of the generation plants in the supply stations.

Table 3.1 Installed thermal and electrical power of the supply stations.

Supply station	Heat generation	Units	Total installed power
CCC	Gas-fired internal combustion engines Heat pumps Gas boilers	5 5 3	11 MW_{th} (11.25 MW_e) 2.0 MW_{th} 25.5 MW_{th}
CRV	Waste heat from foundry	1	1.1 MW_{th}
CSD	Gas boilers	3	3.4 MW_{th}

Centro Città network is supplied simultaneously by CCC, CSD and CRV. Consequently, an order of priority can be summarized in the following table (the priority is adaptable at any time). CRV recovers waste heat, so it always has priority. CCC has priority in winter because it has a large capacity to cover the winter thermal load. In summer, it is unnecessary to use all that power because the thermal load is low, so CSD has priority over CCC.

Table 3.2 Order of priority in the heat supply for CRV, CCC and CSD supply stations, respectively, winter and summertime.

Supply station	PRIORITY	
	Winter	Summer
CRV	1	1
CCC	2	3
CSD	3	2

The following paragraphs provide a brief description of the three supply stations and their operating logic to allow a better contextualisation of the research work.

3.1.1.1 Centrale Centro Città - CCC

The main supply station of the Centro Città DH network is Centrale Centro Città (CCC), with an installed thermal power of approximately 38 MWt. The pump head is set in the CCC station depending on the circulating flow rate, in line with the curve shown in Figure 3.3. This curve, obtained empirically from the DH network operator, allows a sufficient pressure difference and therefore circulating mass flow rate even at the critical point of the network. In summer, when the circulating mass flow rate in the network falls below a predetermined threshold (150 m^3/h), the pumps in CCC stop, and the flow regulation is delegated to the CRV supply station.

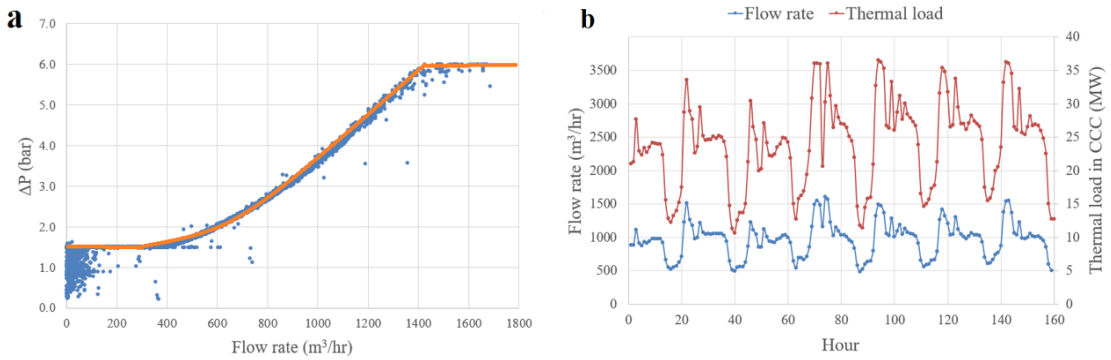

Figure 3.3 Current mass flow control in CCC: (a) theoretical (red line) and measured (blue dots) pressure difference versus mass flow rate; (b) mass flow rate and heat load over time. (Courtesy of AGSM)

Regardless of the pressure difference and the circulating flow rate, the CCC automation system manages the start-up of the heat generators (gas boilers and CHP units) in sequence, starting or stopping them, to always guarantee a constant supply temperature equal to 80°C. The thermal load is followed by the CHP units , turning on or off the individual units, and when in operation, they always work at nominal load. In addition, each CHP unit has a heat

pump installed (five heat pumps in total), which consumes part of the electrical energy produced by the combustion engine (100 kW) to produce about 300 additional thermal kW. The water-to-water heat pumps are installed outdoors in a dedicated space, as shown in Figure 3.4. They use glycol water from the low-temperature cooling circuit of the cogeneration engines as a heating source. Each gas engine has an independent cooling circuit. Therefore each heat pump recovers heat from one of these circuits, independently of the other heat pumps in the system. The flow rate required for each evaporator is taken by tapping from the delivery piping of the cooling circuit and returned, after use in the evaporator, directly into the same piping. Each heat pump delivers the heat to the district heating network in parallel with the other heat pumps and the other production units on the condenser side.

So, when the heat pumps operate, the characteristics of the combustion engines change. They will have less electrical efficiency and more thermal efficiency. The operation of the heat pumps is on/off, and it depends on the energy prices. The thermal power produced by the combustion engines is almost constant, but the heat recovery, i.e. the heat supplied to the district heating network, can be variable, especially in mid-season. Each engine can dissipate up to 50% of its thermal power. 50% of the power comes from the oil/water cooling circuit, which is usually not dissipated. Another 50% comes from the heat recovery on the exhaust fumes, which can be dissipated into the atmosphere through a bypass valve on the exhaust fume manifolds.

Figure 3.4 Heat pumps of the CCC supply station. (Courtesy of AGSM).

3.1.1.2 Centrale ADV-Pittini - CRV

A second thermal power station on the same district heating network, named CRV Station, recovers waste heat from a foundry (Acciaierie di Verona of Pittini group) in Lungadige Galtarossa. The existing heat recovery system has a recoverable capacity of 1 MWt. CRV is designed to be operated in automatic mode and supply the base thermal load request of the DHN. Therefore it operates with priority over all other supply stations.

3.1.1.3 Centrale Sede AGSM - CSD

In addition to the two supply stations mentioned above, a third station is called Centrale Sede AGSM (CSD). The CSD station allows transferring the thermal energy produced by the three boilers to the network, both in winter and summer. As shown in Figure 3.5, the primary circuit (supply station side) consists of three boilers with a total capacity of approximately 3,000 kWt (boiler 1: 1,200 kWt; boiler 2: 1,200 kWt; boiler 3: 600 kWt), two circulation pumps of 7.5 kWe each, powered by inverter, and a plate heat exchanger with thermal power of 3,000 kWt. Instead, the secondary circuit (network side) comprises the heat exchanger previously described, a 55 kWe inverter-driven circulation pump and a system minimum flow valve regulated by a pressure transducer. Unlike CRV, which serves the base thermal load, CSD is mostly used as a support station (towards CCC in winter and CRV in summer) and as a reference station if CRV should not be available, for example, in case of maintenance.

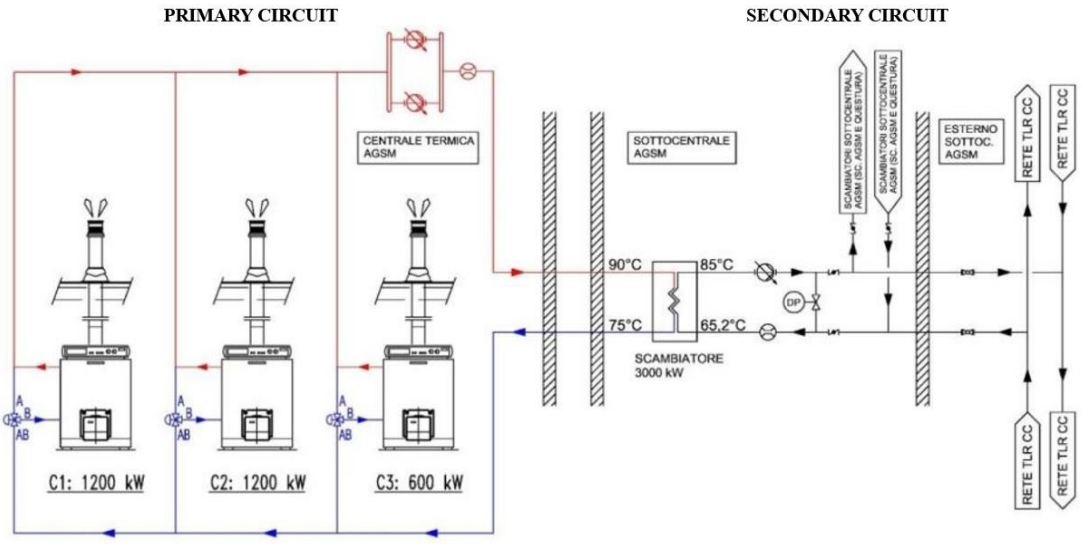

Figure 3.5 Simplified scheme of CSD supply station with primary and secondary circuits. (Courtesy of AGSM)

3.1.2 The monitored building stock

The selected building dataset consists of two schools, two hotels, three offices and nine residential units. Some general information about the investigated buildings is shown in Table 3.3.

Table 3.3 General information of the selected user substations.

Typology	**Age**	**Floors**	**Height [m]**	**F. area [m^2]**
Office A	1990	4	13	3350
School A	1870	3	9	1080
Office B	1980	3	9	445
Condominium A	1960	6	22	788
Condominium B	1960	6	22	788
Condominium C	1930	6	19	167
Condominium D	1930	5	16	148
Hotel A	1950	6	19	119
Condominium E	1960	6	19	540
Condominium F	1920	5	16	729
Hotel B	1910	4	13	534
Office C	1940	4	13	324
Condominium G	1930	6	19	162
Condominium H	1970	4	13	94
Condominium I	1970	6	19	292
School B	1960	3	9	2325

As said, the DHN of Verona Centro Città is connected to 247 user substations, but just for 26 of these 247, the monitoring was provided. The latter started in October-November 2019 and ended in March 2020. The monitoring of energy use in the substations serviced by AGSM was carried out by Gizero Energie, a specialized company in energy monitoring. These measures included:

• Maximum, minimum and mean power [kW] for each hour;

• Water flow [m^3/h];

• Supply and return temperature [°C].

The data regarding the pressure in the supply and return pipes was also provided for some substations. In addition, extra measures such as humidity and temperature in the substations, useful for maintenance, were added to these data concerning energy monitoring. These measures are all corresponding to the primary circuit of the heat exchanger installed at each user. The measuring devices installed are all ultrasonic compact energy meters suitable for

measuring the energy consumption of district heating systems. The principle of operation of these meters is static and based on the transit time measurement. In particular, ultrasonic meters are characterized by the absence of moving parts, thus preventing mechanical wear of the metering components, low-pressure losses, low start flowrate and good tolerance to suspended particulates in the water flow. On the whole, the ultrasound principle assures stable and accurate measuring results. Furthermore, for these buildings, some key information was provided by the energy supplier AGSM Energia Spa, including:

• Call sign;
• ID number;
• Address;
• Heat exchanger size (in kW) for heating and eventually for DHW;
• Year of plant installation;
• Invoiced energy demand referred to 2017.

The measured data and all nominal data were analysed to evaluate the level of reliability of the energy supplier's information. Therefore, the data relating to energy demand were first checked. Then, the monitored consumption was carried over to the entire year 2019 using degree days and then normalized to 2017 to compare the invoices referring to the same year. A discrepancy emerged from the comparison between energy demands for some buildings that have been excluded from the analysis. In addition, other buildings were excluded by the data set due to uncertain end-use. This led to the final group of 16 buildings. In the figure below, an overview of the 16 buildings in the Verona city centre is shown, while a satellite view of each building is shown in Figure 3.7.

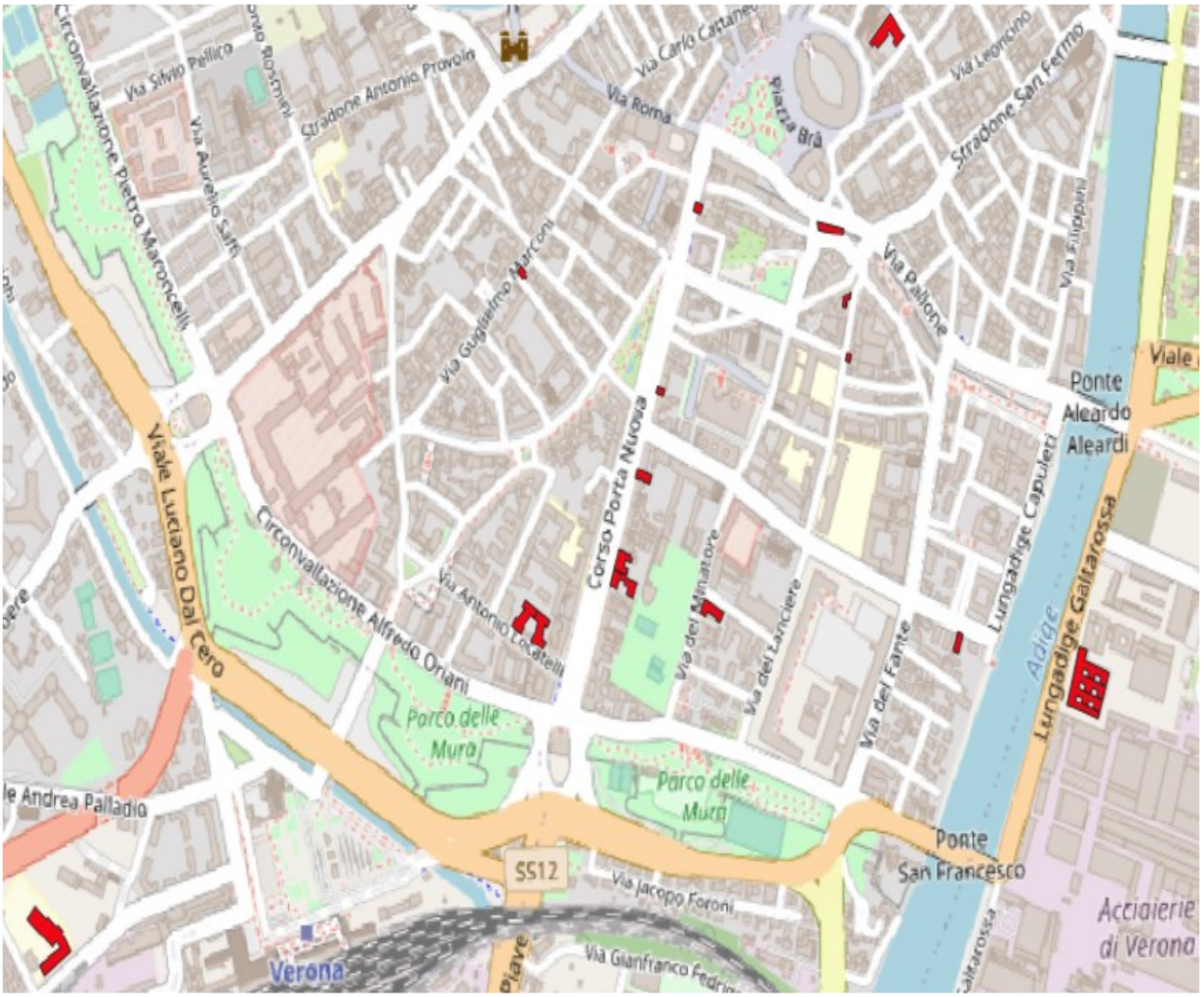

Figure 3.6 Satellite image of the area under investigation.

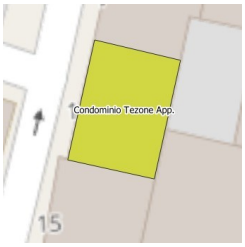

(a) Cond. H

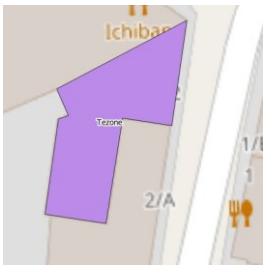

(b) Cond. G

(c) School B

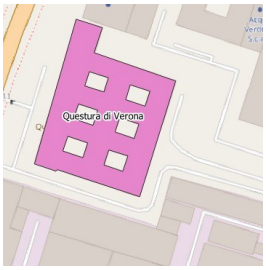

(d) Office A

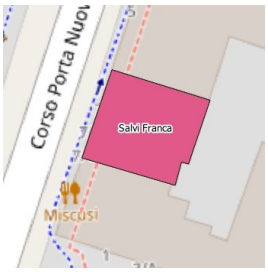

(e) Cond. C

(f) Cond. I

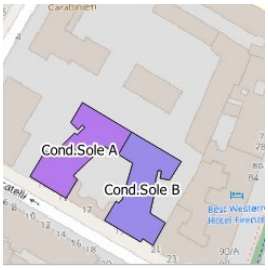

(g) Cond. A and B

(h) Office C

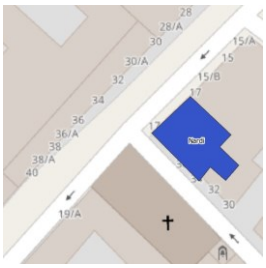

(i) Cond. D

(j) Hotel A

(k) School A

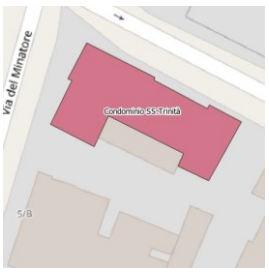

(l) Cond. E

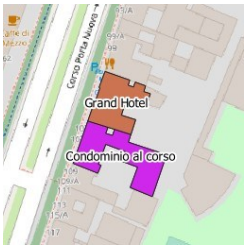

(m) Cond F, Hotel B

(n) Office B

Figure 3.7 Satellite images of the monitored substations

CHAPTER 4 MODELS

Models developed with different software were used to analyse the energy flexibility sources in a district heating network (Chapter 5 and 6).

In this chapter, first, the tool used for modelling the district heating network and the model's assumptions are described. Secondly, the geometric and energy models of two buildings connected to the district heating network of Verona are presented.

4.1 District heating network model

In this study, the concept was to consider the district heating network as a source of energy flexibility and take advantage of the thermal capacitance of the water inside the pipelines. The differences between this system with the traditional storage system (e.g. storage tank) made it necessary to consider a dynamic model to assess the actual thermal capacitance of the network.

4.1.1 Network pre-processing

The Verona's district heating network was simulated using *NeMo*, a finite difference method model, and it describes the network's topology using graph theory [74] [75]. A plug flow is assumed, which implies that the velocity of the heat carrier fluid is uniform in the radial direction (one-dimensional model). The network is represented by a set of nodes and oriented branches, and an adjacency matrix determines their mutual connections. In problems of forced convection, the velocity of the heat carrier fluid does not depend on the temperature distribution. Therefore, the hydraulic and thermal problems can be uncoupled. This allows the calculation of the mass flow rates and the pressures across the network in a first step; then, given the mass flow rates, the energy balance is solved to determine the temperature distribution. The overall structure of the model is illustrated in Figure 4.1. The model was developed using MATLAB [76].

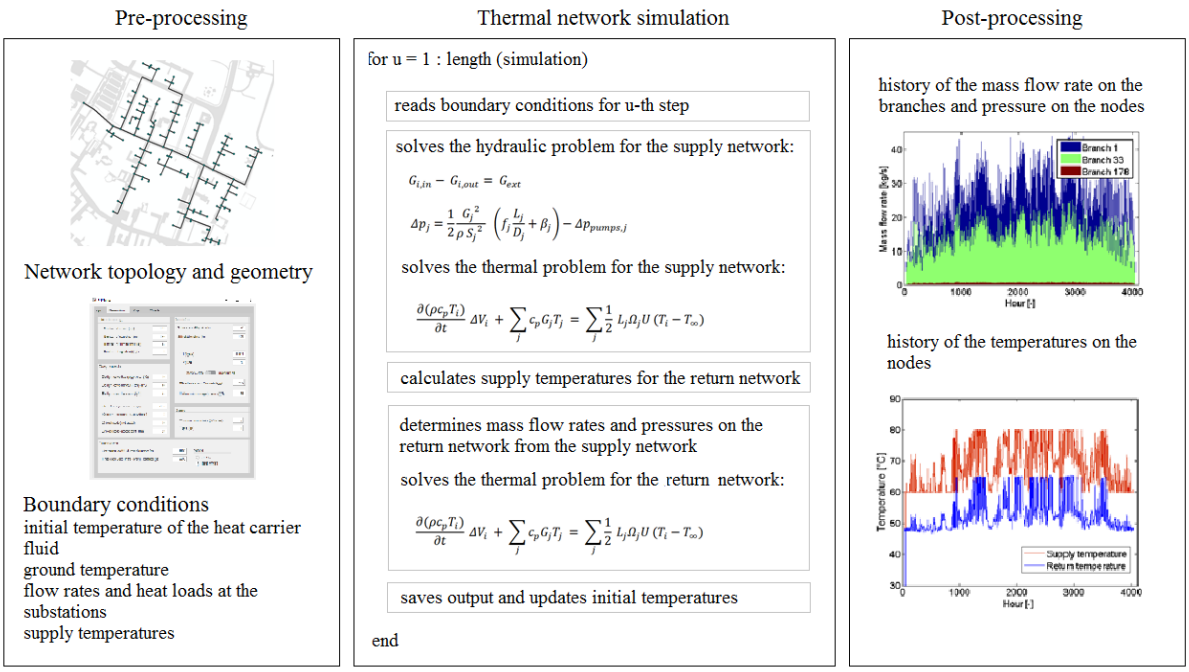

Figure 4.1 Structure of the model NeMo [74].

4.1.2 The hydraulic balance

Due to the incompressible nature of the heat carrier in modern DH systems –pressurized water, two equations are sufficient to describe the flow and pressure distribution: the *continuity equation* and the *momentum equation*. Equation (4.1) applies the law of conservation of mass to the *i*-th node of the network:

$$G_{i,in} - G_{i,out} = G_{i,ext} \tag{4.1}$$

where G_{ext} is the *nn*1* vector of mass flow rates exiting/entering the system from/in the nodes. Equation (4.2) applies the Navier-Stokes equations to the *j*-th branch of the network, including both distributed pressure losses due to viscosity and concentrated losses due to geometrical irregularities:

$$\Delta p_j = \frac{1}{2}\rho \left(f_j \frac{L_j}{D_j} + \sigma_j \right) {v_j}^2 - \Delta p_{pump,j} \tag{4.2}$$

Velocities are linked to mass flow rates through Equation (4.3):

$$G_j = \rho S_j v_j \tag{4.3}$$

By substituting Equation (4.3) in Equation (4.4), the following holds true:

$$\Delta p_j = r_j {G_j}^2 - \Delta p_{pump,j} \tag{4.4}$$

Where all the constant terms that refer to the *j*-th pipe are grouped into the constant *r*:

$$r_j = \frac{1}{2\,\rho\,{S_j}^2}\left(f_j \frac{L_j}{D_j} + \sigma_j\right) \tag{4.5}$$

Thus, all mass flow rates and pressures can be found by solving two systems of equations that can be written in matrix form:

$$A\,\dot{G} + \dot{G}_{ext} = 0 \tag{4.6}$$

$$A^T P = r\,\dot{G}^{\,2} - h \tag{4.7}$$

Where *G* and *P* are the *nb*1* vectors of mass flow rates and the *nn*1* vector of pressures. The heads provided by the pumps $\Delta p_{pump,j}$ are stored in the *nb*1* vector *h*. Thus, the overall system has *nn*+*nb* equations and the same amount of unknown variables. These systems are coupled because *G* appears in both equations. Moreover, the overall system is nonlinear because the pressure drops depend on the square of the flow rates. To solve the overall system represented by Equations (4.6) and (4.7), the model uses the semi-implicit method for pressure linked equations, also known as SIMPLE method[77]. In this method, the pressure field is determined by first calculating an intermediate velocity field based on an estimated pressure field; and then obtaining appropriate correction to satisfy the continuity equation. The momentum equation is linearized by expressing the first term as a product of a hydraulic resistance *R* (expressed in Equation (4.5)) and of the mass flow rate *G*. Therefore, Equation (4.4) can be rewritten as:

$$\Delta p_j = R_j G_j - \Delta p_{pump,j} \tag{4.8}$$

In matrix notation:

$$A^T P = R(\dot{G})\,\dot{G} - h \tag{4.9}$$

A guess-value vector for mass flow rates is used to calculate the *nb*nb* diagonal matrix of hydraulic conductances, *Y*, where $Y_{j,j} = 1/R_j$. Then, a guess-value vector for pressures P^* is assumed and used to calculate a new vector of mass flow rates G^* in Equation (4.10). The latter equation is obtained by left-multiplying both members of Equation (4.9) by *Y*:

$$G^* = Y\,A^T P^* + Y\,h \tag{4.10}$$

With this new vector G^*, the new conductance matrix Y^* can be calculated. Then, assuming that $Y=Y^*$ and using Equation (4.6), both pressures and flows can be corrected simultaneously:

$$A\,Y^* A^T \Delta P^{corr} = -AG^* - G_{ext} \tag{4.11}$$

$$\Delta G^{corr} = Y^* A^T \Delta P^{corr} \tag{4.12}$$

The pressure correction can be obtained by solving the linear system represented by Equation (4.11). Then, the resulting vector can be used to calculate the mass flow rate correction, as shown in Equation (4.12). Finally, under-relaxation factors can be used to calculate the new vectors of G and P that can be used as inputs for the next iteration. The iteration loop ends when the norm of the residuals of both G and P is lower than a tolerance, set to 0.01 kg/s and 50 Pa, respectively. Since the momentum equation provides pressure differences, the pressure in one node must be fixed as a boundary condition. After the convergence, the guess vectors for pressures and mass flow rates are updated using those of the previous time-step to reduce the computation time.

4.1.3 The thermal balance

The heat propagation in the network is described by the energy balance performed on the volume of heat carrier fluid around the network's nodes. The control volume of the *i*-th node corresponds to half of the heat carrier fluid volume of all the branches connected to it, as shown in Figure 4.2. The model neglects the heat conduction through the wall pipe along the axial direction; the heat transfer in the radial direction considers the convection between the heat carrier fluid and the inner pipe surface, the thermal resistance of the pipe and its thermal insulation, as well as the thermal resistance of the surrounding ground. However, the thermal capacitance of the surrounding ground is not considered.

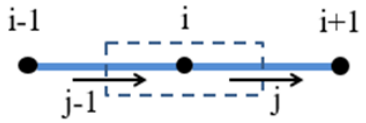

Figure 4.2 Control volume of the i-th node.

Applying the energy balance to the node shown in Figure 4.2 leads to Equation (4.13):

$$\rho \mathrm{V_i} \mathrm{c_p} \frac{\partial \mathrm{T_i}}{\partial \mathrm{t}} = G_{j-1} c_p T_{j-1} - G_j c_p T_j - \frac{1}{2} (\mathrm{L_j} \Omega_\mathrm{j} U_j + \mathrm{L_{j-1}} \Omega_\mathrm{j-1} U_{j-1})(\mathrm{T_i} - \mathrm{T_g}) \quad (4.13)$$

where G is the mass flow rate, V is the volume of heat carrier fluid enclosed in the control volume, Ω is the perimeter of the pipe section, U is the radial heat transmission coefficient from fluid to the ground and T_g is the undisturbed ground temperature. The temperature of the branches is then associated with the temperature of the corresponding upwind nodes, according to the well-known upwind scheme. Therefore, Equation (4.13) becomes:

$$\rho \mathrm{V_i} \mathrm{c_p} \frac{T_i^{(t)} - T_i^{(t-\Delta t)}}{\Delta t} = G_{j-1} c_p T_{i-1}^{(t)} - G_j c_p T_i^{(t)} - \frac{1}{2} (\mathrm{L_j} \Omega_\mathrm{j} U_j + \mathrm{L_{j-1}} \Omega_\mathrm{j-1} U_{j-1}) \left(T_i^{(t)} - \mathrm{T_g}\right) \quad (4.14)$$

Equation (4.14) can be represented in matrix form as:

$$\mathrm{M}\, \dot{T} = s - K\, T \quad (4.15)$$

Where M and K are respectively the mass matrix and stiffness matrix. The temperature at the inlet node is fixed (Dirichlet condition). In a previous version of the software [29], the first-order ordinary differential equation (ODE) was formulated as by Equation (4.15) and solved by MATLAB's ODE solver ode15s which implements the Numerical Differentiation Formulas (NDF) [78]. This formulation was abandoned because the ODE solvers do not allow to set the calculation time-step. Therefore, Equation (4.15) was linearized as follows:

$$\frac{M}{\Delta t} (T - T_0) = s - K\, T \quad (4.16)$$

where T_0 represents the temperature vector of length *nn* with the temperature values of the preceding time-step (initial network temperature at the beginning of the simulation). Equation (4.16) can then be rewritten in the classical form of a linear system ($A\, x = b$) as follows:

$$\left(K + \frac{M}{\Delta t}\right) T = \left(s + \frac{M}{\Delta t} T_0\right) \quad (4.17)$$

The linear system of Equation (4.17) can then be solved with Gauss-elimination methods. First, the mass matrix is zero at the inlet nodes to set the temperature at the system boundaries (Dirichlet condition); the missing mass is attributed to the adjacent nodes.

In the current model *NeMo*, the user can choose the resolution method for the transient heat propagation problem between the ODE solver and the linear system solver. However, the latter requires the user to set the internal calculation time-step Δt.

4.1.4 Modelling assumptions

Although the model would be able to deal with hundreds of consumers in a reasonable computation time, this was avoided by aggregating them based on a proximity criterion. Consequently, the number of substations was reduced from 247 to 65. This choice was made to facilitate both the pre-processing phase and the analysis of the simulation results without compromising their accuracy and by obtaining, on the other hand, shorter computation times. The heat demand and mass flow rate profiles of the single substations were simulated using the thermal load profiles measured at the supply stations and the users' annual energy bill for heating. The procedure to obtain the heat demand profiles of the 65 equivalent substations consisted of the following three steps:

1) An equivalent thermal load profile, equal to the sum of the three heat supply stations (CCC, CRV and CSD) minus the heat losses of the network, was calculated.

2) 65 normalized coefficients (the sum is equal to 1) in proportion to the customer's heat invoices belonging to the 65 equivalent substations were calculated.

3) The equivalent profile obtained in point 1 was divided among the 65 equivalent users using the coefficients calculated in point 2.

The heat losses in point 1 were evaluated using a constant value corresponding to the average of the considered week. The procedure described above smears the consumption of individual users evenly over time. In reality, users may or may not require heat due to the differences between technical systems (e.g. presence or absence of domestic hot water heat exchangers) or different user behaviour (e.g. constant set-point or night-time setback). The above procedure for creating heat demand profiles ignores this diversity between users. Reducing the number of users means that service pipes' number, length, and diameter need to be adapted. Table 4.1 shows the difference between the original data and the final model used in the study. It can be seen that the total length of the network was significantly reduced due to the lower number of service pipes.

Moreover, having more users connected to the same equivalent service pipe requires a higher mass flow rate and, therefore, a higher diameter to avoid excessive pressure drops. Thus, the model's pipe lengths were further decreased to have the same volume of water as the real network -approximately 700 m^3. This study assumes that all the heat produced by the three stations is supplied by station CCC. This choice was taken to better analyze the correlation

between mass flow rate and thermal load profile at the supply station, i.e. without "disturbance" due to mass flow rate injected from distant supply points.

Table 4.1 Topological difference between real and modelled network.

Parameter	Real network	Modelled network
Number of substations	247	65
Number of heat supply points	3	1
Total length [km]	22.6	16.3
Length of transmission pipes [km]	15.0	12.0
Length of service pipes [km]	7.6	4.3
Loops	11	11

4.2 Model of the buildings at district scale

Appropriate dynamic models are necessary both during the early design stages of buildings and when retrofitting solutions for existing ones are evaluated. On the other hand, in this particular situation, the dynamic model is necessary to evaluate the flexibility potential determined by the thermal capacitance of the buildings. Therefore, the geometric and energy modelling of two of the 16 monitored buildings was considered. These are respectively the School A and the Condominium I. To define the geometry was used the drawing software SketchUp, while for the energy analysis, was used EnergyPlus.

4.2.1 Dynamic model of a school

4.2.1.1 Geometric modelling and stratigraphy of a school

About School A, located in the historical centre of Verona, only the data related to the external plan, the number of floors, the overall height and the stratigraphy of the building was available. The structure is characterized by three floors, the surface occupied by the building is 1080 m^2 and the height is equal to 9.45 m^2. Regarding the geometric model, the intent was to make a model as realistic as possible to carry out an accurate energy analysis. So, it was necessary to know the school's internal planimetry. However, not having the internal distribution, it was considered that of another elementary school, i.e. the Leonardo da Vinci school at Gazzo (PD). This building has two floors, and the internal plan is shown in Figure 4.3.

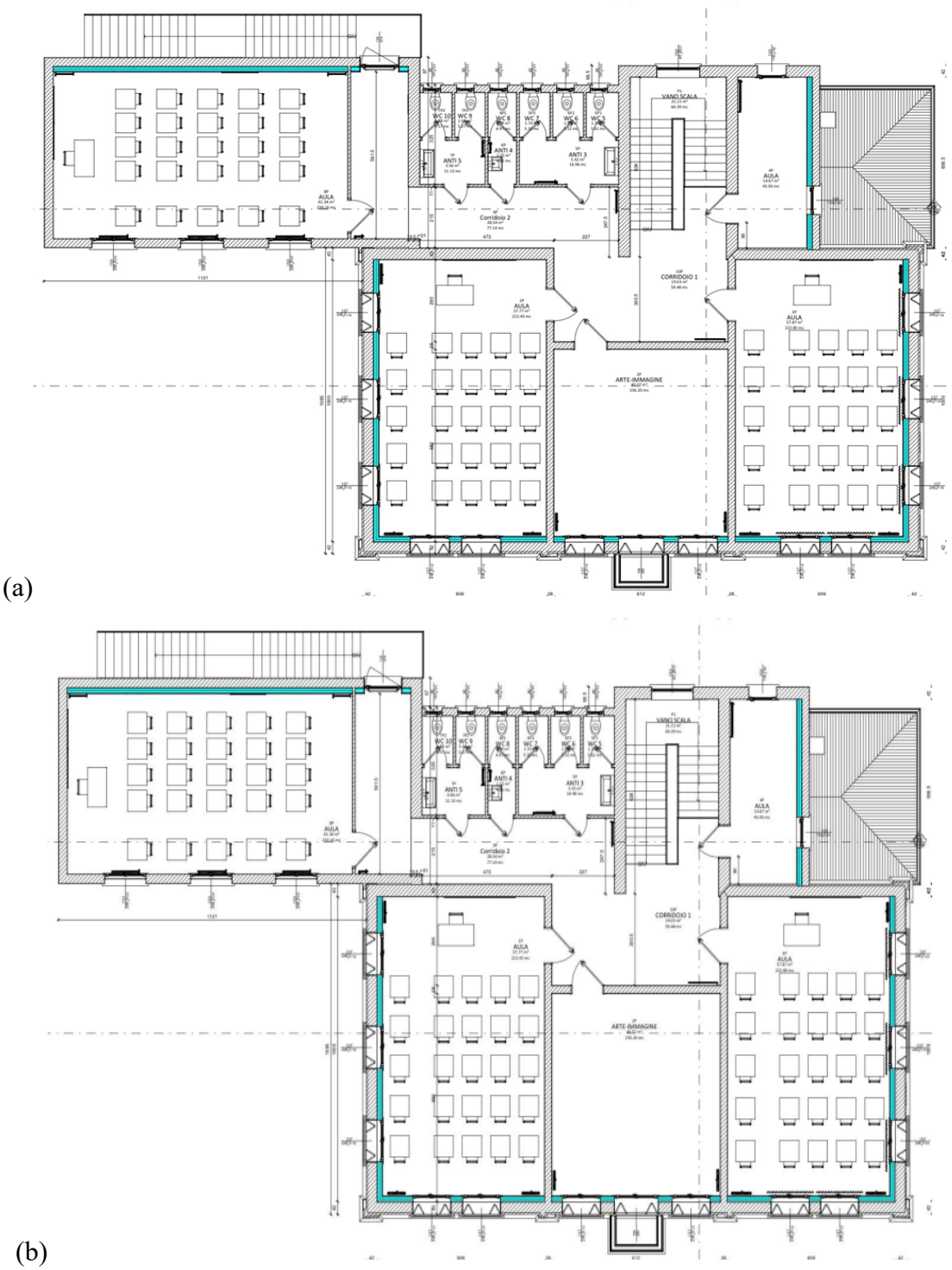

(a)

(b)

Figure 4.3 Reference planimetry of the school for the ground floor (a) and first floor (b).

The floor area of each indoor environment was reported and scaled based on the ratio between the total floor area of the reference school and the School A. This was done as long as the scaled surface did not prove to be too large for its use. In this case, it was decided to increase the number of rooms rather than the size. This method was applied to decide the size of the classrooms. In Table 4.2, the list of the internal rooms has been provided.

Table 4.2 List of rooms in the school building.

Ground floor	**First floor**	**Second floor**
Gym	Classroom 1 FF	Classroom 1 SF
Canteen	Classroom 2 FF	Classroom 2 SF
Closet	Classroom 3 FF	Classroom 3 SF
Bathroom GF	Classroom 4 FF	Lab 1
Hallway GF	Teachers' bathroom FF	Lab 2
Classroom 1 GF	Hallway FF	Hallway SF
Classroom 2 GF	Classroom 5 FF	Auditorium
Office GF	Classroom 6 FF	Classroom 4 SF
Teachers' bathroom GF	Classroom 7 FF	Bathroom SF
Teachers' room	Bathroom FF	Office SF
	Office FF	

As far as the glazed surface is concerned, it was decided to base the decision on the window/floor surface ratio. The size of individual windows and doors was determined by dividing that ratio by the number of total windows and doors identified by visually analyzing the building.

The adjustment of the internal reference distribution (Leonardo da Vinci school) in the building under consideration (School A) was carried out based on practical considerations, according to the regulations in force and based on the restrictions due to the external geometry of the school. The approximate nature of these choices will not substantially affect the thermal analysis's quality since the objective is not to analyse the thermal behaviour of this specific building but of this type of building, characterized by a certain thermal capacitance and subject to specific internal loads. In Figure 4.4 it is shown the result of geometric modelling on SketchUp .

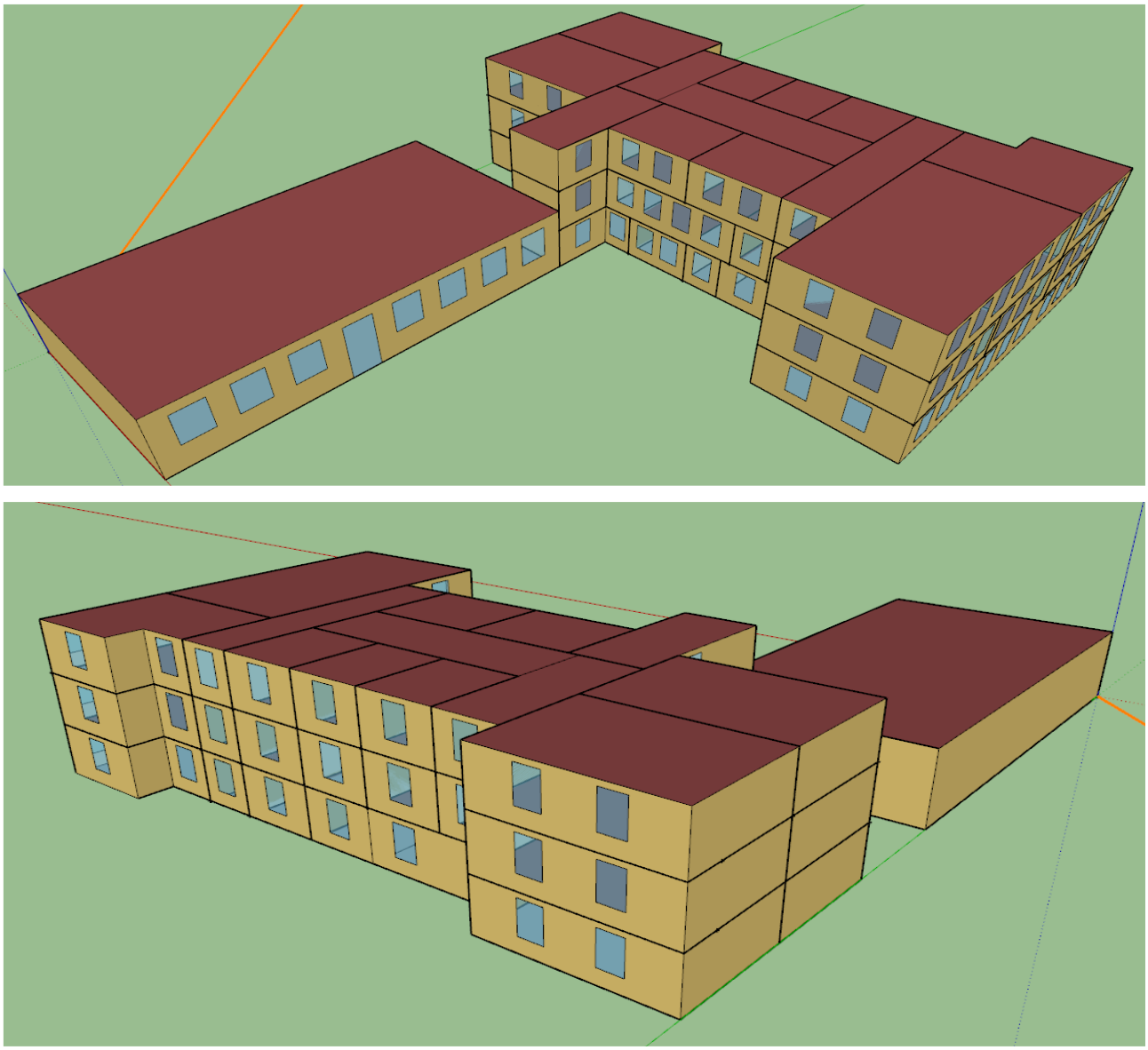

Figure 4.4 SketchUp geometric model of the School A.

Surrounding buildings and shading from them were not considered.

The knowledge of stratigraphy is fundamental to correctly evaluate the structure's dynamic behaviour from the thermal point of view. Therefore, all values have been reported in the following table.

Table 4.3 Stratigraphy of the school building structure.

Structures	Materials	Thickness [m]	Conductivity [W/(m K)]	Density [kg/m^3]	Specific heat [J/(kg K)]	Heat absorption
Wooden roof (no insulation)	Tiles	0.015	0.58	1800	840	0.9
	Wood	0.12	1.16	2000	670	0.7
Concrete slab	Gravel	0.3	1.2	1700	1000	0.7
	Screed	0.1	1.16	2000	670	0.7
	Cement mortar	0.02	1.4	2000	670	0.7
	Stoneware	0.015	1.47	1700	1000	0.7
Wooden beam ceiling	Stoneware	0.015	1.47	1700	1000	0.7
	Wood	0.06	0.18	710	2700	0.7
	Beams and dead spaces	0.2	1.11	1.2	1000	0.7
	Plywood	0.01	0.1	450	1000	0.7
	Plaster (internal)	0.02	0.7	1400	1000	0.9
Stonemasonry	Plaster (external)	0.02	0.9	1800	910	0.9
	Stone blocks	0.4	2.4	2500	1000	0.7
	Plaster (internal)	0.02	0.7	1400	1000	0.9
Hollow flat block and plaster	Plaster	0.015	0.7	1400	1010	0.7
	Hollow flat block	0.06	0.69	600	1000	0.7
	Plaster	0.015	0.7	1400	1010	0.7

In addition to the reference case, a retrofitted version was considered. It was decided to insulate the exterior walls and roof with a 15 cm layer of polystyrene with the characteristics summarized in Table 4.4. So, the transmittances of the different elements of the retrofitted and non-retrofitted structure are resumed in Table 4.5.

Table 4.4 Thermal characteristics of the insulating layer.

INSULATING LAYER	
Thickness [m]	0.15
Conductivity [W/(m K)]	0.04
Density [kg/m^3]	30
Specific heat [J/(kg K)]	1220
Heat absorption	0.7

Table 4.5 Total transmittances of the elements of the retrofitted and non-retrofitted structure.

RETROFITTED STRUCTURE	
Total transmittances [W/(m^2 K)]	
Insulated external wall	0.38
Interior wall	2.57
Exterior floor	2.77
Intermediate floor ceiling	1.1
Insulated roof	0.29

NON-RETROFITTED STRUCTURE	
Total transmittances [W/(m^2 K)]	
External wall	2.58
Interior wall	2.57
Exterior floor	2.77
Intermediate floor ceiling	1.1
Roof	3.34

For the calculation of the total transmittances of the structures, a convective heat transfer coefficient equal to 7.7 W/m^2 K was considered for the interior surface and of 25 W/m^2 K for the exterior one, as suggested by [39]. Finally, a transmittance of 5.7 W/m^2 K was considered for the windows, and their g-values were assumed equal to 0.82.

4.2.1.2 Thermal modelling of a school

Thermal modelling of the building requires dividing the building into thermal zones. A thermal zone can include several rooms, but from the point of view of the heating/air conditioning system is a single room to be maintained at the required temperature. Therefore, adjacent rooms subjected to similar internal and external thermal loads can be incorporated within the same thermal zone. However, in the case of schools, an accurate subdivision is preferable, as the rooms can be large and subject to very different uses, and therefore loads. This is why it was decided to consider a thermal zone for each room.

The detailed data of the internal loads of the structure were not available, so it was necessary to consider the EN 16798-1 standard to obtain an approximate profile of the internal loads and heating setpoint. These data were collected and summarized in daily schedules (Table 4.6). Note that the standard only provides specific data for classrooms.

Table 4.6 Schedules of internal loads and temperature setpoint, for weekdays (a) and weekends (b).

(a)	Weekday				
Load	**Classroom occupancy**	**Lighting**	**Infiltration**	**Ventilation**	**Set point**
Unit of measurement	[W/m²]	[W/m²]	[h^{-1}]	[h^{-1}]	[°C]
Nominal value	13.8	8	0.2	0.0038	-
1:00	0	0	1	0	16
2:00	0	0	1	0	16
3:00	0	0	1	0	16
4:00	0	0	1	0	16
5:00	0	0	1	0	16
6:00	0	0	1	0	16
7:00	0	0	1	0	16
8:00	0	0	1	0	21
9:00	0.6	0.6	1	1	21
10:00	0.7	0.7	1	1	21
11:00	0.6	0.6	1	1	21
12:00	0.4	0.4	1	1	21
13:00	0.3	0.3	1	1	21
14:00	0.7	0.7	1	1	21
15:00	0.6	0.6	1	1	21
16:00	0.4	0.4	1	1	21
17:00	0.2	0.2	1	1	16
18:00	0	0	1	0	16
19:00	0	0	1	0	16
20:00	0	0	1	0	16
21:00	0	0	1	0	16
22:00	0	0	1	0	16
23:00	0	0	1	0	16
0:00	0	0	1	0	16

(b)	Weekends				
Load	**Classroom occupancy**	**Lighting**	**Infiltration**	**Ventilation**	**Set point**
Unit of measurement	[W/m²]	[W/m²]	[h^{-1}]	[h^{-1}]	[°C]
Nominal value	13.8	8	0.2	0.0038	-
1:00	0	0	1	0	16
2:00	0	0	1	0	16
3:00	0	0	1	0	16
4:00	0	0	1	0	16
5:00	0	0	1	0	16
6:00	0	0	1	0	16
7:00	0	0	1	0	16
8:00	0	0	1	0	16
9:00	0	0	1	0	16
10:00	0	0	1	0	16
11:00	0	0	1	0	16
12:00	0	0	1	0	16
13:00	0	0	1	0	16
14:00	0	0	1	0	16
15:00	0	0	1	0	16
16:00	0	0	1	0	16
17:00	0	0	1	0	16
18:00	0	0	1	0	16
19:00	0	0	1	0	16
20:00	0	0	1	0	16
21:00	0	0	1	0	16
22:00	0	0	1	0	16
23:00	0	0	1	0	16
0:00	0	0	1	0	16

The setpoint schedule shown in Table 4.6 for weekdays is not that suggested by the standard for school buildings, but it is a modified version based on the results obtained during the simulations. In fact, with the standard schedule, the internal temperature around 8 am was not sufficient to ensure the minimum comfort required. Furthermore, the maximum temperature suggested of 20 °C was insufficient because an ancient structure is always very disadvantageous for the operative temperature (temperature related to the perception of comfort). Therefore, it was decided to raise the maximum temperature by 1°C and to anticipate the setpoint increase by one hour. This allowed lower discomfort values. The occupation schedules in Table 4.6 were considered only for the classrooms. The other rooms were assumed to be almost empty all the time or with a negligible presence of people. An

exception was the gym, for which a sensible thermal load of 188 W/person was considered due to physical activity. Instead, for the canteen, a schedule that foresees the presence of people from 12 noon to 2 p.m. was adopted, assuming a nominal value of sensitive load equal to 80 W/person, due to the thermal emission of the serving dishes.
Regarding the ventilation of rooms other than classrooms, the UNI 10339 [79] and the UNI 16798-1 [80] were taken as reference. The reference schedules adopted were the same as for classrooms. Only the nominal value changed. All values are summarized in Table 4.7.

Table 4.7 Nominal values of ventilation by room type.

Nominal value		
Auditorium	0.01	m^3/s person
Bathroom	8	1/h
Hallway	0.000254	m^3/s
Laboratory	0.11	m^3/s
Canteen	0.65	m^3/s
Gym	1.32	m^3/s
Office	0.006	m^3/s

The schedules already implemented in the OpenStudio environment for small offices, obtained from AHSRAE Standar 90.1 [81], were used. They are summarized in Table 4.8 for weekdays.

Table 4.8 Schedules of the internal loads in the offices.

	Weekday		
Load	**Occupancy (Sensitive)**	**Lighting**	**Devices**
Unit of measurement	[W/person]	[W/m²]	[W/m²]
Nominal value	132	10.6	7
1:00	0	0.05	0.4
2:00	0	0.05	0.4
3:00	0	0.05	0.4
4:00	0	0.05	0.4
5:00	0	0.05	0.4
6:00	0	0.1	0.4
7:00	0.1	0.1	0.4
8:00	0.2	0.3	0.4
9:00	0.85	0.9	0.9
10:00	0.85	0.9	0.9
11:00	0.85	0.9	0.9
12:00	0.85	0.9	0.9
13:00	0.5	0.9	0.8

14:00	0.85	0.9	0.9
15:00	0.85	0.9	0.9
16:00	0.85	0.9	0.9
17:00	0.85	0.9	0.9
18:00	0.7	0.7	0.8
19:00	0.4	0.5	0.6
20:00	0.4	0.5	0.6
21:00	0.1	0.3	0.5
22:00	0.1	0.3	0.5
23:00	0.05	0.1	0.4
0:00	0.05	0.05	0.4

For simulation purposes, it was necessary to carry out a basic dimensioning of the heating system of the building. It was decided not to define a specific heating system but to use a specific tool of EnergyPlus called "Ideal Load Air System", which was set for each thermal zone. It was used the software itself to calculate the design power required by each thermal zone during the coldest day of the winter season since it was not possible to use the Standards. Furthermore, as the demand profile varies over time, it was decided not to use the peak values measured during the setpoint increase from 18 to 21 °C, but to consider the thermal power values required two hours after the increase. In this way, it was avoided to oversize the system. The design loads obtained have been summarised in Table 4.9.

Table 4.9 Design power of school building thermal zones.

Ground floor	**Design power [kW]**	**First floor**	**Design power [kW]**	**Second floor**	**Design power [kW]**
Gym	82.4	Classroom 1 FF	2.7	Classroom 1 SF	3.3
Canteen	39.6	Classroom 2 FF	2.7	Classroom 2 SF	3.2
Closet	3.3	Classroom 3 FF	2.0	Classroom 3 SF	2.4
Bathroom GF	8.5	Classroom 4 FF	2.5	Lab 1	7.2
Hallway GF	8.8	Teachers' bathroom FF	5.1	Lab 2	7.2
Classroom 1 GF	2.4	Hallway FF	8.7	Hallway SF	10.2
Classroom 2 GF	2.4	Classroom 5 FF	3.0	Auditorium	5.9
Office GF	3.5	Classroom 6 FF	2.7	Classroom 4 SF	3.3
Teachers' bathroom GF	4.9	Classroom 7 FF	2.8	Bathroom SF	8.9
Teachers' room	4.8	Bathroom FF	8.7	Office SF	4.6
		Office FF	3.8		

4.2.2 Energy plus models of a residential building

4.2.2.1 Geometric modelling and stratigraphy of a residential building

The second case study consists of a large residential building, Condominium I, built in the '70s. The area occupied by the building is 291 m^2 and its height equal to 18.9 m^2. Six floors characterize the structure, and the number of internal apartments is 12, two for each floor. The internal distribution of the apartments was not available, so the planimetry of another residential building (shown in Figure 4.5) was adopted as a reference. Two apartments characterise the latter for each floor, divided by a hallway and a stairwell. The apartments on each floor are equal and mirrored.

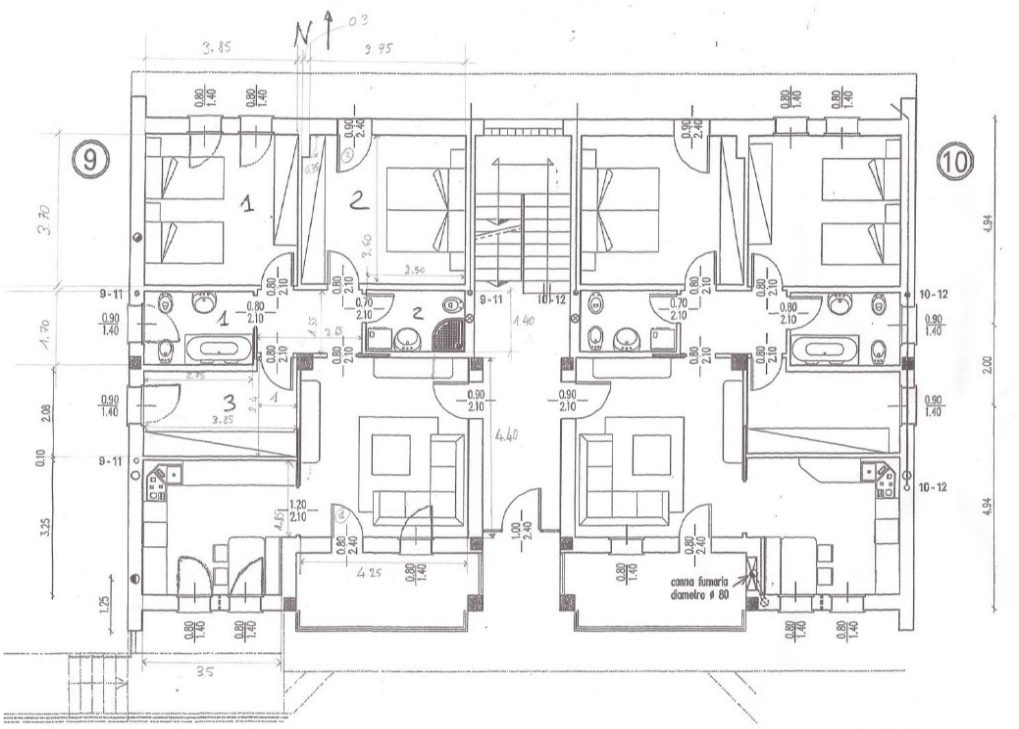

Figure 4.5 Ground floor planimetry of the reference residential building.

The reference apartment was adapted to Condominium I by scaling the surfaces according to the ratio between the total base areas of the two buildings. The distribution of the window surfaces has been determined, finding a balance between the real distribution, the distribution in the reference case and the window/floor surface ratio. The dimensions of the window frames are the same as in the reference case. Glass doors have not been considered as they are not present in the real case, except in the stairwell on the ground floor. As shown in Figure 4.5, in the reference apartment, there is a gap between the kitchen and the living room in correspondence with the veranda. Since this gap is not present in the Condominium

I, the veranda was included in the living room. Moreover, the apartments on the north side are slightly smaller than those on the opposite side due to the lack of symmetry in the real building along the S-N axis. So, the two apartments measure a gross floor of respectively 126.9 m² and 139 m². By considering a height of 2.70 metres for each room (a standard measure in line with the overall height of the building), the result in Figure 4.6 was obtained using SketchUp.

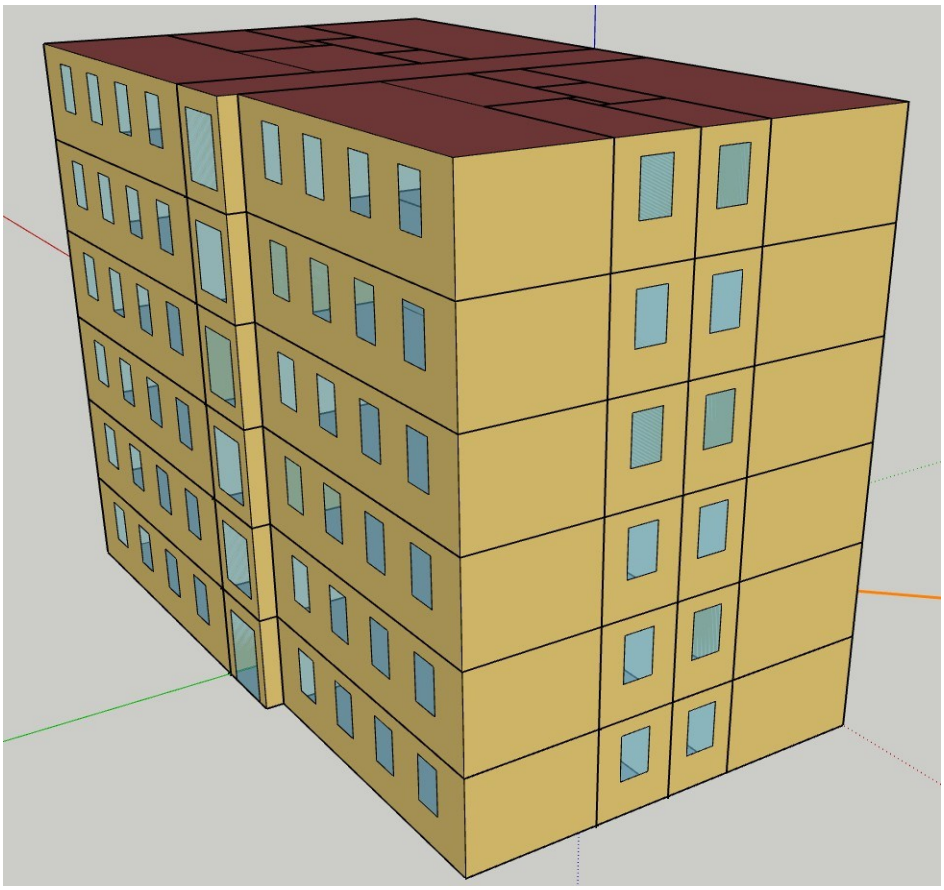

Figure 4.6 Geometric modelling of the Condominium I with SketchUp.

The data concerning the stratigraphy are reported in the following tables.

Table 4.10 Stratigraphy of the Condominium I structure.

Type of stucture	Structures	Materials	Thickness [m]	Conductivity [W/(m K)]	Density [kg/m^3]	Specific heat [J/(kg K)]	Heat absorption
ROOF	Concrete slab, traditional screed	Waterproof coating	0.01	0.17	1200	1000	0.8
		Cement screed	0.12	1.16	2000	670	0.7
		Cement mortar	0.03	1.4	2000	1000	0.7
		Reinforced concrete	0.04	1.4	2400	1000	0.7
		Steel beams and hollow bricks	0.16	0.48	900	1000	0.7
		Plaster	0.02	0.7	1400	1000	0.9
OUTWARD-FACING FLOOR	Reinforced concrete slab, traditional screed	Gravel	0.3	1.2	1700	1000	0.7
		Screed	0.1	1.16	2000	670	0.7
		Beams and dead spaces	0.2	1.11	1.2	1000	0.7
		Stoneware	0.015	1.47	1700	1000	0.7
INTERIOR CEILING	Concrete slab - lightweight screed	Stoneware	0.015	1.47	1700	1000	0.7
		Cement mortar	0.02	1.4	2000	1000	0.7
		Lightweight cement screed	0.06	0.58	900	1000	0.7
		Cement mortar	0.02	1.4	2000	1000	0.7
		Concrete and hollow brick	0.16	0.49	900	1000	0.7
		Plaster (internal)	0.02	0.9	1800	910	0.9
EXTERNAL WALLS	Hollow brick masonry	Plaster (external)	0.02	0.9	1800	910	0.9
		Hollow bricks	0.12	0.39	800	1000	0.7
		Air gap (6 cm)	0.06	0.33	1.2	1005	0.7
		Hollow bricks	0.12	0.39	800	1000	0.7
		Plaster (internal)	0.02	0.7	1400	1000	0.9
INTERNAL WALLS	Hollow flat block and plaster	Plaster	0.015	0.7	1400	1010	0.7
		Hollow flat block	0.06	0.69	600	1000	0.7
		Plaster	0.015	0.7	1400	1010	0.7

Also in this case, it was considered a retrofitted version of the structure, insulating the walls and replacing the windows and doors. It was decided to use a 10 cm layer of polystyrene for the thermal insulation. The characteristics are summarised in Table 4.11.

Table 4.11 Thermal characteristics of the insulation layer.

INSULATING LAYER	
Thickness [m]	0.10
Conductivity [W/(m K)]	0.045
Density [kg/m^3]	30
Specific heat [J/(kg K)]	1220
Heat absorption	0.7

For the calculation of the total transmittances of the structures, the values 7.7 W/m^2 K and 25 W/m^2 K were considered as convective heat transfer coefficients for the internal and external surfaces, respectively. Table 4.12 lists the transmittances of the envelope elements.

Finally, a transmittance of 4.9 W/m^2 K was considered for the windows, and their g-values were assumed equal to 0.82.

Table 4.12 Transmittances of the elements of the retrofitted and no retrofitted structure.

RETROFITTED STRUCTURE	
Total transmittances [W/(m^2 K)]	
Insulated external wall	0.31
Interior wall	2.57
Exterior floor	0.5
Intermediate floor ceiling	1.33
Insulated roof	0.34

NON-RETROFITTED STRUCTURE	
Total transmittances [W/(m^2 K)]	
External wall	0.98
Interior wall	2.57
Exterior floor	0.50
Intermediate floor ceiling	1.33
Roof	1.34

4.2.2.2 Thermal modelling of a residential building

Usually, the residential buildings are divided into living and sleeping areas to make it easier to analyse and control the system. Further increasing the subdivision is useless because it determines a higher complexity of the simulation, but it does not significantly increase the overall accuracy. Within the living area, the following rooms have been grouped: kitchen, living room, bathroom 1 and 2, room, hallway. While in the sleeping area, the bedrooms were considered. This subdivision was applied to each building apartment (Figure 4.7). The stairwell was not considered within any thermal zone as it is an unheated room.

Figure 4.7 Distribution of thermal zones for the apartments.

The internal loads of the structure are not available in detail, so EN 16798-1 was used to obtain an approximate but reliable profile of the internal loads. Table 4.13 lists the load types

with their nominal values and daily schedules, valid for weekdays and weekends. The infiltrations totally provided the ventilation.

Table 4.13 Schedules of the residential building internal loads.

Load	**Occupancy weekdays**	**Occupancy weekend**	**Appliances**	**Lighting**	**Infiltration**
Unit of measurement	[W/m²]	[W/m²]	[W/m²]	[W/m²]	[h^{-1}]
Nominal value	2.8	2.8	3	3	0.2
1:00	1	1	0.5	0	1
2:00	1	1	0.5	0	1
3:00	1	1	0.5	0	1
4:00	1	1	0.5	0	1
5:00	1	1	0.5	0	1
6:00	1	1	0.5	0	1
7:00	0.5	0.8	0.5	0.15	1
8:00	0.5	0.8	0.7	0.15	1
9:00	0.5	0.8	0.7	0.15	1
10:00	0.1	0.8	0.5	0.15	1
11:00	0.1	0.8	0.5	0.05	1
12:00	0.1	0.8	0.6	0.05	1
13:00	0.1	0.8	0.6	0.05	1
14:00	0.2	0.8	0.6	0.05	1
15:00	0.2	0.8	0.6	0.05	1
16:00	0.2	0.8	0.5	0.05	1
17:00	0.5	0.8	0.5	0.2	1
18:00	0.5	0.8	0.7	0.2	1
19:00	0.5	0.8	0.7	0.2	1
20:00	0.8	0.8	0.8	0.2	1
21:00	0.8	0.8	0.8	0.2	1
22:00	0.8	0.8	0.8	0.2	1
23:00	1	1	0.6	0.15	1
0:00	1	1	0.6	0.15	1

Regarding the indoor temperature setpoint, the standard provides a fixed setpoint of 20 °C for the whole day and year. However, a constant value is not interesting for analysing the dynamic behaviour of the building. Therefore, it was decided to consider a setpoint of 21 °C from 6 am to 10 pm and 18 °C from 10 pm to 6 am.

The EN 12831-1 Standard was considered to calculate the design power of the heating system. This provides a simplified method for the calculation. Since the analysed case is a residential building, it was decided to calculate three types of apartments: ground floor, intermediate floor, and top floor. Those on the ground floor and, in particular, the top floor

are the most disadvantaged ones, as they are directly exposed to the outside air or the ground. In contrast, those at the intermediate floors are adjacent above and below to heated flats. There was also the problem of the different surface areas of the apartments. The largest ones (139 m2) were considered a reference to avoid underestimating transmission losses.
In addition, to the design power calculated using the simplified method, the heating power for the intermittent operation was considered. The heating-up power is the design power that allows a building to be heated in a short period after the system has been switched off for a long period. Therefore, assumptions had to be made to calculate it, considering 2 hours for the recovery time and 3K for the temperature drop due to inactivity. The calculated design powers are summarised in the following tables for reference (Q ref) and retrofitted (Q ret) cases.

Table 4.14 Design power for the different apartments in the residential building with heating-up power.

	With heating-up power	
	Q ret (kW)	**Q ref (kW)**
Ground floor	6.4	8.7
Top floor	7	12.7
Intermediate floor	5.8	8

The total installed power for the whole building is 61.2 kW in the retrofitted case and 107.6 kW in the reference one.

Table 4.15 Design power for the different apartments in the residential building without heating-up power.

	Without heating-up power	
	Q req (kW)	**Q ref (kW)**
Ground floor	2.9	5.2
Top floor	3.5	9.2
Intermediate floor	2.3	4.6

In this case, the total installed power for the whole building is 26.4 kW in the retrofitted version and 72.6 kW in the reference one. In particular, the latter value is very close to the nominal power of the heat exchanger installed at the user's substation (77 kW).

CHAPTER 5 ANALYSIS OF LOAD SHIFTING STRATEGIES

5.1 Exploiting the thermal capacitance of the heat carrier fluid

The thermal capacitance of the heat carrier fluid enclosed in the network pipelines can be used to decouple the thermal load profile at the supply station from the heat demand of the users. This solution becomes particularly important when space constraints prevent the installation of large size hot water tanks. However, the network itself is different from a traditional heat storage system in that (i) the storage system is not separated from the supply and return pipelines (ii) the fluid inside the DHN performs two functions simultaneously: to transfer and accumulate heat. The higher the flow rate and the average velocity of the transfer fluid, the faster these phenomena occur. So, it was necessary to assess the district heating network's thermal behaviour through simulations performed with a model. The considered tool was NeMo.

5.1.1 Method

Since the supply temperature is kept constant in Verona DHN, the only way to charge/discharge the network is to increase/decrease the mass flow rate to increase/decrease the water temperature in the return pipe. So, the present analysis's approach consisted of simulating the thermal and hydraulic behaviour using NeMo with current and modified flow profiles. First, the same heat demand profiles at the users' substations were imposed. Then, the resulting thermal profiles at the main supply station (CCC) were compared to the reference ones using the indicators listed in Section 5.1.1.2. To summarize, the mass flow rate must increase or decrease compared to the current pumping strategy to charge or discharge the network. The profile differences are described using five dimensionless parameters shown in Figure 5.1.

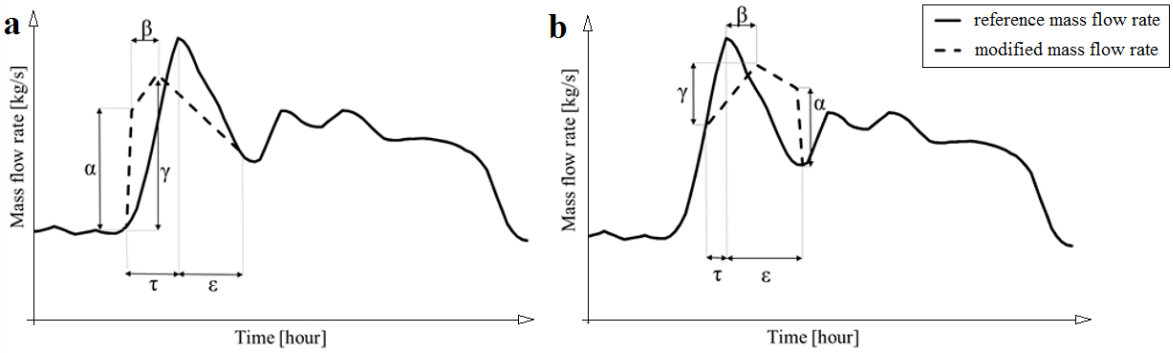

Figure 5.1 Parameters used to change the mass flow rate for the network (a) pre-charge and (b) post-charge.

Parameter τ indicates how many hours in advance the mass flow rate must be adjusted with respect to the peak load to produce the desired change in the thermal load pattern at the central station (CCC). Parameter ε defines the number of hours after the predicted peak load at which the mass flow rate adjustment ends. Thus, τ and ε define the time interval when the mass flow profile deviates from the reference one. In the current mass flow control, the time with the maximum mass flow coincides with the peak load request at the central station. Parameter β identifies the time instant in which the flow peak of the modified flow profile is reached; it varies between 0.1 and 1 and indicates respectively whether the peak is immediately after the start of adjustment or whether it coincides with the peak load as in the reference profile. Parameter α identifies the flow rate value at the start of regulation; this value is chosen between the flow rate value of the reference profile at the time detected by τ (α = 0) and the peak value of the reference profile (α = 1). The last parameter, γ, establishes the maximum mass flow rate value. As a result, α, β and γ, determine the shape of the mass flow profile, so they can be defined shape parameters. To limit the number of simulations and at the same time to have mass flow rate profiles with different shapes, three combinations of the parameters α, β and γ were chosen, as shown in Table 5.1. As far as the pre-charge process is concerned, the sensitivity analysis included three shape parameters combinations (C1, C2, C3) with four values of parameter τ: 1.5, 2.5, 3.5 and 4.5 hours. For all 24 simulations carried out (12 for February and 12 for April), the parameter ε was constant and equal to 3 hours. The same approach was adopted for the post-charge process, where τ was set to 1 hour and other 24 simulations arose from the combination of C4, C5, C6 parameters with four values of ε (1.5, 2.5, 3.5 and 4.5 hours). Therefore, the analysis included

48 simulations with modified mass flow rate and two reference simulations (one per reference week) with the existing pump head control strategy.

Table 5.1 The three considered combinations of parameters α, β and γ.

Thermal load	Combination	α [-]	β [-]	γ [-]
Pre-charge	C1	0.2	0.5	0.8
	C2	0.1	0.1	0.9
	C3	0.7	0.5	0.7
Post-charge	C4	0.4	0.4	0.5
	C5	0.8	0.4	0.4
	C6	0.4	0.1	0.3

5.1.1.1 Simulation assumptions

As suggested by van der Hejide et al. [82], it is possible to consider typical days which adequately represent the district heating behaviour for the entire year. Consequently, two representative weeks were chosen to study the load shifting strategies:

- A cold winter week, from February 27th to March 5th. The thermal load ranges between 7 and 30 MW_t, and an average value of 14.15 MWt characterizes i_t. It is supplied by the cogeneration plants, which run almost always under full-load, the heat pumps, the heat recovered from the foundry, and the gas boilers, which supply the remaining part of the thermal load;
- A week during the middle season, from the 24th to 30th of April, in which the thermal load ranges from 2.5 to 10 MW_t and its average value is equal to 4.8 MW_t. The heat demand is provided by a single CHP (2.2 MW_t) always at full load, the heat pump connected to the operating CHP, the waste heat, and the gas boilers.

The undisturbed ground temperature T_g in Verona at a depth of 1 meter was considered equal to 3°C in February and 13°C in April, considering the seasonal effect of the location.

5.1.1.2 Key Performance Indicators

As already mentioned, the objective of this analysis is to shift the heat supply over time and not to save energy directly. The results were analysed using six indicators. The first three of them can be considered as Key Performance Indicators (KPI) because they quantify the

impact of the control strategy in terms of peak shaving, peak shifting, and amount of energy shifted.

The indicator Δq_{max} indicates the damping of the thermal peak load at the power plant with the modified pumping strategy, while $\Delta t_{q_{max}}$ indicates the phase shift of the peak compared to the reference one. Negative values indicate anticipation of the peak, while positive values indicate a delay in the phase shift compared to the reference case.

$$\Delta q_{max} = \frac{q_{max,ref} - q_{max,mod}}{q_{max,ref}} \tag{5.1}$$

$$\Delta t_{q_{max}} = t_{max,mod} - t_{max,ref} \tag{5.2}$$

In addition to lowering the peak, an important objective for the district heating operators is to shift the thermal load over time. This flexibility could make it possible to sell electricity produced by CHP units or consume the electricity required by heat pumps at times with higher or lower electricity prices. Therefore, the proposed control strategy could help district heating operators become more economically competitive. The amount of thermal energy shifted with the flow adjustment strategy is the *available network capacity* (C_{net}) calculated as follows:

$$C_{net} = \int_{t_0}^{t_1} \left(q_{mod} - q_{ref}\right) dt \tag{5.3}$$

where t_0 is the time when the mass flow regulation starts and t_1 is the time instant when $q_{mod} = q_{ref}$. The available network capacity C_{net} is positive when the network is pre-charged to anticipate the thermal load and negative during post-charge events to postpone the thermal load.

Three other indicators were defined to determine the impact of this regulation on the operation of the network in relation to the current situation.

A discomfort indicator was used to assess whether the control method applied to the district heating network could lead to local discomfort to the users. The latter was considered to be approximately proportional to the drop of the return temperatures in each substation for the entire duration of the flow adjustment strategy, as the thermal behaviour of the buildings was not considered. In fact, a lower return temperature due to the limited mass flow rate could result in longer warm-up times inside buildings before the indoor air temperature setpoint is reached.

This index was calculated in relative terms (PD_{rel}), by evaluating the lowering of the temperature compared to that of the reference simulation. Thus, the following equation holds true:

$$PD_{rel} = \begin{cases} \int_0^{168} \left(T_{r,ref} - T_{r,mod}\right) dt, & T_{r,ref} > T_{r,mod} \\ 0 & T_{r,ref} \leq T_{r,mod} \end{cases} \quad (5.4)$$

The discomfort index was given a central role in this analysis because the district heating utility must always guarantee a quality of service to its customers. Then, the other two indicators measure if the flexibility brought by the modified control strategy leads to higher energy consumption. The first indicator indicates the variation of thermal energy supplied by the plant compared to the reference simulation:

$$\Delta Q_t = \frac{Q_{t,mod} - Q_{t,ref}}{Q_{t,ref}} \quad (5.5)$$

Similarly, the second indicator ΔW_{el} measures the variation in electrical energy required for pumping compared to the reference case:

$$\Delta W_{el} = \frac{W_{el,mod} - W_{el,ref}}{W_{el,ref}} \quad (5.6)$$

5.1.1.3 Practical measures for method implementation

From a practical point of view, the district heating operator cannot directly set the mass flow rate circulating in the network, which depends on the opening degree of the valves in the user's substations. The greater the demand for thermal power by the user substations, the greater the opening of the valves and, therefore, the total flow rate circulating. The operator must guarantee a minimum pressure difference on all customers' substations. In this way, the circulating mass flow rate is guaranteed for all consumers even when the maximum pressure drop along the network occurs, i.e. when all substations require high mass flow rates. A possible solution to adjust the circulating mass flow rate in the network consists of installing some bypasses between the supply and return lines. The district heating network operator may perform daily planning of the flow rate based on heat load forecasts. Then, the desired change compared to the current situation would be achieved by a proportional opening of the bypass valves when the mass flow rate must be increased and by a proportional decrease of the pump head when the mass flow rate must be reduced. Therefore,

another set of simulations was carried out to show how the number and position of the bypasses affect the thermal profile in the plant compared to the one obtained by distributing flow variations evenly across all the user substations. Four layout configurations were examined, as summarized in Figure 5.2. This set of simulations included only the network pre-charge process with the combination C1 and τ = 3.5 hours in both representative weeks.

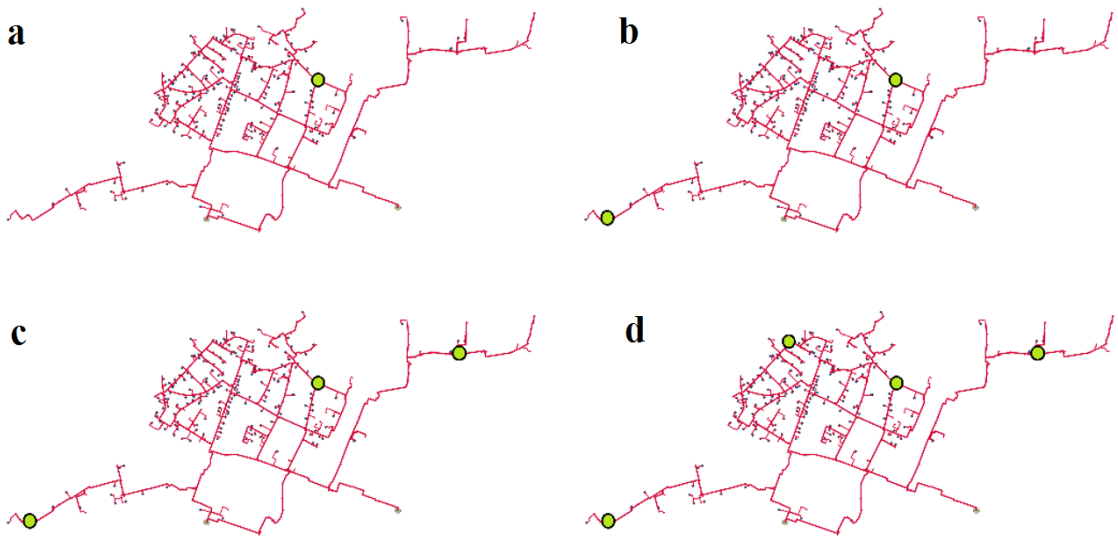

Figure 5.2 Position of the bypasses in the selected layouts: (a) BP1, (b) BP2, (c) BP3, (d) BP4.

Moreover, the operator should consider the thermal expansion involved in the injection of a water flow at 75-80°C into the return network. Indeed, this thermal transient may result in a local temperature rise of about 25-30°C in the piping close to the bypass. Therefore, appropriate expansion joints (where not already present) should be installed to prevent damage due to the pipes' elongation. In the case of networks with multiple suppliers, the third-party suppliers should communicate the heat production forecasts to the DHN manager. This way, the latter will set the bypass valves openings according to the total circulating mass flow (including that injected by third party suppliers). There are three supply stations in the considered case study: two managed by the DHN operator and one (CRV) by a third-party supplier.

5.1.2 Results

This section shows how a change in the mass flow rate profile brings to a variation in the thermal load profile at the heat supply station. Here, the effects of the parameters that characterize the mass flow rate profile are separately analysed in both pre-charge and post-charge mode. In this first set of simulations, the surplus/deficit of mass flow rate was evenly distributed among all customer substations. Finally, in Section 5.1.2.4, a subset of simulations was conducted to evaluate how the results change by concentrating the flow rate injection through a limited number of bypasses. Additional results derived from the implementation of the proposed method with regard to primary energy-saving potential and cost-saving potential can be found in [20] and [45], respectively.

5.1.2.1 Pre-charge of the network

As explained in Section 5.1.1, the combination of the parameters α, β, γ indicates the shape of the modified mass flow profile. Figure 7 shows the different power profiles obtained by varying τ (from 1.5 to 4.5 hours), for a given combination (C1), on Tuesdays in the April reference week. As it can be seen, the power peak of the reference profile was replaced by two smaller peaks: one earlier and one later than the initial peak. The two peaks represent (i) the effect of the change in mass flow rate and (ii) the reference thermal load profile. The energy supplied to the users was the same, so the variation in mass flow rate resulted in a variation of the average temperature difference between supply and return pipes. Since the temperature difference in the supply station did not decrease at the same speed at which the mass flow rate was increased, thermal energy accumulated in the network, and the peak occurred in advance. Then, the temperature difference at the supply station did not increase quickly enough to face the decrease in the mass flow rate introduced during the power peak of the reference case. As a result, an early peak occurred, followed by a valley and by a delayed peak. These variations occur all the more rapidly, the higher the speed of the heat carrier fluid in the pipelines. The thermal behaviour is very different depending on the season considered: during the coldest months, the average speed of the fluid is much higher than in the mild months. Depending on a number of factors, including the combination of parameters chosen, the average fluid velocity in the network and the original thermal load profile, one of the two peaks prevails. The greater between the two peaks was considered to define the

peak shifting and the peak shaving indicators. Figure 5.3 shows that an increased peak shaving goes together with an increased peak shifting for both delayed and anticipated peaks. Therefore, the best peak shaving values Δq_{max} correspond to the highest phase shifts Δt_{max} of the modified power peak.

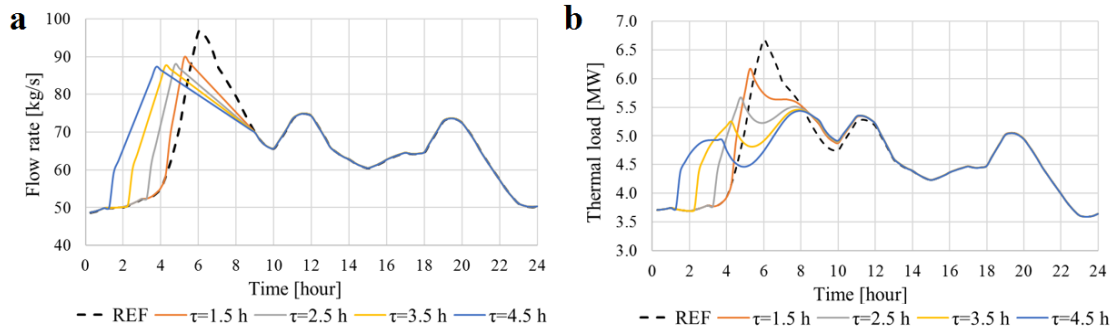

Figure 5.3 Thermal load profiles obtained by varying τ on Tuesday, April week.

Table 5.2 shows that considering combination C1, the key performance indicators (peak shaving Δq_{max}, peak shifting Δt_{max}, available network capacity C_{net}) and discomfort index PD_{rel} progressively increase when τ increases from 1.5 to 4.5 hours. The same holds true for combinations C2 and C3. The results were analysed day by day because the daily thermal load profile sometimes leads to daily deviations from the trends observed weekly. In Table 5.2, for each simulation of both representative weeks, two typical days were chosen: a working day (Tuesday) and a weekend day (Sunday). The peak load reduction (Δq_{max}) shows a limited increase in February during both Tuesday (approximately from 7.5% to 8.7%) and Sunday (from 11.8% to 12.8%) and a significant increase in April: from 7.6% to 18.5% on Tuesday and from 2.0% to 17.0% on Sunday.

Furthermore, Table 5.2 shows that the peak is always delayed in February, whereas in April, the peak is anticipated below a certain τ and delayed for higher values (higher than 3 hours on Tuesday and higher than 4 hours on Sunday). In general, greater sensitivity of the results to the variation of τ emerged in the week of April compared to the week of February. This depends on the lower speed of the heat carrier fluid, which slows down the propagation of heat through the network. In addition, the increase of τ involved an increase of the thermal energy stored in the network during the pre-charge process: C_{net} increased from 1.4 MWh to 7.5 MWh in February and from 0.1 MWh to 2.8 MWh in April. Improving the performance indicators by anticipating the start of the modified control strategy led to higher thermal discomfort indexes. During winter time, when the heat demand of the users is high,

more heat can be stored in the network before the peak hours. However, the thermal discomfort index was 2 to 4 times bigger than in the reference week of April.

Concerning the energy-related indicators, the thermal energy needs ΔQ_t increases from 0.36 MWh (equal to 0.09% of the daily reference thermal energy supplied) to 1.17 MWh (0.33% of the daily reference thermal energy) in February's representative week, whereas in April, the increase is limited to 0.21 MWh (0.19% daily). The difference in electrical energy needs for pumping between the mass flow adjustment strategy and the reference case shows more consistent variations: ΔW_{el} ranges from -0.18 MWh (-9%) to 0.10 MWh (+6.7%) during February, whereas the increase is almost negligible in April.

Table 5.2 Effect of τ on key performance indicators, considering combination C1.

Week	$q_{max,ref}$ [MW]		τ [h]	Δq_{max} [%]		Δt_{max} [h]		C_{net} [MWh]		PD_{rel} [°C h]	
	TUE	SUN		TUE	SUN	TUE	SUN	TUE	SUN	TUE	SUN
FEB	25.71	20.64	1.5	7.5	11.8	0.50	1.00	1.36	2.06	10	12
			2.5	8.5	12.4	0.75	1.00	3.25	4.56	14	14
			3.5	8.7	12.8	0.75	1.25	6.06	5.63	16	15
			4.5	8.7	12.8	0.75	1.25	7.46	6.98	17	15
APR	6.67	6.69	1.5	7.6	2.0	-0.75	-0.50	0.08	0.08	4	3
			2.5	14.9	6.9	-1.25	-1.00	1.48	0.45	5	6
			3.5	18.2	13.3	1.75	-1.50	2.24	1.39	5	7
			4.5	18.4	17.0	2.00	1.25	2.80	2.31	5	7

Table 5.3 shows the effect of the chosen shape combinations (C1, C2 and C3) on the performance indicators for a given τ the intermediate value of 2.5 hours was chosen. Figure 5.4(a) and (b) show the different profiles of the modified mass flow rate and how they affect the thermal load profile. When the network was pre-charged, the peak occurred earlier than the reference one, for all the considered combinations in April. In February, the peak was always delayed except for Sunday with the combination C2, i.e. when the thermal load was low, and the flow rate increased sharply. Together, these two conditions led the first power peak to exceed the second, as shown in Figure 5.4(b). In April, the same condition resulted in an increase of the thermal peak load of the network of approximately +3% compared to the reference control strategy. This indicates that the day of the week also greatly influences the results. This is particularly evident in the difference between the damping of the thermal peak load (Δq_{max}) on Tuesday and on Sunday in April representative week. The comparison between the different combinations showed that C1 was the best choice to damp the daily

power peak. In contrast, the combinations C2 and C3 made it possible to obtain a marked translation before the reference power peak.

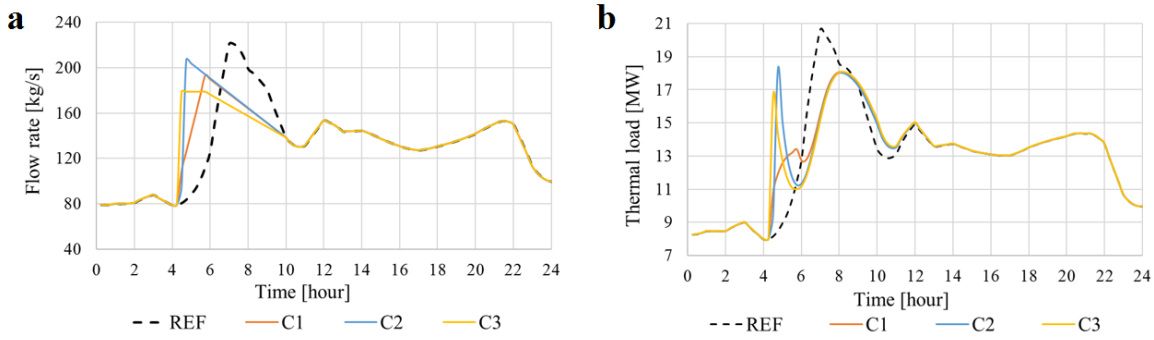

Figure 5.4 Different shapes of the modified (a) flow rate and (b) power profiles associated to the combinations C1, C2, C3 for Sunday, week of February.

With all the considered combinations, the discomfort index during February was always higher than in April, and the highest values characterised the combination C3. This condition is more likely to cause discomfort, especially during cold winter days. In this analysis, the probability of discomfort was evaluated in relative terms, i.e. compared to the reference simulations.

Regarding the energy indicators ΔQ_t and ΔW_{el}, the flow adjustment did not imply significant variations in the thermal energy supplied by the plant (ΔQ_t < 0.2% for all the considered combinations). In April, these variations became negligible. The electrical energy consumption for pumping depends on the combination: in almost all the considered simulations, they range between - 170 and +40 kWh.

Table 5.3 Effect of the different combinations on performance indicators (τ =2.5).

Week	$q_{max,ref}$ [MW]		Comb	Δq_{max} [%]		Δt_{max} [h]		C_{net} [MWh]		PD_{rel} [°C h]	
	TUE	SUN		TUE	SUN	TUE	SUN	TUE	SUN	TUE	SUN
FEB	25.71	20.64	C1	8.5	12.4	0.75	1.00	3.25	4.56	14	14
			C2	8.7	11.6	0.75	-2.25	4.84	5.14	14	14
			C3	8.5	12.4	0.75	1.00	5.05	4.79	18	17
APR	6.67	6.69	C1	14.9	6.9	-1.25	-1.00	1.48	0.45	5	6
			C2	3.8	-3.0	-2.25	-2.00	2.04	0.95	4	6
			C3	11.9	4.1	-2.50	-2.25	1.85	1.05	6	7

5.1.2.2 Post-charge of the network

Similarly to Table 5.2, Table 5.4 shows the results for a given combination (C5) and for different values of ε, which denotes the duration of the mass flow rate adjustment after the peak load. The value of parameter τ was set to 1 hour to operate in the same range of discomfort of the pre-charge cases to make the results of the two control strategies comparable. Figure 5.5 shows the mass flow rate (a) and thermal load (b) profiles obtained with different values of ε on Tuesday, April week. The peak shaving effect was reduced during February and April compared to that obtained with the pre-charge strategy. As shown in Table 5.4, the peak was always delayed, and the lags of peak load were not significantly affected by the values of parameter ε.

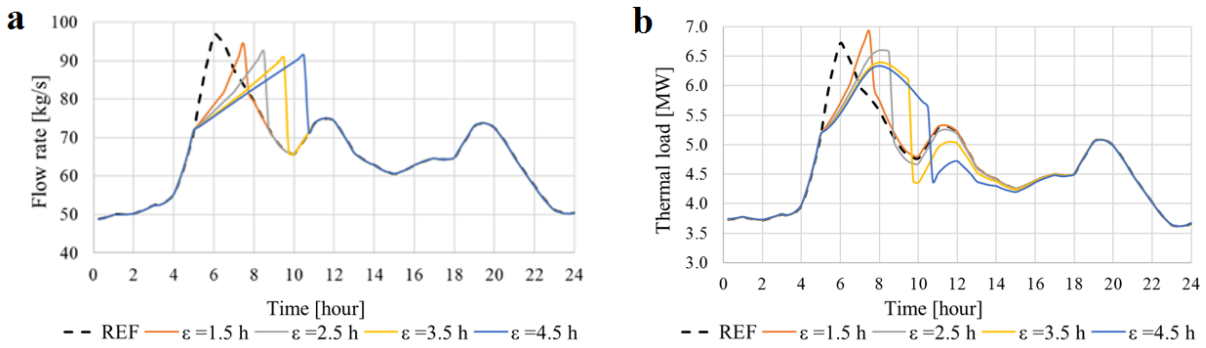

Figure 5.5 The different mass flow rate (a) and power profiles (b) obtained by varying ε between 1.5 and 4.5 hours on Tuesday, April week.

Furthermore, Table 5.4 outlines that, in absolute terms, the values of available network capacity C_{net} during February are always higher than those of April for a given ε, similarly to what was found out in the network pre-charge process for a given τ. The values range between -2.3 MWh and -4.6 MWh in February and between -0.25 MWh and -1.3 MWh in April. In the same way, the discomfort index during February was always higher than in April. The thermal energy needs ΔQ_t with the modified control strategy showed a negligible variation compared to the reference simulations. The energy need for pumping ΔW_{el} increased from 70 kWh (-6% on Sunday) to 240 kWh (equal to 12% on Monday) in February, whereas the increase was negligible in April.

Table 5.4 Effect of ε on key performance indicators.

Week	$q_{max,ref}$ [MW]		ε [h]	Δq_{max} [%]		Δt_{max} [h]		C_{net} [MWh]		PD_{rel} [°C h]	
	TUE	SUN		TUE	SUN	TUE	SUN	TUE	SUN	TUE	SUN
FEB	25.71	20.64	1.5	-1.8	-6.3	0.75	1.25	-2.29	-3.03	8	12
			2.5	0.9	-0.2	0.75	1.50	-2.52	-3.74	10	17
			3.5	1.8	3.1	0.75	1.25	-2.67	-4.30	11	20
			4.5	2.1	3.7	0.75	1.50	-2.78	-4.56	11	21
APR	6.67	6.69	1.5	-2.8	2.3	1.50	0.75	-0.88	-0.25	4	1
			2.5	1.7	2.8	2.00	1.00	-1.16	-0.28	5	1
			3.5	4.8	3.2	2.00	0.75	-1.29	-0.31	6	2
			4.5	5.7	3.3	2.00	1.00	-1.33	-0.33	6	2

Figure 5.6 (a) and (b) show how the different shapes of the modified mass flow rate profiles corresponding to the three combinations affect the thermal load profile. Table 5.5 summarizes the results achieved considering ε equal to 2.5 hours, while the mass flow rate profile was modified with the combinations C4, C5 and C6. Comparing the different combinations shows that C6 was the best choice to damp the daily power peak in both representative weeks. With the combination C5, it was possible to determine the highest displacement in advance of the peak load and to obtain the best load shifting results (higher values of C_{net}). With all the considered combinations, the discomfort index during April was always lower than in February, and the combinations C5 and C6 were characterised by the highest discomfort values.

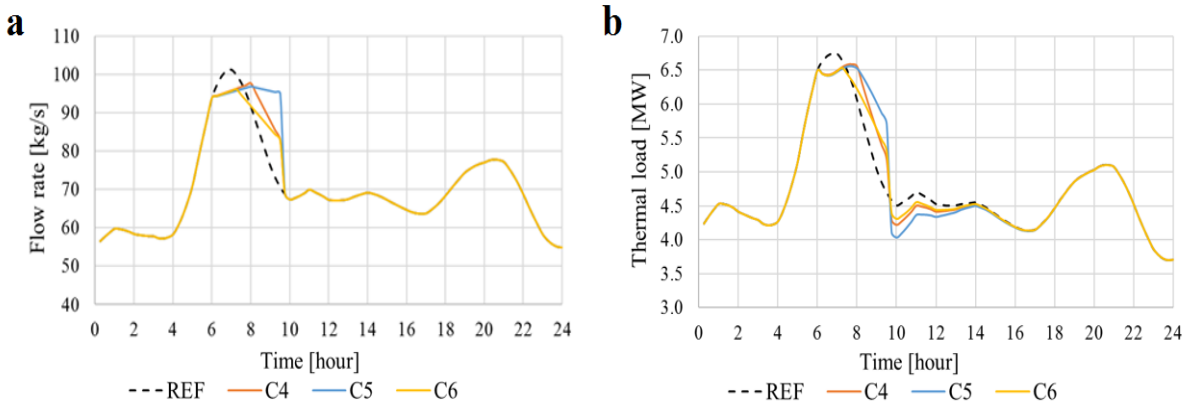

Figure 5.6 Different shapes of the modified (a) flow rate and (b) thermal load profiles associated to the combinations C4, C5, C6 for Sunday, week of April.

Table 5.5 Effect of the combinations C4, C5 and C6 on performance indicators (ε =2.5).

Week	$q_{max,ref}$ [MW]		Comb	Δq_{max} [%]		Δt_{max} [h]		C_{net} [MWh]		PD_{rel} [°C h]	
	TUE	SUN		TUE	SUN	TUE	SUN	TUE	SUN	TUE	SUN
FEB	25.71	20.64	C4	0.0	0.6	0.75	1.00	-2.35	-3.11	9	15
			C5	0.9	-0.2	0.75	1.50	-2.52	-3.74	10	17
			C6	2.7	3.3	0.50	1.25	-2.38	-3.53	10	17
APR	6.67	6.69	C4	6.0	2.8	1.25	1.00	-1.00	-0.26	4	1
			C5	1.7	2.8	2.00	1.00	-1.16	-0.28	5	1
			C6	7.1	3.0	1.75	0.50	-1.13	-0.26	5	2

5.1.2.3 Comparison between pre-charge and post-charge

Figure 5.7 shows the amount of thermal energy shifted through the indicator C_{net} as a function of the discomfort index PD_{rel} on Tuesdays in February and April representative weeks. The two weeks are represented by two different colour scales: orange for April and blue for February. Colour intensity is proportional to the τ (ε) parameter in the pre-charge (post-charge) cycle, which ranges from 1.5 hours to 4.5 hours, as shown in the tables above. As it can be seen, considering the same range of discomfort index, the thermal energy stored in the network with the pre-charge strategy was about twice that "not supplied" during the first part of the post-charge process. As a result, the pre-charge cycle achieved much better load-shifting results than the post-charge cycle. Furthermore, as an increase of C_{net} and of the relative discomfort index was observed with the rise of τ for the pre-charge process, the increase of ε involved an increase of C_{net} (in absolute terms) and of the discomfort index in the post-charge process.

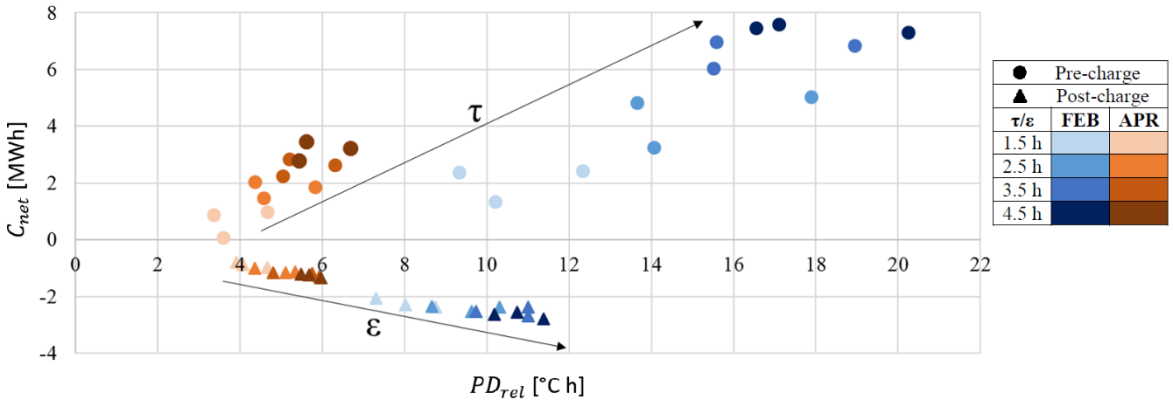

Figure 5.7 C_{net} versus PD_{rel} in pre-charge (post-charge) cycles under different τ (ε) values on Tuesdays in February and April representative weeks.

Considering the simulations results of Tuesday only, a change in τ during the pre-charge process leads to a change in both the amount of energy shifted and the probability of discomfort, which was higher than that determined by an equal change of ε during a post-charge process. In other words, greater sensitivity of these indexes to the variation of the time parameters occurred in the pre-charge simulations. The solicitation produced by the thermal network operator with the proposed flow variations, quantified by PD_{rel}, must not affect the thermal comfort conditions in the indoor environment. Therefore, the suitability of high PD_{rel} values in the real operation of the network depends on the energy flexibility of the connected buildings, i.e. on their ability to manage their energy demand according to local climate conditions, user needs and system requirements. In this case, "system requirements" refers to the needs of the DH network operator, whose objective could be manifold: shaving peaks, reducing operating costs etc. This evaluation should be carried out in particular for the oldest uninsulated buildings, considering the thermal capacitance provided by the building structures, the possible presence of thermal energy storage systems, and the initial indoor temperature conditions when the solicitation occurs. Assessing whether the calculated values of PD_{rel} bring discomfort for these buildings would need a detailed analysis of their dynamic thermal behaviour, which goes beyond the scope of this analysis.

5.1.2.4 Practical measures for method implementation

The mass flow rate and the heat demand profiles at the customers' substations determine the thermal load profiles at the supply station. Although the effect of the heat carrier velocity was considered by simulating the district heating network in two different periods of the heating season, the variability of the thermal load profiles due to the spatial distribution of the mass flow was not considered. This aspect plays a crucial role because the number of bypass pipes and their position determines how the network's mass flow rate is distributed. The latter determines the amount of water participating in the thermal storage process and, in turn, the resulting thermal load profile at the supply station. The meshed structure of the network makes it difficult to assess the resulting thermal load profiles at the supply station *a priori*. Thus, a sensitivity analysis was carried out according to the assumptions reported in Section 5.1.1.3. Figure 5.8 shows that the number and position of the bypass pipes influence the resulting thermal load profiles. Layouts BP1 and BP2 (one and two bypass pipes) led to similar profiles, as well as those with three and four bypasses (BP3 and BP4).

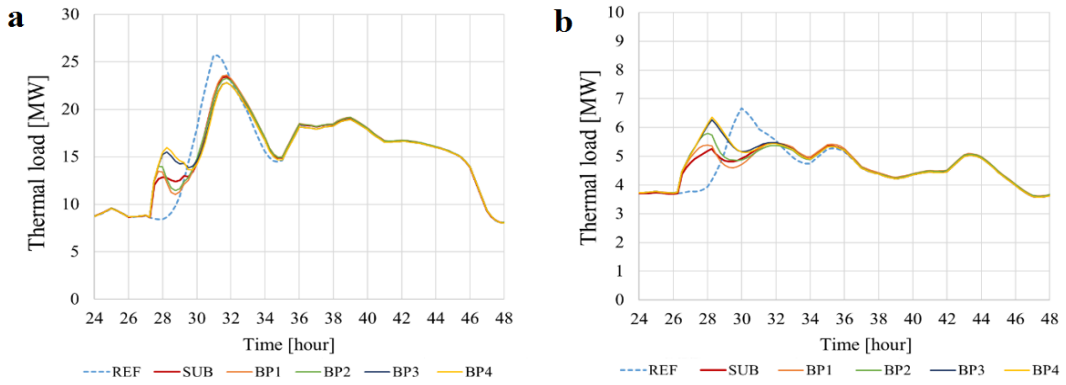

Figure 5.8 Thermal load profiles obtained at the main supply station with different bypass layouts.

Table 5.6 confirms the results reported in Figure 5.8: the layouts BP3 and BP4 entailed a significant increase in the amount of thermal energy shifted C_{net} if compared to the initial simulation (indicated with the acronym SUB), where the mass flow rate variation was evenly distributed among all the substations. This trend is evident in both reference weeks. These layouts improved the peak shaving in February (e.g. from -12.7% to -15.3% on Sunday), whilst in April, the peak increased as long as more bypasses were considered, as shown in Figure 5.8(b). This occurred because the first thermal power peak exceeded the second due to the increase in mass flow rate through the opening of the bypass valves. This fact suggests that during middle seasons the mass flow rate circulating through the bypass pipes should be high enough to attain the desired thermal load shift, but not too high if the operator aims at reducing the peak load.

Table 5.6 Influence of the number of bypass pipes on the flexibility indicators with combination C1 and τ = 3.5 hours.

Week	$q_{max,ref}$ [MW]		Number of bypasses	Layout	Δq_{max} [%]		C_{net} [MWh]	
	TUE	SUN			TUE	SUN	TUE	SUN
FEB	25.71	20.64	0	SUB	8.7	12.7	6.06	5.63
			1	BP1	8.1	11.8	5.43	5.35
			2	BP2	9.4	13.3	6.14	5.98
			3	BP3	11.3	15.3	9.68	9.83
			4	BP4	11.3	15.3	9.88	9.96
APR	6.67	6.69	0	SUB	18.2	13.3	2.22	1.39
			1	BP1	18.0	12.6	2.61	1.82
			2	BP2	13.2	6.9	3.28	2.10
			3	BP3	6.0	3.5	4.03	2.05
			4	BP4	4.6	2.2	4.17	2.16

NeMo software features a post-processing visualization toolbox to help the user analyze the simulation outputs. Once the coordinates of the nodes are provided, *NeMo* can generate an animated plot to show how the desired variable (mass flow rate, pressure or temperature) changes over time and space. This functionality has proven very useful to explore the spatial distribution of the considered variables.

Figure 5.9 shows the water temperature difference in the return pipes between the simulation with the three bypass pipes (BP3 configuration) and the reference simulation with the existing pump head control strategy. In detail, Figure 5.9 shows the evolution of the temperature difference during the pre-charge process on Tuesday in February's reference week with τ = 3.5 hours and combination C1. Before the start of the modified control strategy at 3 a.m., there was no difference between the two simulations and the whole network was coloured green. As it can be seen in the colour bar on the right, the temperature difference becomes yellow in case of the return temperature increases compared to the benchmark simulation. In contrast, it turns from green to blue when the return temperature falls below the values of the reference simulation. At 3:30 a.m., the bypass valves opened, and the supply temperature at 80°C started being supplied to the return pipes. The hot water spread across the network and mixed with colder water –see the network at 4 a.m. The hot temperature front reached almost all parts of the network, but a tree-shaped branch was on the upper side of the network. The temperature reached by the water in a certain pipe depends on its distance from the bypass pipes. Indeed, one hour before the peak load (5 a.m.), the return temperature was almost equal to that of the supply pipes (80°C) close to the bypasses, whereas it was lower in the south-eastern part of the network. The latter showed a modest temperature increase of approximately 5°C. Then, the thermal load started rising and reached its peak at 6 a.m. Consequently, the return pipes cooled down and rapidly returned to their usual temperature, corresponding to 0 K on our scale. At 6:15 a.m., the bypass valves were closed, and the thermal load was still very high. As a result, the water-cooled down, and the network turned blue. It can be seen that this variation was not uniform across the network: in the peripheral branches –especially the north-eastern one- the thermal transient was much slower due to the very low heat demand of the connected users. This evidence points out the need to accurately choose the share of mass flow rate surplus to be circulated through each bypass. In this case, circulating less water in the bypass on the north-east branch would have been beneficial to exploit the thermal capacitance of the network better. As long as the

thermal load decreased, the return temperature returned to its standard values. At 10 a.m., the modified control strategy ceased, and the mass flow rate supplied by the central station was the same as in the benchmark simulation. One hour later, the return temperature variation approached zero everywhere but in the north-eastern branch, where the transient was not yet finished.

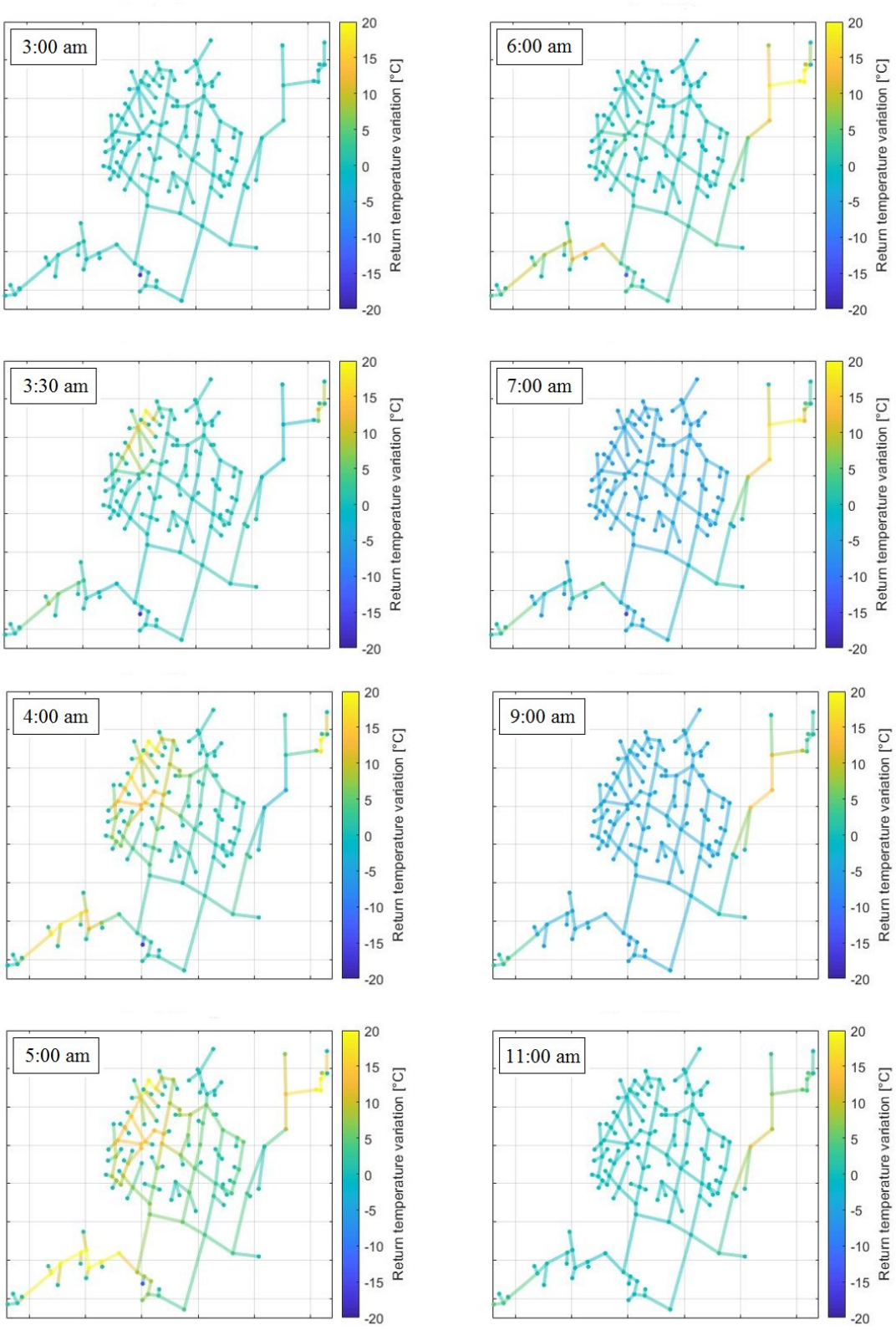

Figure 5.9 Return temperature variation with the layout BP3.

5.2 Exploiting the thermal capacitance of the building envelope

The thermal capacitance of the buildings' structure can be a source of energy flexibility for the demand side management (DSM) of the user substations connected to a district heating network. The considered DSM strategy consists of Active Demand Response (ADR) simulations in this research work. This means to vary the thermal load profile of the users from their current/normal pattern in response to a specific change in the boundary conditions. The study considered two building types belonging to the user substations connected to the district heating network of Verona, respectively, a school and a residential building. The energy model of these two case studies has been described in Section 4.2. The innovative character of the analysis lies in the fact that it takes into account large buildings. The flexibility potential of the two considered buildings was assessed by analysing the heat demand pattern modification and its impact on thermal comfort. Furthermore, the influence of the building envelope type, the user behaviour and the weather conditions were considered.

5.2.1 Method

The method for assessing the flexibility potential of the building structure consisted of comparing two simulations with the Energy Plus model of the buildings for each ADR event: a reference simulation and an ADR simulation. The ADR events were determined by modifying the setpoint schedule, anticipating or delaying the switch on of the eating system. This resulted in a different thermal load profile from the reference case.

Two types of ADR events were considered:

- Upward event: an event that increases the temperature setpoint before the thermal load peak, during the heating period.
- Downward event: is when the temperature setpoint is lowered after the thermal load peak, during the heating period.

Figure 5.10a shows the resulting average operating temperature and thermal load implementing an upward event compared with the reference case during the winter. On the other hand, Figure 5.10b compares the reference case and downward event results.

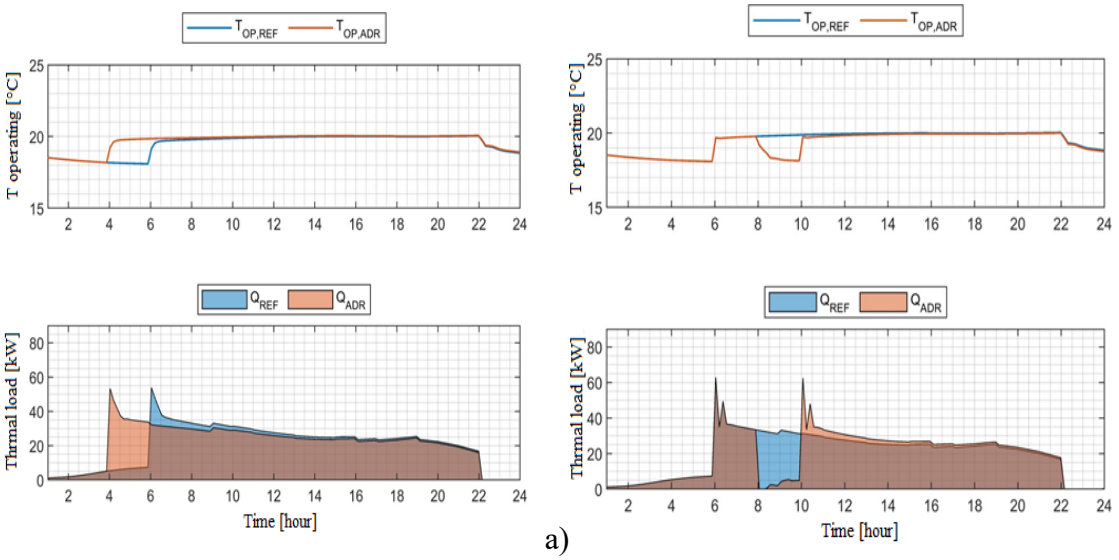

Figure 5.10 Resulting operating temperature and thermal load, respectively, in case of an upward event (a) and downward event (b) and compared with the reference case during the heating period.

5.2.1.1 Key Performance Indicators

The thermal load profile variation allowed defining two key performance indicators (KPI) to assess the energy flexibility of the building envelope. The first KPI is the “available capacity for active demand response", i.e. the capacity to shift the heat load over time. This parameter was defined as:

$$C_{ADR} = \int_0^{L_{ADR}} (Q_{ADR} - Q_{REF}) dt \tag{5.7}$$

Where Q_{REF} represents the heat load value of the reference case and Q_{ADR} in the ADR case, both as a function of time. L_{ADR} is the duration of the event. C_{ADR} is usually expressed in terms of kWh of energy moved. Generally, C_{ADR} is evaluated on an average basis depending on the number of events implemented, as shown in Equation 5.8. In this study, the monthly average value of this parameter was considered.

$$C_{ADR} = \frac{\sum_1^N C_{ADR_i}}{N\, L_{ADR}} \tag{5.8}$$

Where N is the number of ADR events implemented in the considered period. It was necessary to consider also the concept of ADR efficiency to carry out a complete analysis of the ADR events. This KPI is defined in the equation below.

$$\eta_{ADR} = 1 - \frac{\int_0^{\infty} (Q_{ADR} - Q_{REF}) dt}{\left| \int_0^{L_{ADR}} (Q_{ADR} - Q_{REF}) dt \right|} \tag{5.9}$$

In a simplified way, it is the ratio between the blue area (Q_{REF}) and the red area (Q_{ADR}) represented in the thermal load diagram of Figure 5.10a or Figure 5.10b. The ratio between

these areas can't be unitary because thermal losses through the envelope or due to ventilation must be considered. Furthermore, ADR events cause alterations in the behaviour of the heating system, leading to variations in the internal comfort of the building. Therefore, the following indicator called "thermal discomfort degree-hours" was considered to evaluate discomfort. It is based on the calculation of the operating temperature of a given environment and is defined as follows:

$$TDDH = \int_0^{Occ} \left| T_{OP} - T_{OP,LIM} \right| dt \quad (5.10)$$

Where L_{OCC} represents the time that people are present in a certain environment, and $T_{OP,LIM}$ the extreme reference value for comfort assessment. The lower limit was considered equal to 20°C and the upper 25°C.

5.2.1.2 Simulation framework

The results of Vivian et al. [39] were used as a reference for the choice of ADR events duration and time. Their analyses concluded that from the point of view of C_{ADR} and ADR efficiency the best events are those located close to the load peaks, immediately before for upward events and immediately after for downward events, with a duration of 2 hours. As far as the setpoint is concerned, according to Vivian et al. [39], a variation of ±3 K is optimal for residential cases. So, the setpoint was increased from 18°C to 21°C for the upward event, and it was decreased from 21°C to 18°C for the downward one.

Since the considered buildings are user substations connected to the Verona district heating network, only events during the heating period envisaged for the Verona area (climate zone E), i.e. from 15 October to 15 April, were considered. During this period, an ADR event occurred once a week, on Wednesdays. The decision to impose an event once a week is necessary to avoid that one event could influence the next, distorting the analysis and results. In fact, by analysing the simulations, it has been seen that the average duration of the "rebound effect" (the alteration of the load profile compared to the reference one) lasted for a maximum of 5 days. In the ADR simulations, the trend of the defined KPIs was determined by varying different boundary conditions. First, the change in the building envelope was assessed, considering a reference case, which corresponds to the real case for both the school and the residential building, and a retrofitted case. Then the effect of the design power of the heating system was evaluated: without heating-up power, with heating-up power and without power limit. In these simulations, the ADR events were implemented in the whole building

or only in some parts. For example, in some simulations of the residential case, the ADR event was applied only on the second floor of the building, while different setpoint schedules were considered in the neighbouring floors: with reference schedule and with the heating system off (as a separate single dwelling).

The software that allowed to carry out the simulations is Energy Plus. In this study, it was decided not to consider a specific heating system. On the other hand, with this software, it is impossible to set a priori the share of the heat supplied in a convective and radiant way without defining a specific heating system. However, it is possible to use an "Ideal-Air Load" tool that implements an ideal all-air system specifically designed to carry out performance analysis without defining any specific heating system. This system behaves in the same manner as a VAV terminal. So, the convective fraction of heat delivered is 100%. A limitation of this tool is that it has to be applied to each thermal zone defined in the geometric model of the building: so, it was necessary to calculate the design powers for each zone.

The simulations were carried out for the two considered case studies (residential building, school), setting up a timestep of 10 minutes. Then, thermal load and operating temperature were obtained for each thermal zone as the output for the reference and the ADR simulations.

5.2.2 Residential building analysis results

The KPIs were evaluated for a 2-hour upward modulation event from 5 to 7 am and a 2-hour downward modulation event from 9 to 11 am. Both were applied to the Condominium I under different boundary conditions. In a first step, the influence of the building envelope was evaluated, then the effect of the design power of the heating system was considered. The KPIs values obtained from the simulations have been reported in histograms as monthly average values to damp the local effect of any events that turn out to be anomalous compared to those of the same period.

5.2.2.1 Effect of building envelope in the residential building

The typology of the building envelope results in a significant impact on the performance of active demand response events. It has been considered the real typology and the retrofitted one. As mentioned in paragraph 4.2, a thermal coat was added to requalify the building, and windows and doors have been replaced.

In Figure 5.11, the monthly average results of ADR efficiency ($\eta_{ADR\ average}$) are shown for the reference and retrofitted case, considering the ADR schedules applied to all apartments (a,b), to the apartments of a single floor (c,d) and to a single floor as a separate dwelling (e,f). In addition, in this first analysis, the design power of the heating system was considered equal to the case with heating-up power.

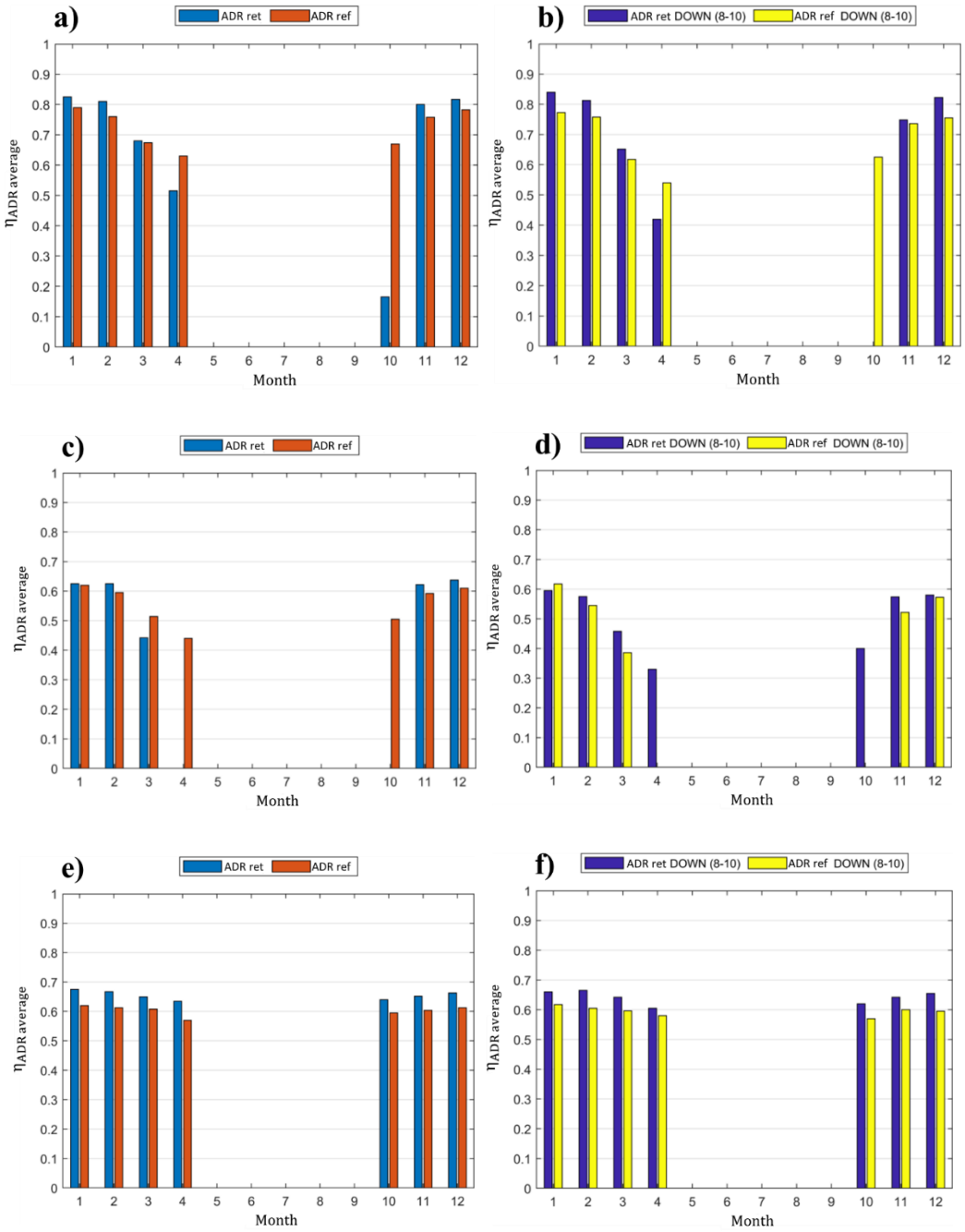

Figure 5.11 Monthly average ADR efficiency for the reference and retrofitted case, with ADR schedules applied to all apartments (a,b), apartments of a single floor (c,d) and a single floor as a separate dwelling (e,f).

As shown in Figure 5.11, the ADR efficiency of the retrofitted case (ADR ret) is usually higher than the reference case (ADR ref) for both upward and downward events.

The fact that the monthly average values of ADR efficiency decreased going towards the warmer months does not seem to make physical sense because transmission losses decrease, and efficiency should increase rather than decrease. This last thing and the lower ADR efficiencies of the retrofitted case compared to the reference one for April and October (in Figure 5.11 a and b) are due to the influence of the design power of the heating system. This particular behaviour will be discussed in detail in the following section on the heating system power limit effects.

In addition, in Figure 5.11 b, c and d, the zero values of the ADR efficiency in April and October are because the heating system was not switched on in that periods. This is due to insulation or the heated floors above and below, which allow the indoor temperature to never fall below the set point.

The case in which the ADR events were applied to the whole building (Figure 5.11a and b) made it possible to reach higher ADR efficiency values than the other cases in the coldest months. This happened because the same event on all the floors made the transmittance losses in the vertical direction practically nil for the interior floors, making the inter-floor slabs adiabatic. So, the average seasonal ADR yield for cases (a) and (b) was higher than in the other cases, as shown in Figure 5.12. On the other hand, on average, cases (c) and (d) of Figure 5.11 are the most inefficient. This result was because, in this case, there are transmission losses through inter-floor slabs towards the adjacent apartments of the other floors and because the ADR event's efficiency was assessed on the considered floor, not the whole building. So, the benefit that the heating of a single part of the building has on the rest did not count. The latter case is difficult to apply to the user substations of a DHN. However, it was interesting to understand the effects on the considered KPI if events are applied only to a part of a building.

Finally, the trend of the single floor as a separate dwelling (Figure 5.11e and f) was very stable during the heating season, with no significant variation for both the retrofitted and the reference case.

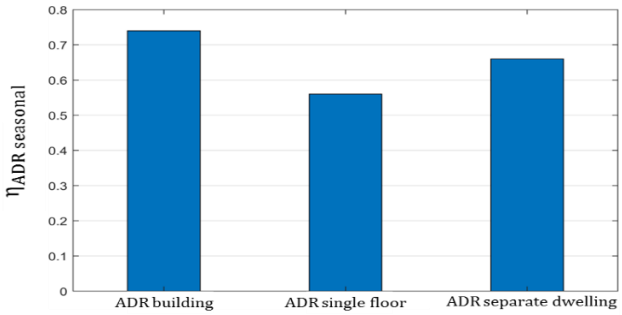

Figure 5.12 Seasonal ADR efficiency for the retrofitted case, with ADR schedules, applied to the entire building, a single floor, and a single floor as a separate dwelling.

As well as the efficiency, also the energy moved (C_{ADR}) was strongly influenced by the type of building envelope. Figure 5.13 shows that the average monthly C_{ADR} for the reference cases were always much higher than those of the retrofitted ones. This confirms the results obtained by Vivian et al. [39]. The higher thermal capacitance of the no retrofitted case allowed to shift much more energy, independently from the type of ADR event (upward or downward) or whether it was a residential building (Figure 5.13 a and b), the apartments of a single floor (Figure 5.13 c and d), or a separate dwelling (Figure 5.13 e and f).

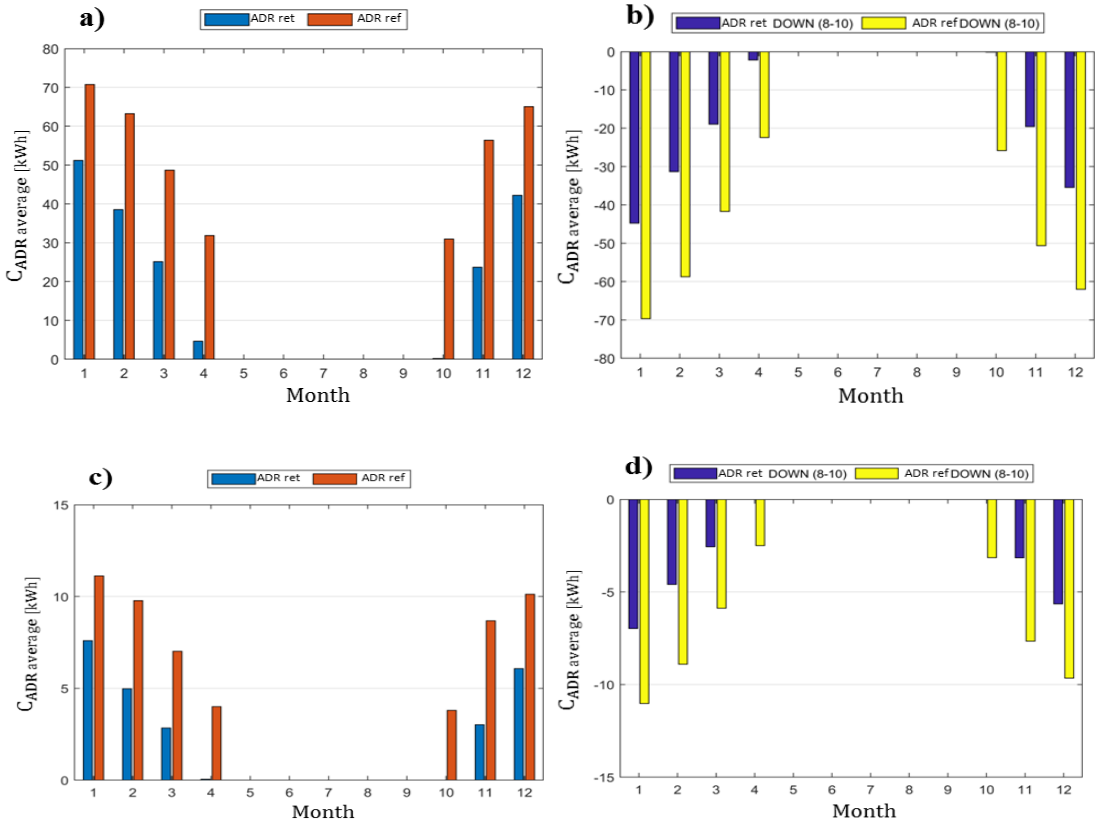

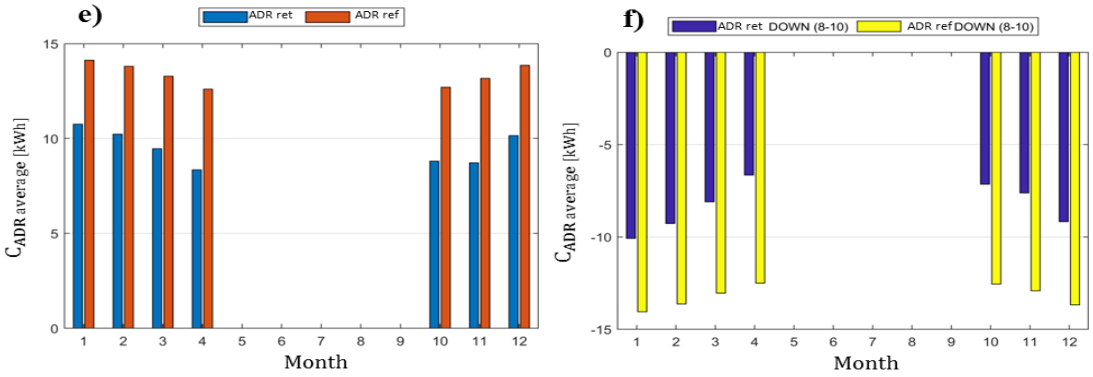

Figure 5.13 Monthly average C_{ADR} for the reference and retrofitted case, with ADR schedules applied to all apartments (a,b), apartments of a single floor (c,d) and a single floor as a separate dwelling (e,f).

Figure 5.14 shows the thermal discomfort at each floor considering ADR events on the whole residential building and the heating system designed with the heating-up power. For the retrofitted case, the discomfort with the upward events is shown in Figure 5.14a and with the downward events in Figure 5.14b, while for the reference case with the upward events in Figure 5.14c and with the downward ones in Figure 5.14d. Lower values of TDDH characterised the simulations in the retrofitted cases compared to the reference ones. Furthermore, in both retrofitted and reference cases, it is possible to see that while the TDDH decreased for upward modulation events, it increased for downward ones. In all cases, the highest discomfort values were obtained in January due to the very low external temperature values. Regarding the distribution of discomfort along with the floors of the building, the central floors, particularly the second floor (P2), present lower levels of discomfort than the first floor (P1) and 5^{th} floor (P5). This trend changes in the reference case during the October-December period (Figure 5.14c and d), with the ground floor being characterised by lower discomfort values than other floors. With both types of building envelope, the discomfort index is dependent on the external temperature as it is high in the colder months of the season and much lower in the warmer ones.

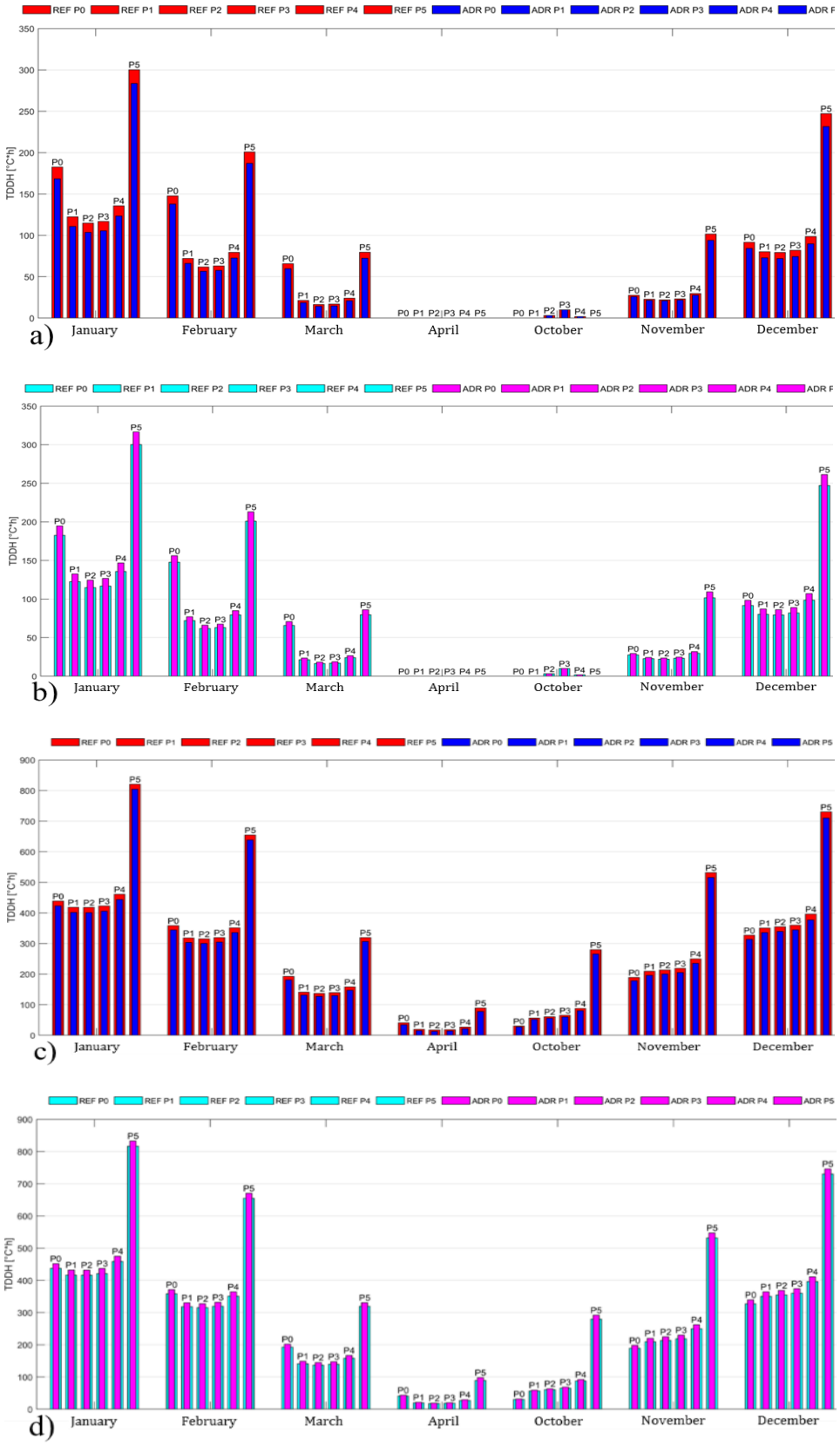

Figure 5.14 Thermal discomfort (TDDH) at each floor with heating-up power, for upward events (a) or downward events (b) on the whole building in the retrofitted case, and upward events (c) or downward (d) in the reference case.

5.2.2.2 Effect of the heating system design power in the residential building

As mentioned in the previous section, the influence of the design power was very strong, so that events in the coldest months were more efficient, despite the higher transmission losses through the envelope. In Figure 5.15, the monthly average results of ADR efficiency ($\eta_{ADR\ average}$) are shown for the case with no limit of heating system design power, with heating-up power and without heating- up power, considering the ADR upward schedules applied to all apartments (a), to the apartments of a single floor (b) and a single floor as a separate dwelling (c). Furthermore, these ADR simulations were carried out for the retrofitted case of the residential building.

As shown in Figure 5.15 a and b, the $\eta_{ADR\ average}$ were always penalised by the progressive lowering of the design power limit in each month considered. On the other hand, the design power limit, with no heating-up power, imposed for the separate dwelling (Figure 5.15c) was disadvantageous only in the colder months. At the same time, there was a reversal of the trend in March-April and October-November. In fact, in this last case, a slight improvement of the $\eta_{ADR\ average}$ towards warmer months can be seen. So, in the case with ADR events applied to the apartments of a single floor as a separate dwelling and with a sufficiently low design heating power limit (no heating-up power), the influence of the thermal loss trend was more important. In fact, the monthly average ADR efficiency was higher in the heating season's warmer months.

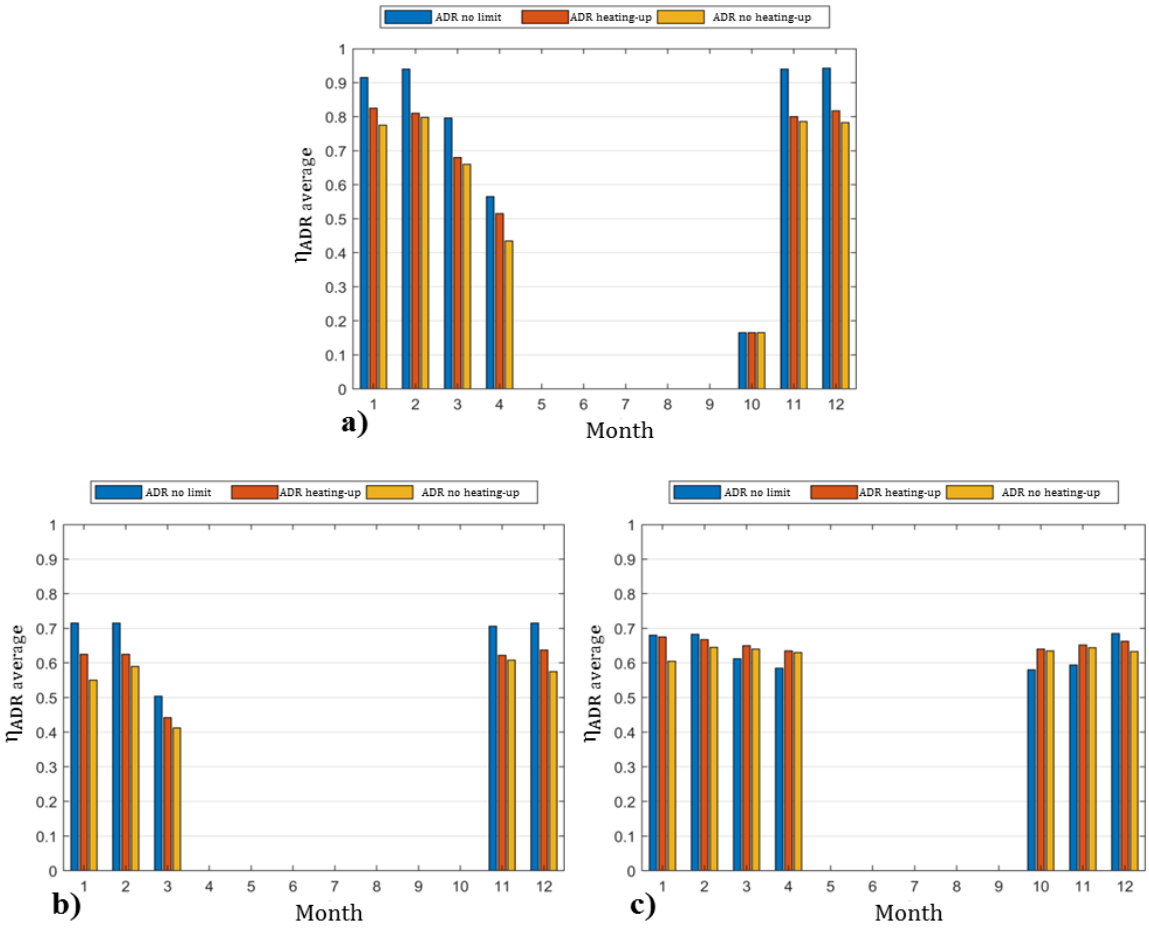

Figure 5.15 Monthly average results of ADR efficiency for the retrofitted case with three different heating system design powers, considering ADR schedules applied to all apartments (a), apartments of a single floor (b) and a single floor as a separate dwelling (c).

Furthermore, the average seasonal ADR efficiencies were investigated, considering the three different heating system design powers. The results are summarised in Table 5.7.

Table 5.7 Seasonal ADR efficiency for the different heating system design powers and with the ADR modulation events applied in different ways.

	Seasonal ADR efficiency		
	ADR all apartments	ADR single floor	ADR separate dwelling
NO LIMIT	0.85	0.64	0.64
HEATING-UP POWER	0.74	0.56	0.64
NO HEATING-UP	0.71	0.52	0.63

The data in Table 5.7 shows that in the case with ADR modulation events applied in the apartments of the whole building, the design power of the heating system had a great influence on the seasonal ADR efficiency, which varied from 0.85 to 0.71. The more the

heating system was oversized, the higher the average seasonal ADR efficiency. In this perspective, the case without a power limit represented a sort of maximum ADR efficiency obtainable by modulating the design power. On the other hand, the seasonal η_{ADR} with ADR events applied to the case of the separate dwelling were less influenced by the design power variation (the seasonal ADR efficiency varied between 0.64 and 0.63), confirming what was seen in the previous analysis of the monthly average ADR efficiencies.

It remains to understand why variations in heating system design power affected the ADR efficiency. The reason is linked to the dynamic behaviour of the heating system.

Considering the thermal load and average operating temperature profiles resulting with upward events in all apartments of the residential building in the mid-season period, Figure Figure 5.16b (no limit of the heating system design power) shows that when there is an increase of the setpoint from 18 to 21 °C, a peak of the thermal load occurs, which is followed by a brief shutdown of the system. This behaviour determines a decrease in the monthly average η_{ADR}. On the other hand, on winter days (Figure Figure 5.16a and c), when transmission losses are higher, the system does not perform an intermittent start-up, but it continues to operate even after the start-up peak. So there isn't the same decrease in ADR efficiency seen in the previous cases. Finally, in figure Figure 5.16f, even if the mid-season period is considered, as the design power of the heating system is characterised by a lower limit (no heating-up), there is no peak in the thermal load profile followed by the shutdown of the system. Therefore, the ADR efficiency does not decrease as in other mid-season cases. It can be concluded that the behaviour of the heating system predominantly influenced the trend of the monthly average ADR efficiency with the ADR events applied to the whole building.

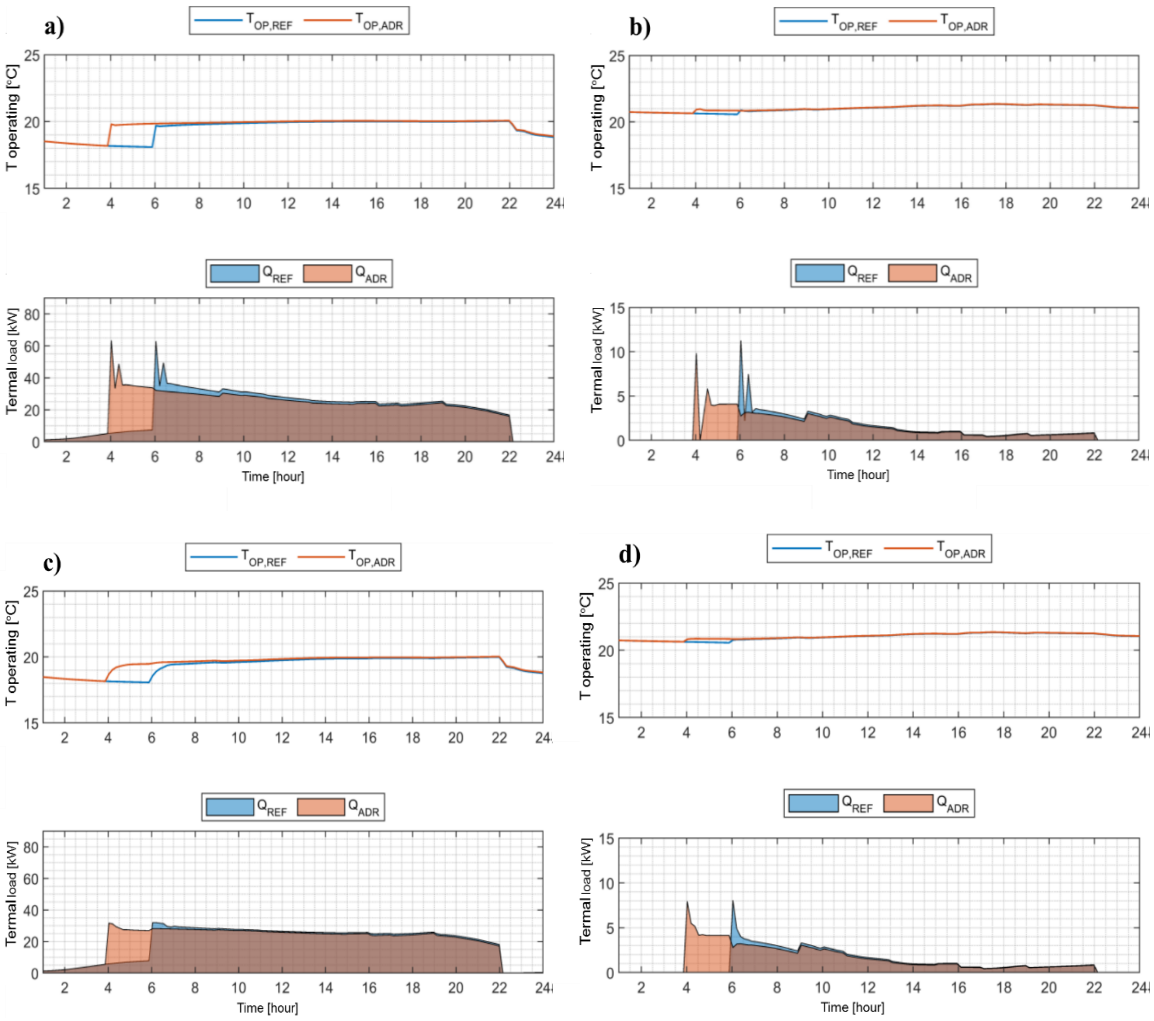

Figure 5.16 Thermal load and average operating temperature profiles with upward events in all apartments of the residential building for (a) 18/01 no limit power, (b) 22/03 no limit power, (c) 18/01 no heating-up power, (d) 22/03 no heating-up power.

As far as the average monthly C_{ADR} is concerned, considering the case with ADR events applied to the apartments of a single floor, and without limit of the heating system design power, for January the average value of the energy moved was 6.8 kWh, as shown in Figure 5.17b. By multiplying this value for the number of floors (6), the result was lower than that obtained in case (a) with ADR events applied to the apartments of the whole building, equal to 47.2 kWh. This phenomenon can be explained because the ground floor and the fifth floor subjected to greater transmission losses allowed more thermal energy to be moved. The case of the separate dwelling (Figure 5.17c) determined the best C_{ADR} considering the same number of apartments in which ADR events were applied. This is because the greatest thermal losses characterised it. That's why it is the one least affected by the design power of the heating system as far as the ADR efficiency.

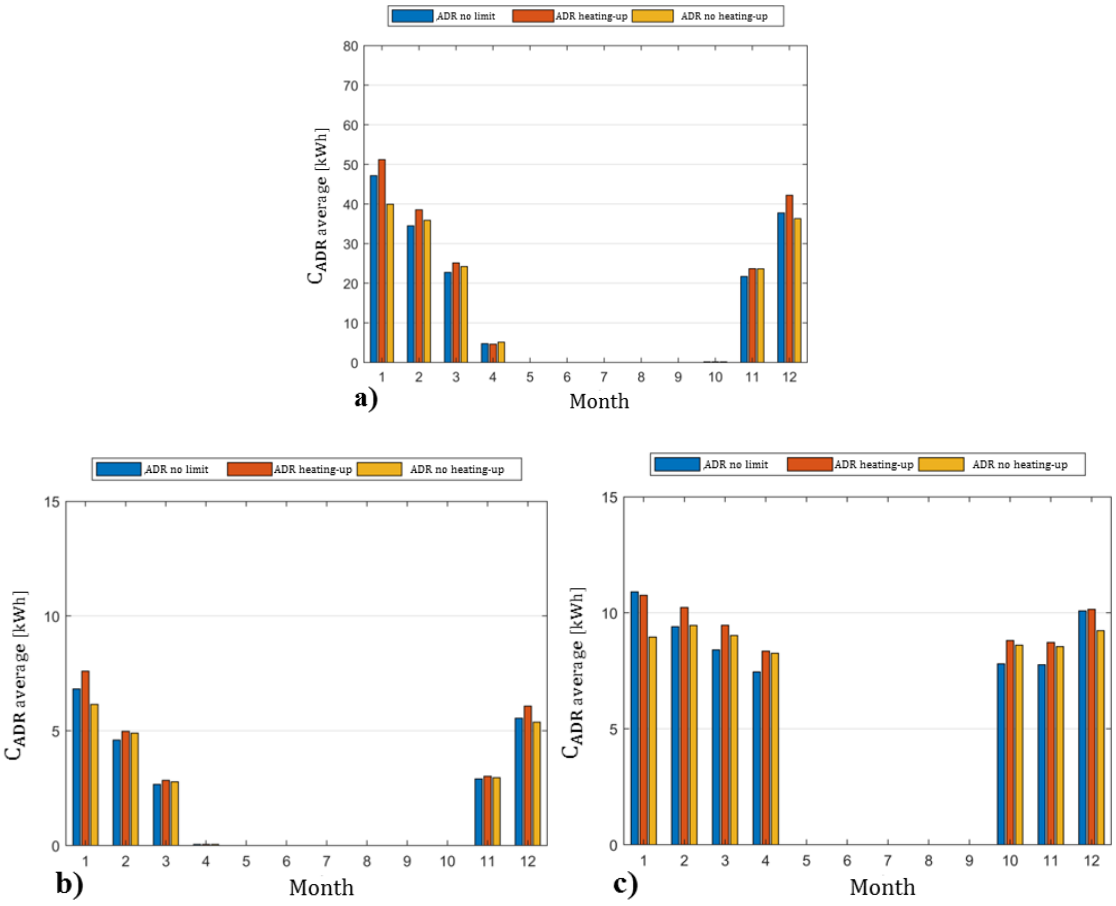

Figure 5.17 Average monthly C_ADR considering the retrofitted case with the three different design powers of the heating system, and with the ADR events applied to the whole building (a), to a single floor (b), and to a single floor as a separate dwelling (c).

Regarding the analysis of the influence of the heating system design power on indoor comfort, considering the retrofitted building with upward modulation events on the whole building, in Figure 5.18, it was found that the case without heating-up power (a) provided worse comfort values than the ideal case without a power limit (b). This is true especially for ADR events in January on the 5th floor (P5), where the high power requirements, due to the higher thermal losses, lead to higher TDDH values with the heating system with a too low power limit (case a).

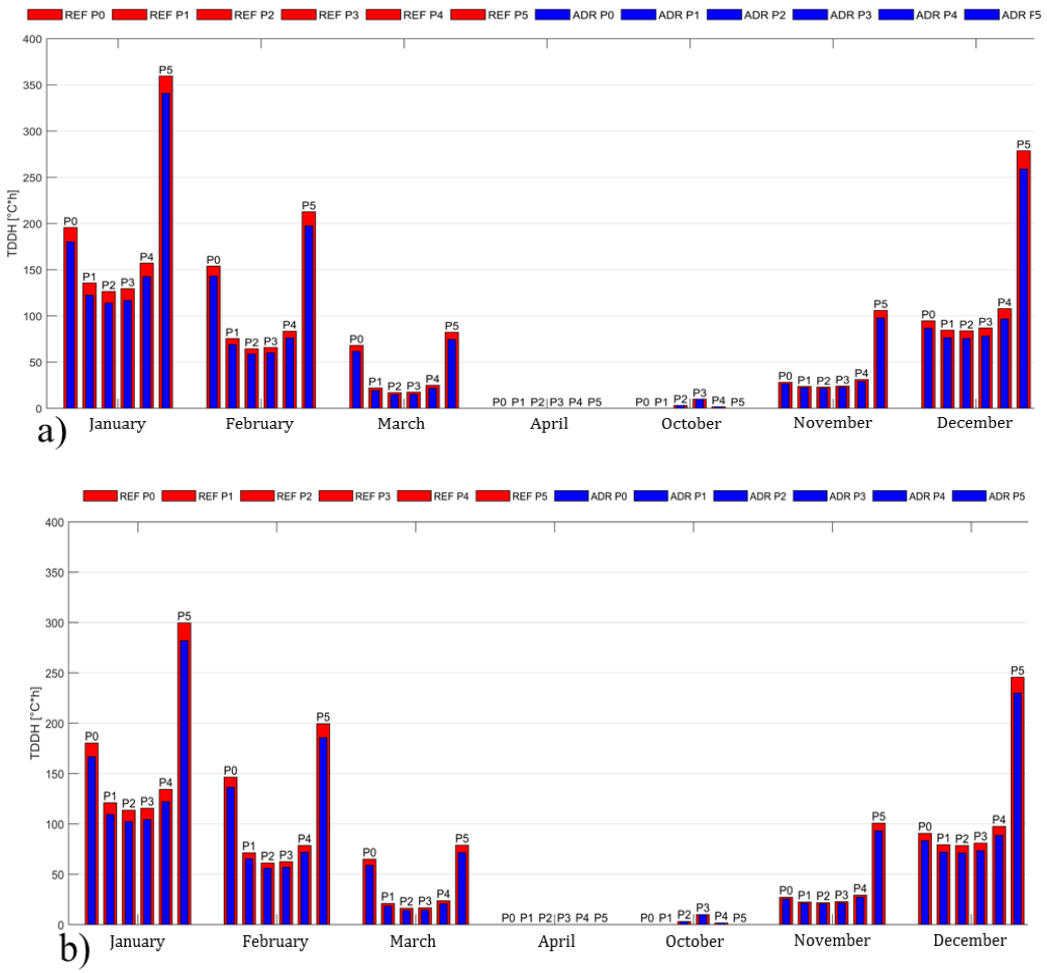

Figure 5.18 Thermal discomfort at each floor for the retrofitted building with upward modulation events on the whole building, and without heating-up power (a), or without power limit (b).

5.2.3 School analysis results

Two different ADR event schedules were implemented for the School A building: an upward modulation event from 5 to 7 and a downward modulation event from 9 to 11, both every Wednesday of the heating season, except for the winter vacation period, when a fixed setpoint of 10°C was considered.

5.2.3.1 Effect of building envelope in the school

Figure 5.19 shows some changes from the residential building. First of all, in case (a), the average value of the ADR efficiency, both for the retrofitted case and the reference one, was considerably lower. In the case of the ADR events implemented in the whole residential building, the average monthly maximum values were above 80%. For the School A, it wasn't

easy to exceed 50%. This marked difference in η_{ADR} was mainly due to the high thermal losses determined by ventilation, as a public environment requires high air changes.

As far as the upward and downward events are concerned, it can be seen in Figure 5.19b that the ADR efficiency is, on average, similar to that of the upward event (Figure 5.19a). Furthermore, the ADR efficiency of the retrofitted case was usually higher than the reference case for both upward and downward events. On the other hand, in the hottest period of the heating season (April and October) for the retrofitted case with the downward events, the average monthly values of η_{ADR} were lower compared to the reference case. This behaviour was because the downward events occurred in the late morning, so the required thermal load was much lower than the heating system's design power considering the heating-up, especially for the retrofitted case. So, the behaviour of the heating system was very intermittent during the start-up phase, as explained in the residential case.

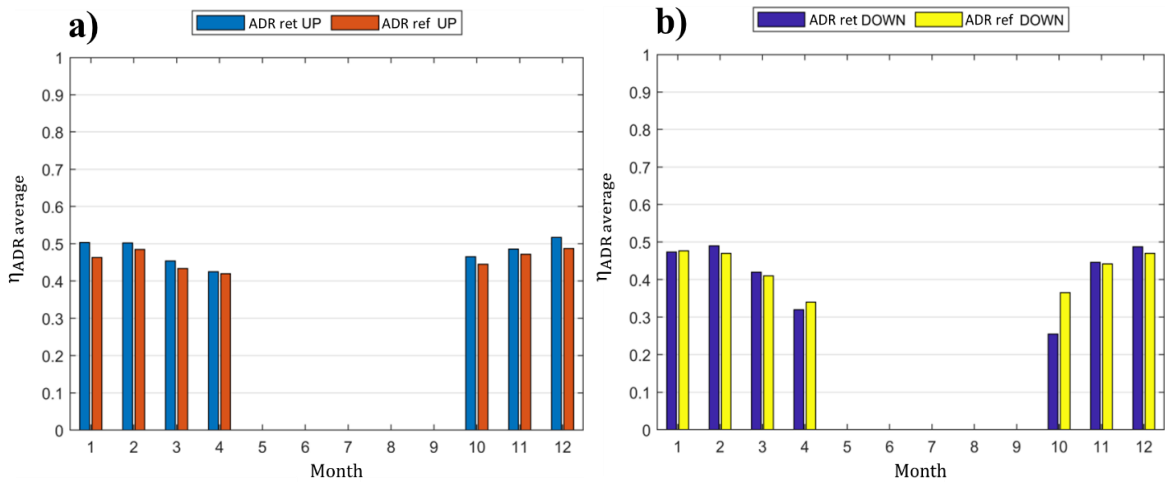

Figure 5.19 Monthly average ADR efficiency for the reference and retrofitted case, with upward (a) and downward (b) modulation schedules applied to the school building, characterised by a heating system with heating-up design power.

As for the residential building, also in the school, the energy moved (C_{ADR}) was strongly influenced by the type of building envelope. For both upward (Figure 5.20a) and downward (Figure 5.20b) modulation events, the average monthly C_{ADR} obtained for the reference cases were always much higher than those of the retrofitted ones.

Analyzing the case with upward events (a), for example, it can be seen that in January, the non-retrofitted building shows an average value that exceeds 120 kWh, and it is just over 100 kWh for the retrofitted case. Moreover, the modulation events lasted 2 hours. So, an

hourly energy displacement capacity of about 60 kWh/h and 50 kWh/h resulted respectively for the reference and retrofitted case. Similar values were obtained for case (b).

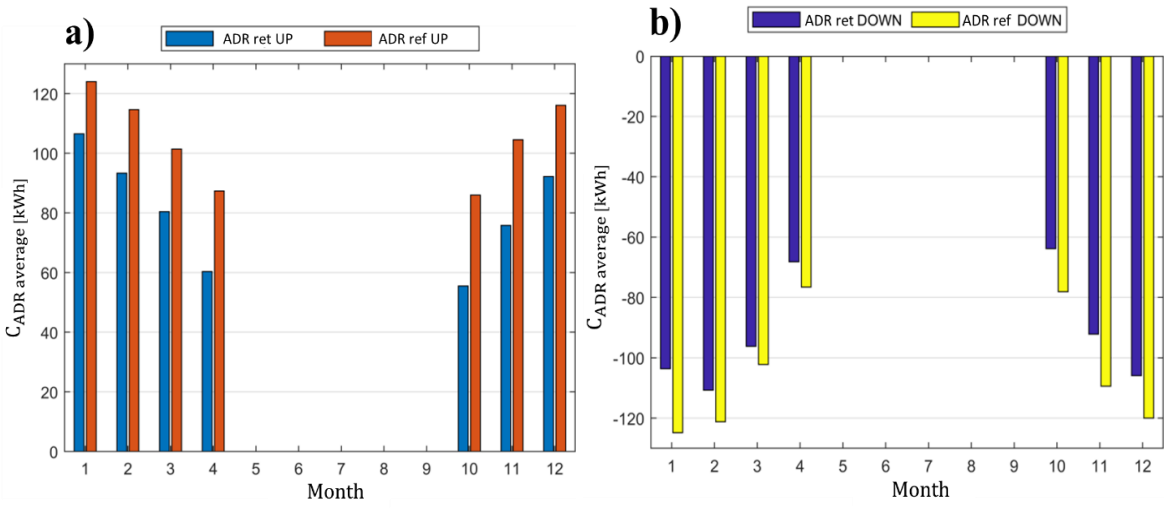

Figure 5.20 Monthly average C_ADR for the reference and retrofitted case, with upward and downward modulation schedules applied to the School A.

Figure 5.21 shows that the perceived discomfort was much higher during January than during all other months. This occurred because January is the coldest month, and at the beginning of this month, school is closed for winter vacations. So, the setpoint was lowered to 10°C. Therefore, bringing the building up to temperature took time during the week of the first ADR event. As a result, the indoor rooms' average operating temperature remained rather low, resulting in high discomfort. Despite the high discomfort values, in January with upward modulation events (Figure 5.21a and Figure 5.21c) there was a much greater TDDH decrease than in other months. On the other hand, the discomfort index with downward events was very high due to the high ventilation required by the public environment. Comparing the retrofitted case (Figure 5.21a and b) and the reference one (Figure 5.21 c and d), the former presented much lower discomfort values, with upward and downward events.

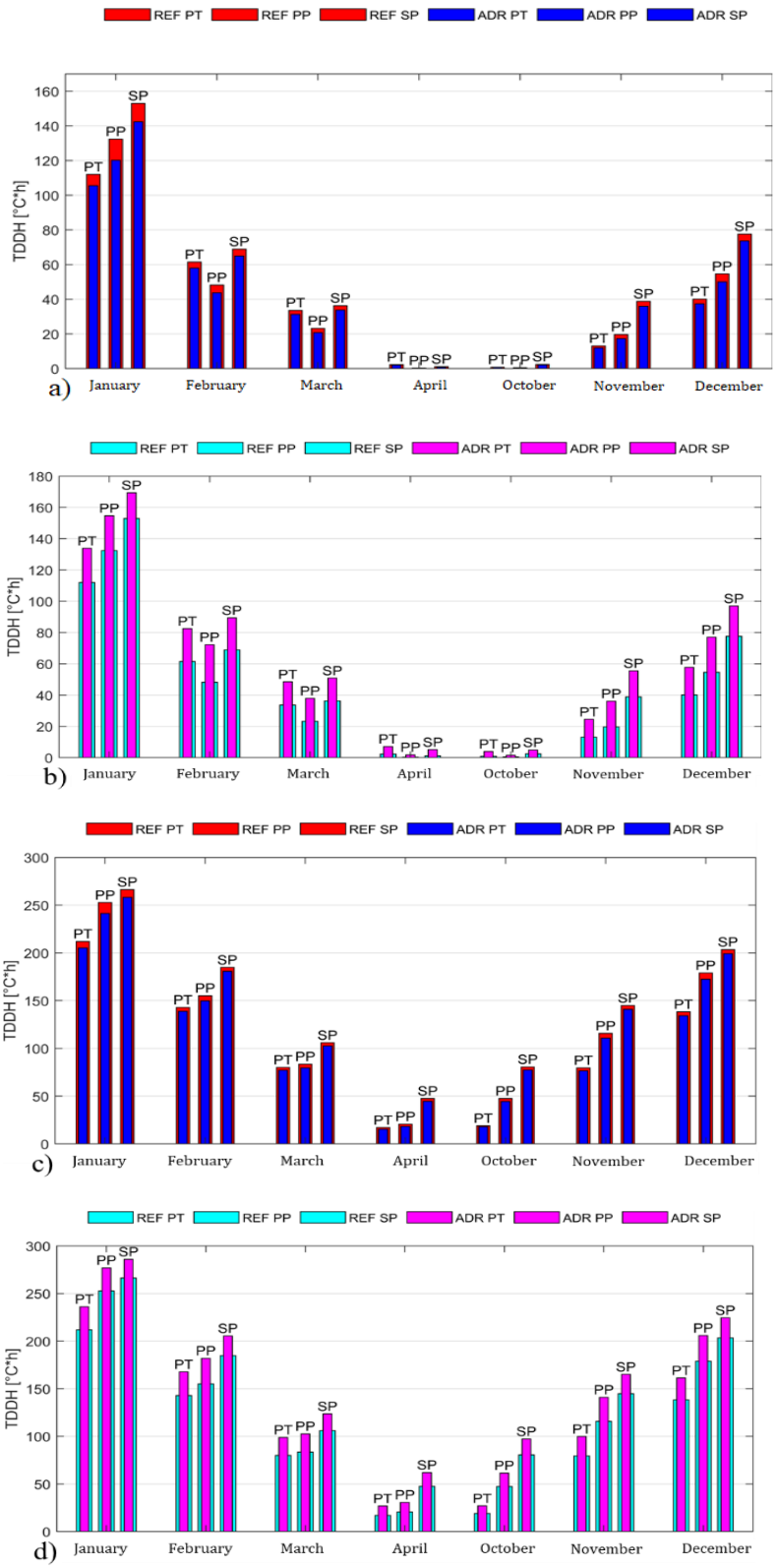

Figure 5.21 Thermal discomfort at each floor of the school building, with heating-up power, and with upward events (a) or downward events (b) for the retrofitted case, and with upward events (c) or downward events (d) for the reference case.

5.2.3.2 Effect of the heating system design power in the school

Two levels of the heating system design powers were chosen for the school case: with heating-up power and without a power limit. The case without heating-up power was discarded as unsuitable for dealing with high ventilation loads.

Figure 5.22 shows that, as in the analysis of the residential building, the ideal case without the design power limitation of the heating system was characterised by better average monthly ADR efficiency results than the case with limited design power. However, this was evident only for upward events (Figure 5.22a), while the difference was very small for downward events (Figure 5.22b).

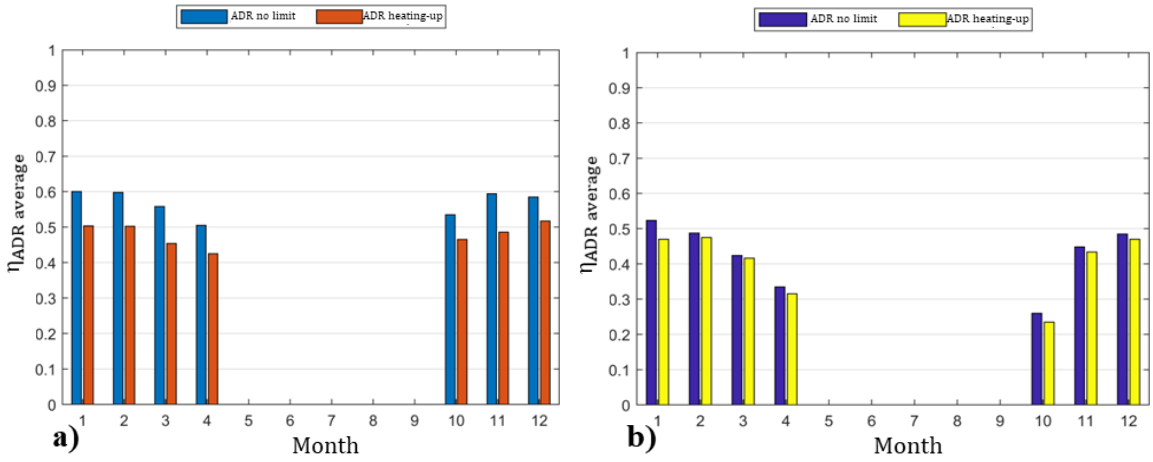

Figure 5.22 Average monthly ADR efficiencies for the school building with the retrofitted envelope and with no design power limit or with heating-up power for upward modulation events (a) or downward modulation events (b).

The monthly average η_{ADR} results of Figure 5.22 can be explained by analyzing the trend of operating temperature and ventilation loads inside the school in Figure 5.23. In particular, the limited increase of ADR efficiency thanks to the unlimited design power of the heating system for the downward event finds an explanation in Figure 5.23b. When the downward event took place, the ventilation loads were high since the lesson was already started. The presence of students implied an increase in the ventilation flow rate. High air exchanges during the downward event led to a decrease in any benefit brought by the unlimited design power of the heating system.

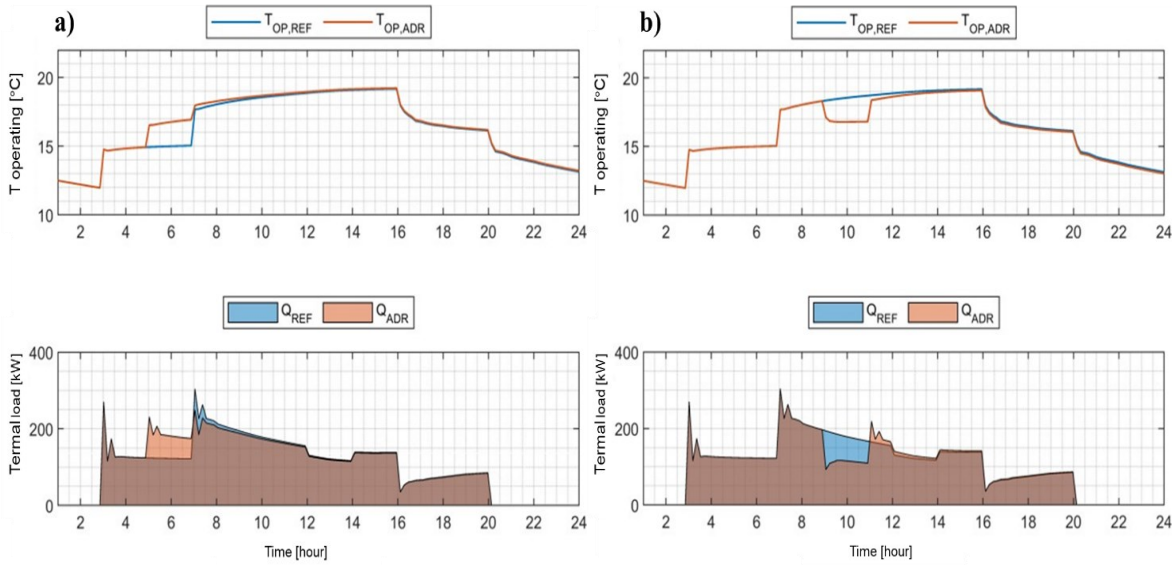

Figure 5.23 Thermal load and operating temperature profiles for the school building with the retrofitted envelope and with no design power limit of the heating system, for upward (a) or downward event (b).

About the analysis of the influence of the heating system design power on the thermal comfort, considering the retrofitted building, the average monthly discomfort (TDDH) was much lower in the case without design power limitation than in the limited one (with heating-up power). However, when the building was subjected to high ventilation loads, as in January, the increase of the heating system design power didn't determine significant gains in thermal comfort with the upward modulation event compared to the reference case. In particular, the higher the design power, the smaller the increase in comfort, as shown in Figure 5.24 a and c. On the other hand, comparing Figure 5.24 b and d in which downward events were implemented, for January, it can be seen that the increase in discomfort due to the lowering of the setpoint between 9 and 11 am was approximately the same both with and without design power limit. This is because, at the time considered, the required load was lower than at the beginning of the morning, so the heating system worked well below the imposed limit. Finally, comparing the two types of events (upward and downward), it can be seen that the variation in the level of comfort determined by a downward event was higher than in the case of an upward event in all months. This is due to the high ventilation that increased the discomfort significantly in the downward case.

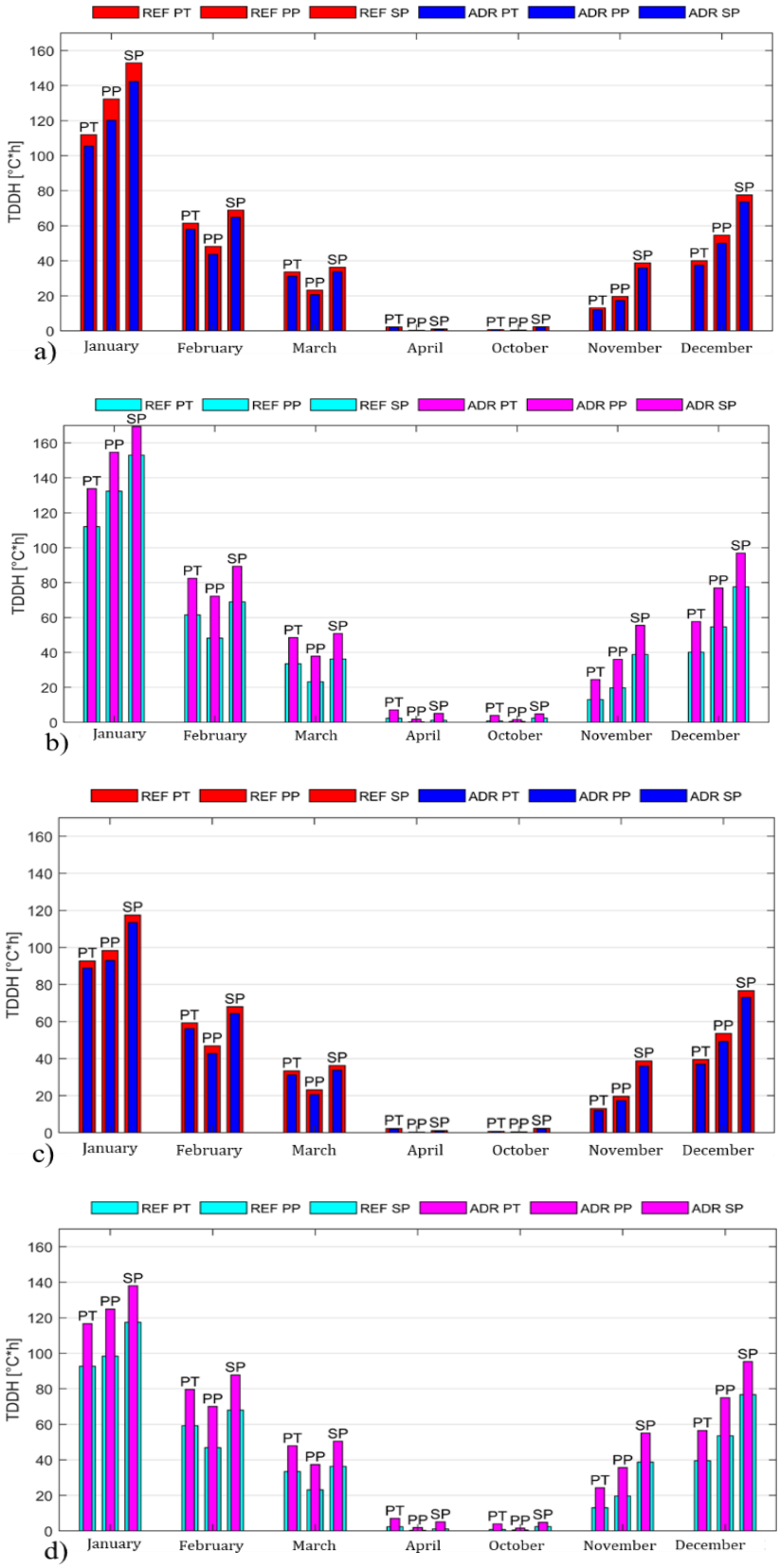

Figure 5.24 Thermal discomfort at each floor of the school building with retrofitted envelope, considering upward (a) or downward event (b) with the heating-up design power and upward (c) or downward event (d) without design power limit.

5.2.4 Conclusions

The study presented in this chapter analyses the sources of energy flexibility that are inherently part of an existing district heating network.

In particular, Section 5.1 shows that by appropriately choosing the mass flow rate circulating through the network, it is possible to shift the thermal load over time, thereby shaving the peak loads. The district heating network of Verona (Italy) was used as a case study. This network operates at constant supply temperature and variable flow rate. The thermal behaviour of the network was simulated using a model based on the finite difference method during two representative weeks –a cold week at the end of February and a mild April week. In the computer simulations, the circulating mass flow rate was varied so that the return temperature increases before (after) the peak load hour to shift the thermal load towards earlier (subsequent) hours. The simulation results showed that the pre-charge process achieves significant results in terms of peak shaving (up to -13% in February and -18% in April) and that the amount of thermal energy shifted in time increases linearly with the number of hours between the start of the flow adjustment strategy and the peak load. A discomfort index has been proposed to evaluate the potential thermal disturbance on buildings served by the network. According to this indicator, the probability of discomfort in the cold representative week is about three times higher than in the week of April. In the same discomfort range, the pre-charge control strategy produces better thermal load displacement and peak shaving results than post-charge simulations.

To produce the desired change in the mass flow rate, the district heating operator would need to install one or more bypass pipes that allow the water flow from the supply to the return pipes. Therefore, the effects of the different flow distribution obtained with a different number of bypasses on the network's dynamic behaviour were investigated. The results showed that introducing three bypass pipes sufficiently far from the main supply station improves both the peak shaving and the amount of thermal energy shifted in both reference weeks. Moreover, adding a fourth bypass pipe would not significantly improve these results, thus giving the district heating operator an important design indication.

In Section 5.2, the simulations allowed to define the behaviour of two different building types under varying boundary conditions. Two different types of ADR events were implemented: an upward event before the peak load and a downward event after, both lasting two hours.

The ADR efficiency values achieved by Condominioum I are much greater than those of the school. In particular, among the cases implemented in the apartment building, an ADR event carried out on all apartments of all floors yields a significantly better ADR efficiency than a single event carried out on a separate equivalent dwelling on the ground floor of the building. Again, the worst case considered in terms of ADR efficiency is that of an ADR event implemented on a single floor. However, a distinction should be made based on the period of the season considered since the separate dwelling performs better than the condominium in the warmer months, although the overall seasonal average performance is still favourable towards the latter.

Regarding the comparison between the requalified case and the reference one, it can be said that the former is generally always better in terms of ADR efficiency. This is especially true with the residential building, while in the case of the school, the high ventilation loads reduce the gap.

Not expected was that the ADR efficiency depended so strongly on the heating system design power. Particularly with the residential building in the requalified version, the ideal case without power limitation performs best with maximum ADR efficiency close to 95%. But what is counter-intuitive is that these high-efficiency values occur in the coldest months when lower external temperatures and higher transmission losses should correspond to lower ADR efficiency. This particular behaviour is due to the specific thermal profile determined when the heating system is oversized. On the other hand, setting a sufficiently limited design power (without heating-up power) reverses the ADR efficiency trend for the case of the separate house, with maximum ADR efficiency values obtained for the warmer months.

As far as thermal comfort is concerned, the requalified version is always the most comfortable. However, the case of the school is worse than the residential building since the high ventilation loads favour the increase of discomfort in the case of downward events while the rise of comfort for upward events is very low.

Regarding the ability to move energy, the separate dwelling is on average more performing than the condominium and the difference increases in the requalified version. In general, the ability to move energy is much lower in the requalified case. This result was expected and perfectly in line with the results seen in the scientific literature.

CHAPTER 6 SYSTEM CONTROL

As a second step, the objective of the research work was to exploit the main sources of energy flexibility that are part of DHN system with two different types of control. These are the Supply Station Control (SSC), which considers centralized thermal storage and the thermal capacitance of the water in the network pipelines, and the Demand Side Control (DSC), which exploits the building thermal capacitance.

6.1 Supply Station Control

The SSC is a model predictive control (MPC), characterized by a MILP optimization problem to schedule the heat supply units of the district heating network of Verona based on heat demand, waste heat availability and electricity price forecasts. Coupling the optimization problem to the model NeMo, allowed to repeat the scheduling with a rolling horizon scheme. The objective of the proposed control strategy was to minimize the operational costs for the DH operator using only the thermal capacitance of the water enclosed in the network pipelines as a thermal buffer in a first phase, and also a thermal storage tank installed in the main supply station, in a second phase.

6.1.1 The optimization problem

The optimization problem relies on a *Mixed-Integer Linear Programming* (MILP) formulation, meaning that all the relations between physical variables (e.g. energy balances) are formulated as linear equality and inequality constraints. This subsection resumes the optimization variables, the constraints and the cost function to minimize. The values of the variables are discretized and considered constant through the time step. The problem has 27 "physical" independent variables summarized in Table 6.1. If the time horizon of the optimization is set equal to 24 hours, there is one schedule of 24 values for each "physical" variable. Therefore, the problem has 27*24 = 648 variables (552 are integers).

Table 6.1 Overview of the optimization variables.

Number	Name	Type	Description
1	T_r	real	Return temperature of the network at the time t
2	n_{chp}	integer	Total number of CHP units in operation at time *t*
3	x_{gb}	integer	On/off status of the gas boiler at time *t*
4	$Q_{gb,mod}$	real	Heat flow rate supplied by the gas boiler at time t over the minimum heat flow rate
5..9	$x_{chp,1}..x_{chp,5}$	integer	On/off status of each CHP unit at time *t*
10..14	$x_{su,1}..x_{su,5}$	integer	Start-up status of each CHP unit: it is 0 unless the

			considered unit starts up at time *t*
15..19	$x_{sd,1}..x_{sd,5}$	integer	Shut-down status of each CHP unit: it is 0 unless the considered unit shuts down at time *t*
20	n_{hp}	integer	Total number of HP units in operation at time *t*
21..25	$x_{hp,1}..x_{hp,5}$	integer	On/off status of each HP unit at time *t*
26	Q_{hs}	real	Heat flow rate supplied by the centralized storage tank at time t
27	T_s	real	Mean temperature of the storage tank at the time t

The network energy balance is considered as a linear constraint, as shown in Equation (6.1). The index *j* in the equations refers to the j-th hour. Thus, the following holds true for *j* = 1...24:

$$\rho \frac{V}{2} c_p \frac{d\boldsymbol{T_r}}{dt} = \boldsymbol{Q_{hs}} + Q_{gb,min}\, \boldsymbol{x_{b,j}} + \boldsymbol{Q_{gb,mod,j}} + Q_{wh,j} - Q_{dem,j} - UA\left(\frac{T_{supp,j}+\boldsymbol{T_{r,j}}}{2} - T_{g,j}\right) \quad (6.1)$$

Where V is the total volume of water enclosed in the network pipelines; $Q_{gb,min}$ is the minimum thermal energy when the gas boiler is in operation; $Q_{wh,j}$ is the available waste heat recovered from an industrial process at j-th hour; $Q_{dem,j}$ is the total heat demand at the user substations at j-th hour; UA is the heat loss coefficient of the pipes; $T_{supp,j}$ and $T_{g,j}$ are the network supply temperature setpoint and the ground temperature at j-th hour. By shifting all the unknown variables to the left side, Equation (6.1) becomes:

$$\left(\frac{\rho V c_p}{\Delta t} + \frac{UA}{2}\right)\boldsymbol{T_{r,j}} - \left(\frac{\rho V c_p}{\Delta t}\right)\boldsymbol{T_{r,j-1}} - \boldsymbol{Q_{hs}} - Q_{gb,min}\,\boldsymbol{x_{b,j}} - \boldsymbol{Q_{gb,mod,j}} = Q_{wh,j} - Q_{dem,j} - \frac{UA}{2}\left(T_{supp,j} - T_{g,j}\right) \quad (6.2)$$

Including the thermal capacitance of the grid $\left(\frac{\rho V c_p}{\Delta t}\right)$ in Equation (6.1) means that the network is modelled as an equivalent thermal storage system, which allows the optimization to store heat in the thermal grid when convenient. According to this strategy, the state of charge of the network is indicated by only one value, which can be interpreted as the average temperature of the heat carrier fluid in the return pipes (T_r).

In Equation (6.3) there is the energy balance of the storage tank, which is considered connected only to cogeneration units and heat pumps, at the generation side.

$$\left(\frac{\rho V c_p}{\Delta t} + UA\right)\boldsymbol{T_{s,j}} - \left(\frac{\rho V c_p}{\Delta t}\right)\boldsymbol{T_{s,j-1}} + \boldsymbol{Q_{hs}} - Q_{chp,nom}\,\boldsymbol{n_{chp,j}} - Q_{hp,nom}\boldsymbol{n_{hp,j}} = UA\,(T_{amb}) \quad (6.3)$$

Where $Q_{chp,nom}$ is the heat production of each cogeneration unit in nominal condition; Q_{hp} the heat production of each heat pump connected to the corresponding CHP unit; T_{amb} the temperature in the supply station where there is the storage tank.
In Equation (6.4), the number of operating cogeneration plants is equal to the sum of the on/off status of each CHP unit:

$$\boldsymbol{n_{chp,j} - x_{chp1,j} - x_{chp2,j} - x_{chp3,j} - x_{chp4,j} - x_{chp5,j} = 0} \quad (6.4)$$

In Equation (6.5), the number of operating heat pumps is equal to the sum of each heat pump's on/off state.

$$\boldsymbol{n_{hp,j} - x_{hp1,j} - x_{hp2,j} - x_{hp3,j} - x_{hp4,j} - x_{hp5,j} = 0} \quad (6.5)$$

The optimization problem is characterised by 648 variables and 96 equations. Therefore, the optimization problem has 552 degrees of freedom, which correspond to the optimal schedules of 23 decision variables. Inequalities (6.6) and (6.7) express that the heat output of the gas boiler is modulated between $Q_{gb,min}$ and $Q_{gb,max}$ and only if the gas boiler is on ($x_{b,j}$= 1). Inequality (6.8) defines the minimum amount of the total thermal output delivered to the network at each time step using the coefficient k_{dem}, which ranges from 0 to 1. In the first case, there could be moments with no heat delivered to the networks, whereas higher values of k_{dem} make the heat production follow the heat demand. Inequalities (6.9)-(6.11) define the moment when a start-up of the CHP occurs ($x_{su,j}$= 1), which is needed to apply a penalty for an excessive number of start-ups. They are repeated five times, once for each CHP unit. Inequalities (6.12)-(6.14), instead, define the moment when a shut-down of any CHP units occurs ($x_{sd,j}$= 1). Therefore, they are also repeated five times. Inequality (6.15) establishes that a heat pump can be switched on only if the corresponding cogeneration engine is running. Inequalities (6.16)-(6.17) establish that at the end of the simulation horizon, the average temperature of the storage tank and the return temperature of the network are greater or equal to the initial ones. These constraints avoid that at the end of the simulation, the tank's energy levels and the network are lower than the initial ones, providing energy for free. Furthermore, inequality (6.18) constrains the heat supplied by the storage tank to the network as a function of the difference between the average temperature inside the tank and the return network temperature, with a heat transfer coefficient (k_{he}).

$$\boldsymbol{Q_{gb,mod,j}} \leq (Q_{gb,max} - Q_{gb,min}) \quad (6.6)$$

$$-Q_{gb,max} * \boldsymbol{x_{b,j}} + \boldsymbol{Q_{gb,mod,j}} \leq 0 \tag{6.7}$$

$$-Q_{chp,nom} * \boldsymbol{n_{chp,j}} - Q_{gb,min} * \boldsymbol{x_{b,j}} - \boldsymbol{Q_{gb,mod,j}} \leq Q_{wh} - k_{dem} * Q_{dem} \tag{6.8}$$

$$\boldsymbol{x_{su1,j}} \geq \boldsymbol{x_{chp1,j}} - \boldsymbol{x_{chp1,j-1}} \dots \boldsymbol{x_{su5,j}} \geq \boldsymbol{x_{chp5,j}} - \boldsymbol{x_{chp5,j-1}} \tag{6.9}$$

$$\boldsymbol{x_{su1,j}} \leq \boldsymbol{x_{chp1,j}} \dots \boldsymbol{x_{su5,j}} \leq \boldsymbol{x_{chp5,j}} \tag{6.10}$$

$$\boldsymbol{x_{su1,j}} \leq 1 - \boldsymbol{x_{chp1,j-1}} \dots \boldsymbol{x_{su5,j}} \leq 1 - \boldsymbol{x_{chp5,j-1}} \tag{6.11}$$

$$\boldsymbol{x_{sd1,j}} \geq \boldsymbol{x_{chp1,j-1}} - \boldsymbol{x_{chp1,j}} \dots \boldsymbol{x_{sd5,j}} \geq \boldsymbol{x_{chp5,j-1}} - \boldsymbol{x_{chp5,j}} \tag{6.12}$$

$$\boldsymbol{x_{sd,j}} \leq \boldsymbol{x_{chp1,j-1}} \dots \boldsymbol{x_{sd,j}} \leq \boldsymbol{x_{chp1,j-1}} \tag{6.13}$$

$$\boldsymbol{x_{sd1,j}} \leq 1 - \boldsymbol{x_{chp1,j}} \dots \boldsymbol{x_{sd5,j}} \leq 1 - \boldsymbol{x_{chp5,j}} \tag{6.14}$$

$$\boldsymbol{x_{hp1,j}} - \boldsymbol{x_{chp1,j}} \leq \boldsymbol{0} \text{ ..... } \boldsymbol{x_{hp5,j}} - \boldsymbol{x_{chp5,j}} \leq \boldsymbol{0} \tag{6.15}$$

$$\boldsymbol{T_{s,0}} - \boldsymbol{T_{s,H}} \leq 0 \tag{6.16}$$

$$\boldsymbol{T_{r,0}} - \boldsymbol{T_{r,H}} \leq 0 \tag{6.17}$$

$$\boldsymbol{Q_{hs}} - k_{he} * (\boldsymbol{T_{s,j}} - \boldsymbol{T_{r,j}}) \leq 0 \tag{6.18}$$

The objective function of the optimization aims to minimize the overall operational costs of the system, as given in Equation (6.19).

$$\begin{aligned} f = \sum_{j=1}^{H} \Bigg(& Q_{chp,nom} \left(\frac{c_{gas}}{\eta_{chp}} - p_{el,sell}\, \delta + c_{man,chp} \right) \Bigg) \boldsymbol{n_{chp,j}} \\ & + \left(Q_{hp,nom} \left(\frac{(p_{el,sell} + a_{hp})}{COP} + c_{man,hp} \right) \right) \boldsymbol{n_{hp,j}} + \left(Q_{gb,min} \left(\frac{c_{gas}}{\eta_{gb}} + c_{man,gb} \right) \right) \boldsymbol{x_{b,j}} \\ & + \left(\frac{c_{gas}}{\eta_{gb}} + c_{man,gb} \right) \boldsymbol{Q_{gb,mod,j}} + c_{wh}\, Q_{wh,j} - c_{TEE} * TEE * Q_{wh,j} \end{aligned} \tag{6.19}$$

where c_{gas} is the cost of the gas used by the gas boilers and the internal combustion engines; $Q_{chp,nom}$ the heat production of each natural gas cogeneration engine operating in nominal condition; η_{chp} the efficiency of each cogeneration engine; $p_{el,sell}$ is the selling price of electricity; δ is the ratio between the power and heat production of the cogeneration engine in nominal condition; $c_{man,chp}$ the maintenance cost of each cogeneration engine; $Q_{hp,nom}$

the heat production of each heat pump operating in nominal condition; a_{hp} is the excise duty paid for the electrical energy used in the heat pump; COP is the coefficient of performance of the heat pump; $c_{man,hp}$ the maintenance cost of each heat pump; η_{gb} is the efficiency of the gas boiler; $c_{man,gb}$ the maintenance cost of the gas boiler; c_{wh} is the cost of the waste heat. The Italian energy efficiency certificates can discount this cost. c_{TEE} is the monetary value of each energy efficacy certificate; TEE is the number of efficiency certificates corresponding to 1 MWh of recovered waste heat. In conclusion, the optimization problem is subjected to equations (6.2) – (6.5) and to inequalities (6.6) – (6.18) and consists of the minimization of the objective function f.

6.1.2 Simulation framework and main assumptions

The optimization problem was executed iteratively within a district heating network simulation of the thermal grid described in the previous section. The coupling of the optimal control problem with the heat distribution in the model predictive control (MPC), allows to (i) assess the benefits of the proposed control strategy on a time interval bigger than the time horizon of the model predictive controller and (ii) consider the deviations of the district heating system from the predictions of the controller, thus improving the reliability of the results.

As shown in Figure 6.1, the set of optimization variables that determine the heat generated at each time step is then used to determine the total mass flow rate circulating in the network. As shown in a previous study [83], the mass flow rate modulation allows the DH system operator to charge and discharge the network to pursue an economic objective. The optimal controller calculates the objective at each time step to minimize the operational costs depending on 24-hours ahead forecasts of heat demand, waste heat availability, and electricity prices. The return network temperature, which is an output of the detailed network simulation, is used as a feedback signal from the system, and it is updated with hourly time-step. So, the decisions taken by the optimal controller are always linked to a measurable physical variable that represents the "current state" of the network. The mass flow rate setpoint is thus the link between the output of the optimization and the input of the district heating network model.

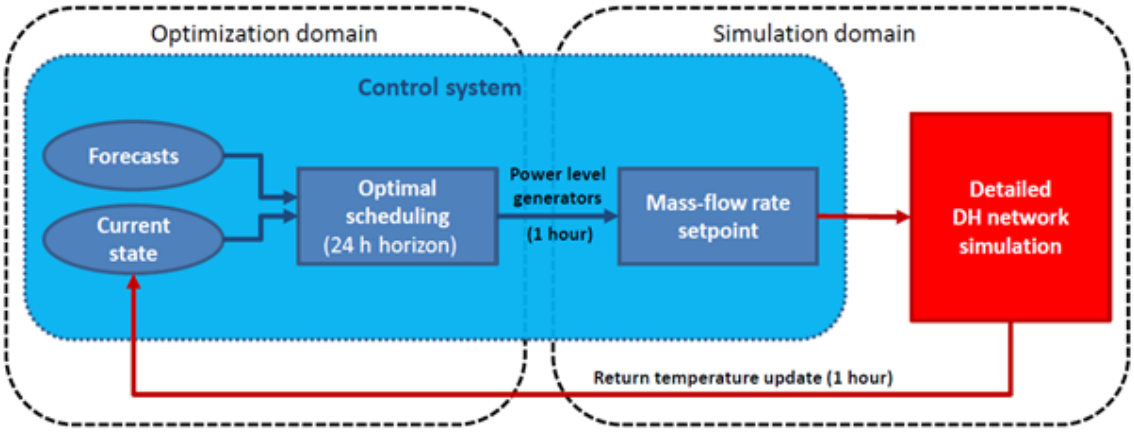

Figure 6.1 Schematic illustration of the coupling between the optimization problem and the detailed district heating network simulation.

In reality, the DH operator does not control directly the mass flow rate but only the head of the circulation pumps. Nonetheless, the operator could vary the circulating mass flow rate by opening and closing a limited number of by-pass valves installed in strategic points of the network. The opening of the valves relies on the mass flow rate setpoint that is currently set through Equation (6.20):

$$G_{tot} = \frac{\alpha\, Q_{gen} + (1-\alpha)\, Q_{dem}}{c_p (T_{supp} - T_r)} \tag{6.20}$$

Equation (6.20) outlines that the mass flow rate setpoint depends both on the current heat demand Q_{dem} and the current heat supply Q_{gen}. When α = 0 the situation is similar to the current flow control, where the mass flow rate only depends on the users heat demand. In the opposite situation (α=1), the mass flow rate only depends on the decisions taken by the optimal controller. This setting would lead to moments when the heat carrier fluid is not circulating and all the heat is provided by the network temperature variation. This situation, predicted by the linear model inside the controller, is not realistic and leads to a very unstable operation of the heat generators. Moreover, a still heat carrier fluid would probably lead to discomfort for the users. The value α=0.3 was found to be a good compromise between the optimal control strategy of the heat generators and the heating needs of the DH customers.

The DH network was simulated over two reference weeks that adequately represent the system behaviour for the entire year:

- A winter week (WW), from February 27th to March 5th. The thermal load ranges between 7 and 30 MW_t with an average value of 14.15 MW_t. It is supplied by the cogeneration plants,

which run almost always under full-load, the heat pumps, the heat recovered from the foundry and the gas boilers, which supply the remaining part of the heat load;
- A week during the middle season (MSW), from the 24th to 30th of April, in which the thermal load ranges from 2.5 to 10 MW_t and its average value is equal to 4.8 MW_t. The heat demand is provided by a single CHP (2.2 MW_t) always at full load, the heat pump connected to the operating CHP, the waste heat and the gas boilers.

The return temperature in the optimization problem can vary between 55°C and 70°C. The average temperature difference between supply and return lines may change between 10°C and 25°C. These values are realistic compared to the temperature difference fluctuations recorded by the DHN operator at the supply station CCC. The mean temperature of the virtual HS (T_s) can range between 95 °C and 75 °C. The aforementioned parameter k_{dem} was set equal to 0.6. The CHP engines, which have a thermal efficiency of 38% in nominal conditions, can be switched either on or off, and the same holds true for the corresponding heat pumps, with COP = 4. Therefore, they behave as "improved" CHP units with higher thermal and lower electrical efficiency than stand-alone internal combustion engines. Start-up and shut-down costs were set empirically so that the engines do not start up more than three times a day, as required by the DHS operator. The gas boilers are indicated here as a unique heat generator called GB, with a thermal efficiency equal to 0.9%. So, it can modulate its thermal output from 0.1 MW to 25.5 MW. The simulation time-step was set to 1 hour.

6.1.3 Results

The optimization problem has been first run without being coupled to the district heating simulation using a one-week horizon for both reference weeks. Therefore, these results represent a benchmark scenario (OPT), i.e. what can be ideally achieved if the (simulated) system perfectly follows the heat supply schedules predicted by the optimization.

Then, the optimization has been coupled to the detailed DH simulation model as described in Section 6.1.2. Finally, the DH is operated with a model predictive controller (MPC) based on the same optimization problem in the simulated scenarios. Both OPT and MPC results consider either the network as the only source of flexibility (net scenario) or the network combination and the additional heat storage (net+hs scenario).

The operational costs were compared to the current ones under the same boundary conditions to evaluate the strategies. The current costs depend on the current regulation explained in the

description of the case study. The selling price of electricity was evaluated using the Italian national market price (PUN) profile of the year 2017. In the WW the average PUN is 48.6 €/MWh and ranges between 30 and 66.9 €/MWh with significant daily cycles. A similar trend occurs in the MSW, with the minimum price falling to 15 €/MWh. An excise duty a_{hp}= 12.5 €/MWh is imposed on the electrical energy consumed by the heat pumps. The cost for the natural gas used for both the gas boilers and the internal combustion engines was assumed equal to approximately c_{gas}= 32 €/MWh after the conversion. The waste heat recovered by the foundry is valued c_{wh}= 20 €/MWh. This cost is discounted by the Italian energy efficacy certificate, which is 250 €. One TEE is obtained, recovering about 7.7 MWh of waste energy. Furthermore, the following maintenance costs have been considered for the different generation plants: $c_{man,chp}$= 7 €/MWh, $c_{man,hp}$= 0.5 €/MWh, $c_{man,gb}$= 1 €/MWh.

6.1.3.1 Optimization results during two representative days

Figure 6.2 and Figure 6.3 show the forecasts (heat demand, waste heat availability and PUN), the heat supplied by the production plants to the network, the schedules calculated by the optimization, the return temperature of the water inside the pipes (T_r) and the temperature inside the storage tank (T_s) for two representative days, -i.e. Monday of both middle season (MSW) and winter weeks (WW).

As far as the results of the typical middle season day are concerned, Figure 6.2a compares the users heat demand (Q_{dem}) with the thermal energy supplied to the district heating network (Q_{supp}). As it can be seen during the first 5 hours, the return water temperature decreases or increases depending on whether the energy supplied by WH, GB and the heat storage tank (HS) is respectively lower or higher than the heat demand. From hour 4 to 8, when the electricity price starts to rise, the CHP increases the supplied thermal energy. Part of the energy produced by the cogeneration units and HP is stored in the tank, increasing T_s, when CHP+HP is greater than HS, as it can be seen in Figure 6.2b and Figure 6.2c. In the same way, the network is charged because Q_{supp} is higher than Q_{dem}. From hour 8 to 14, the CHP production decreases in response to the reduction of the electricity price (Figure 6.2d). From hour 14 to 15, the energy previously stored in the tank is used, and only WH and HS supply heat. From hour 15, the electricity price increases again, the CHP increases the supplied thermal energy and the pattern seen from hour 4 to 15 is repeated. As regards

the level of heat storage in the tank, at the end of the simulation period, the average temperature inside the tank T_s is equal to the initial one (Figure 6.2c), so the constraint defined by inequality (6.16) is respected.

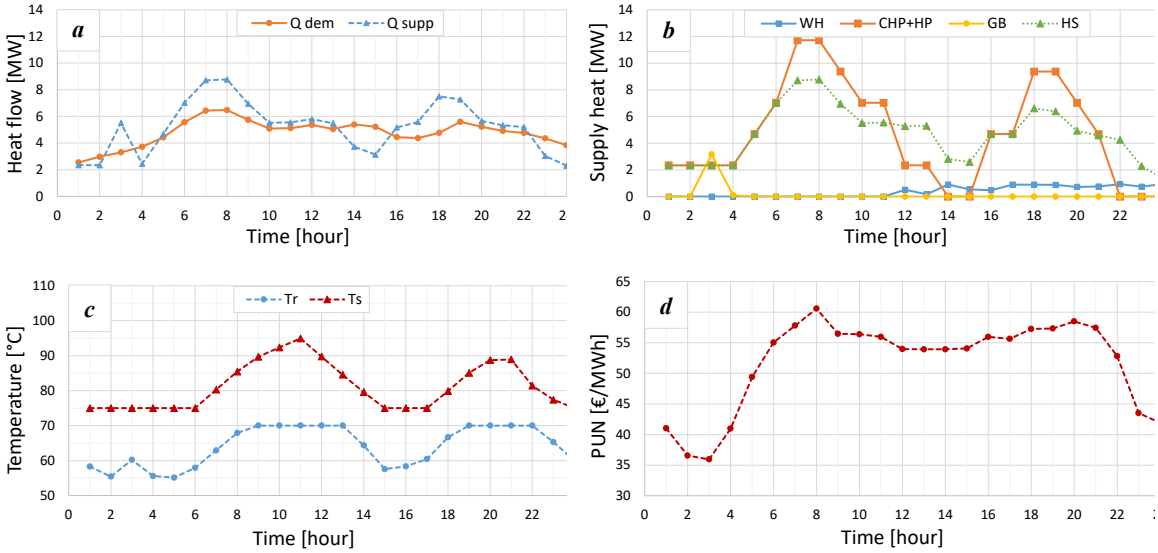

Figure 6.2 Simulation results for a typical middle-season day: (a) heat demand and heat supply; (b) heat supply mix; (c) average return temperature; (d) electricity price.

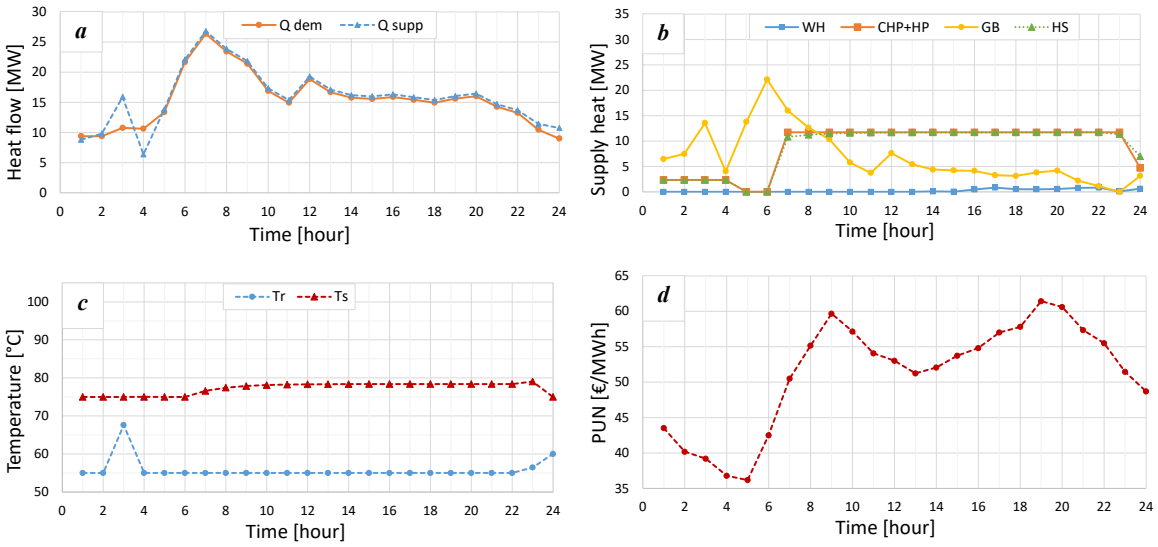

Figure 6.3 Simulation results for a typical winter day: (a) heat demand and heat supply; (b) heat supply mix; (c) average return temperature; (d) electricity price.

During the first three hours of the typical winter day, the network is charged due to the higher thermal input in the network compared to the heat demand. Accordingly, the water temperature inside the pipes increases in these hours, as shown in Figure 6.3c. Furthermore, in the first four hours, the electricity price -see Figure 6.3d- is high enough to produce

thermal power with a CHP unit, as shown in Figure 6.3b. Instead, from hour 4 to hour 5, the electricity price is low, so the heat demand is satisfied by the GB. From hour 7 to hour 23, all the cogeneration engines are running at full capacity, and the GB are modulated to follow the energy demand. About the thermal power supplied by the storage tank, it mostly follows the production of CHP+HP (Figure 6.3b), except from hour 6 to 10 in which it is lower, determining an increase of the temperature inside the tank (T_s) -see Figure 6.3c-, and in the last 2 hours in which is higher.

6.1.3.2 Simulation results of the model predictive control

The most critical part of the simulation framework is coupling the optimization model and the district heating network model to form the model predictive controller (MPC). In general, the MPC output differs from that of the optimization model (OPT). This is because, in the optimization model, the network is considered a one-capacitance model. In contrast, the network behaviour is accurately represented in the simulation using the detailed model NeMo. To match the outputs of the MPC to those of the optimization as much as possible, the mass flow rate has to be controlled as specified in paragraph 6.12. The most significant differences in the outputs of the two models are represented by the return temperatures (T_r), shown in Figure 6.4a, and the thermal power supplied by the storage tank to the network (Q_{hs}) (Figure 6.4b). Figure 6.4a and Figure 6.4b refer to the representative middle season week.

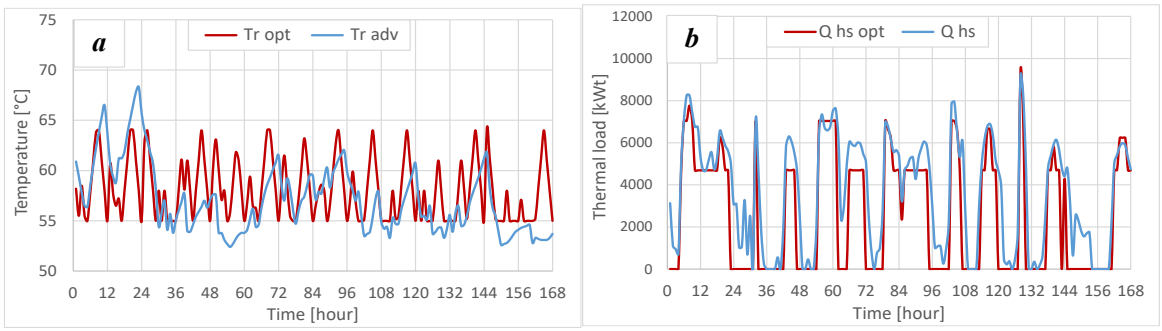

Figure 6.4 Comparison between OPT (red) and MPC (blue) considering respectively the outputs (a) T_r and (b) Q_hs in the MSW.

The difference between the simulation results and the optimisation problem solution determines an increase in the operational cost, as shown in Table 6.2. This is due to the oversimplification of the network thermal behaviour in the optimization constraints, leading to state estimation errors, especially in the middle season week.

Table 6.2 Differences in the operational cost between the OPT, MPC and BAS.

	MSW		WW	
	net	net+hs	net	net+hs
OPT	27,139 €	26,281 €	78,066 €	77,666 €
MPC	29,713 €	27,100 €	80,623 €	80,156 €
BAS	33,953 €		85,595 €	

As mentioned above, the cost values determined by the optimization model in the different cases can be considered a benchmark. Therefore, the cost results of the MPC are between these benchmarks and the operational costs in the basic control (BAS). To analyse more in detail the improvement determined by the advanced control, the scheduling of the basic control (Figure 6.5a) is compared with those of MPC, considering the thermal capacitance of the network (the heat carrier fluid inside the network pipelines), in Figure 6.5b, and of both the network and the storage tank (Figure 6.5c) respectively. The period considered is the MSW.

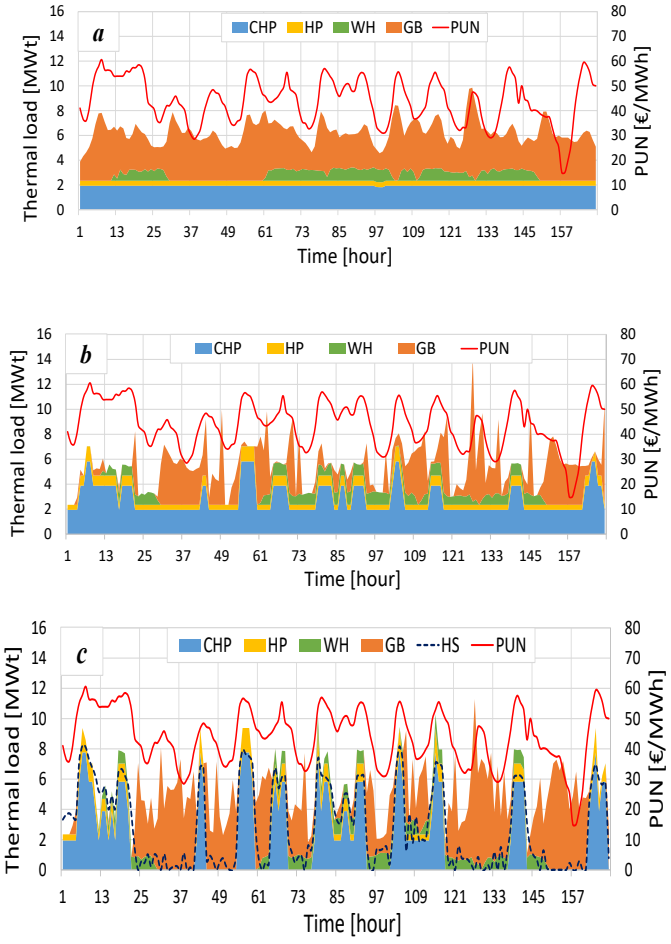

Figure 6.5 Scheduling of the heat generators during the middle season week (a) under current control; (b) under MPC using the thermal capacitance of the network; (c) under MPC using both the network and the storage tank.

The strategy adopted by the advanced control, Figure 6.5b, is to supply heat with a single cogeneration unit and to increase the thermal energy production from CHP only when the value of PUN (the red line in Figure 6.5) is higher than a threshold value (about 45 €/MWh). This determines a higher modulation of CHP units than the basic control case (Figure 6.5a). When the electricity price exceeds the threshold value for a very short period (hours 30 and 128), extra cogeneration units don't turn on to avoid an excessive number of start-ups and shut-downs in a limited period. In Figure 6.5c, considering the thermal capacitance of both the network and the storage tank, the thermal load profile is characterised by higher peak than in Figure 6.5b. This is due to the greater thermal storage capacity of the system, which allows to produce more thermal power with CHP and HP and to accumulate the production in excess in the storage tank when the electricity price is high. On the other hand, when the electricity price is low, the storage tank can supply the stored energy (blu dotted line in Figure 6.5c).

The energy production of the heat supply units and the corresponding share within the heat supply mix, which characterize the different types of control, are shown in Table 4 and 5, respectively, for the MSW and WW.

In the MSW, the strategy adopted by the model predictive control allows a higher share of the heat produced by the CHP units than the basic control (from 31.8% to 49%). As a result, in this last case the MPC allows a reduction of heat produced by gas boiler (53.3% in the BAS, 32% in MPC under "net" scenario). The remaining share of the heat demand is covered by the heat pumps (10%) and by the waste heat sources (9%). Considering also the storage tank, the share of the heat produced by CHP is 37%, so we have an increase compared to the basic control and a decrease compared to the "net" scenario.

On the other hand, in the WW the advanced control determines an increase of heat produced by GB and a reduction of the share supplied by CHP (from 62% in the BAS to 45% in the MPC). This is because, in this case, differently from the basic control, the CHP plants are not in operation when the electricity price is lower than a threshold value. When it is high enough, the total installed power of the CHP plants is not sufficient to supply the entire heat demand. The addition of the storage tank determines a decrease of this share to 41.5%. The heat supplied by the HP is characterised by the same trend of the CHP in both "net" and "net+hs" scenarios. During the simulated periods, the proposed model predictive controller reduces the operational costs of 12.5% and 5.8% in the MSW and in the WW, respectively.

This cost reduction is mainly due to the cost-optimal scheduling of the heat supply units, but also to a reduction in the heat supplied to the customers, as shown in Table 6.3 and Table 6.4. Furthermore, considering a greater thermal storage capacity of the system, determined by the tank, the cost savings increase up to 20% in the MSW and to 6.3% in the WW. So, in the representative middle season week, in which the total installed power of the CHP and HP plants is sufficient to supply the entire heat demand during the peak, the modulation of CHP and HP units has a higher impact, and the percentage increase of the cost reduction determined by the HS is higher.

Table 6.3 Energy and cost balance of the simulated DH network in MSW.

	BAS		MPC net		MPC net+hs	
	[MWh]	[€]	[MWh]	[€]	[MWh]	[€]
CHP	325 31.8%	13,929	458 49%	18,160	343 37%	11,384
HP	67 6.6%	982	94 10%	1,433	70 8%	1,166
GB	545 53.3%	19,927	301 32%	11,000	422 46%	15,428
WH	84 8.3%	-885	84 9%	-880	84 9%	-878
TOT	1,061	33,953	937	29,713	919	27,100
Cost savings	-		4,240 € 12.5%		6,853 € 20%	

Table 6.4 Energy and cost balance of the simulated DH network in WW.

	BAS		MPC net		MPC net+hs	
	[MWh]	[€]	[MWh]	[€]	[MWh]	[€]
CHP	1,612 62%	60,247	1,137 45%	39,631	1,040 41.5%	35,244
HP	309 11.9%	4,898	237 9.5%	3,890	217 8.5%	3,605
GB	587 22.5%	21,449	1,042 41.5%	38,103	1,157 46%	42,307
WH	95 3.6%	-999	95 4%	-1000	95 4%	-1000
TOT	2,603	85,595	2,511	80,624	2,509	80,156
Cost savings	-		4,971 € 5.8%		5,439 € 6.3%	

The three main results and the related discussions are remarked in this section.
In the optimization problem, the oversimplification of the network thermal behaviour results in an underestimation of the operational cost in comparison to the MPC, which considers a detailed district heating network model. This is true especially in the representative middle season week when the cost result of the optimization problem is 8.5% lower than that evaluated by the MPC, in the scenario with the storage tank.
The cost reduction determined by MPC (exploiting the thermal capacitance of the network) compared to the basic control is more relevant in the MSW (-12.5%) than in the winter one (-5.8%). This is in accordance with the results of previous research work [75], in which it was demonstrated that in the coldest period, the flexibility potential of the network is lower.
By adding a centralized storage tank, the cost savings increase much more in the MSW (20%) than WW (6.3%). The result is related to the case study under consideration. The total installed thermal power of the cogeneration engines and heat pumps connected to the centralized storage tank is limited compared to the peak load during WW. In this period, the CHP and HP plants can't produce more energy than the basic control when the electricity price is high. So, a small amount of energy is accumulated in the storage tank, and his flexibility potential is not fully exploited.

6.2 Demand Side Control

The demand side control developed in this research is characterised by many simplifications, described in Section 6.2.1 and 6.2.2, and aimed primarily at giving an idea of the potential of the source of energy flexibility represented by the thermal capacitance of the building envelope.

6.2.1 Concept

The concept is resumed in Figure 6.6. It consisted of considering the substations connected to the DHN as storage tanks to exploit the buildings envelope's thermal capacitance and modify their heat demand pattern. So, each user substation was a virtual storage tank. In accordance with the typology of the substation, the virtual storage tanks were characterized by different values for the volume and the heat transmission coefficient. These parameters were evaluated thanks to Active Demand Response simulations of a residential and a tertiary building (the Condominium I and the School A) analysed in Chapter 5.2. Furthermore, it

was possible to define the new thermal load profiles of the considered user substations from the ADR simulations. Finally, the optimization was performed at the district level, also considering the thermal energy price and the external temperature forecasts and determining the optimized energy demand and the average indoor temperature of each substation.

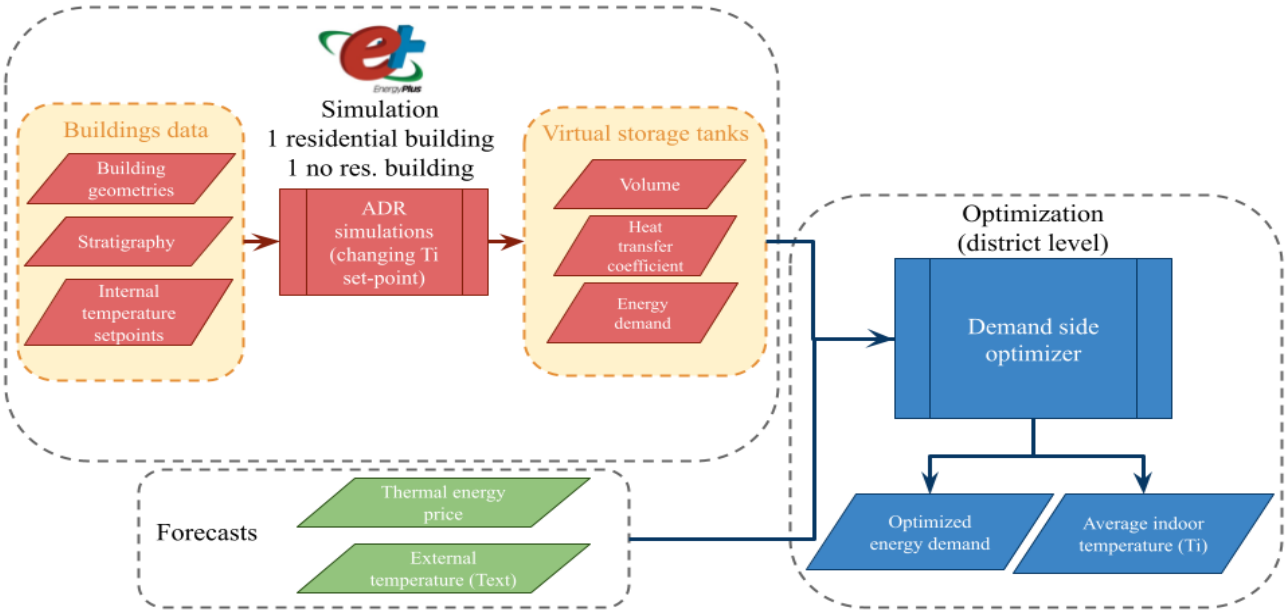

Figure 6.6 Schematic illustration of the Demand Side Control concept.

6.2.2 Method

6.2.2.1 The controlled user substations at the district level

As said in Paragraph 3.1.2, the DHN of Verona Centro Città is connected to 247 user substations, but only for 16 of these the monitoring data was accurate enough. An important monitoring output was the hourly energy consumption. The 16 substations were divided into residential and tertiary buildings. So, the nine residential and seven tertiary structures of Table 6.5 were selected.

Table 6.5 Volume and annual heating demand of the selected monitored substations.

Typology	Volume [m^3]	Annual heating demand [MWh]
Condominium A	18377	407
Condominium B	18377	386
Condominium C	5000	93
Condominium D	3200	78
Condominium E	12449	293
Condominium F	12000	323
Condominium G	10389	285
Condominium H	5371	167

Condominium I	5943	112
Office A	47415	1028
School A	15067	345
Office B	6000	102
Hotel A	2570	148
Hotel B	13670	234
Office C	17000	276
School B	17532	450

In this way, only 5% of the total thermal load of the 247 user substations connected to Verona DHN was considered. Two residential and nine tertiary buildings were added by raising this percentage, increasing the number of the considered substations to 27. Below Table 6.6 shows the general information of these 11 additional substations.

Table 6.6 Volume and annual heating demand of the additional substations.

Typology	**Volume [m^3]**	**Annual heating demand [MWh]**
Condominium J	47000	1280
Condominium K	13822	557
Office D	31272	1462
Office E	106346	1309
Hotel C	40000	1281
Office F	66000	1236
Office G	49000	1024
Office H	40000	1000
Office I	44000	740
Office J	25220	703
Office K	49000	580

The total thermal load profiles of respectively the residential, office, school and hotel substations of Table 6.5 were calculated. The resulting profiles are shown in Figure 6.7. Then the obtained thermal load profiles were scaled for the different buildings in Table 6.6, in relation to their annual heating demand and typology. So, the hourly energy consumptions of the additional buildings were obtained, and about 20% of the total thermal load of all the substations connected to Verona DHN was controlled with the DSC.

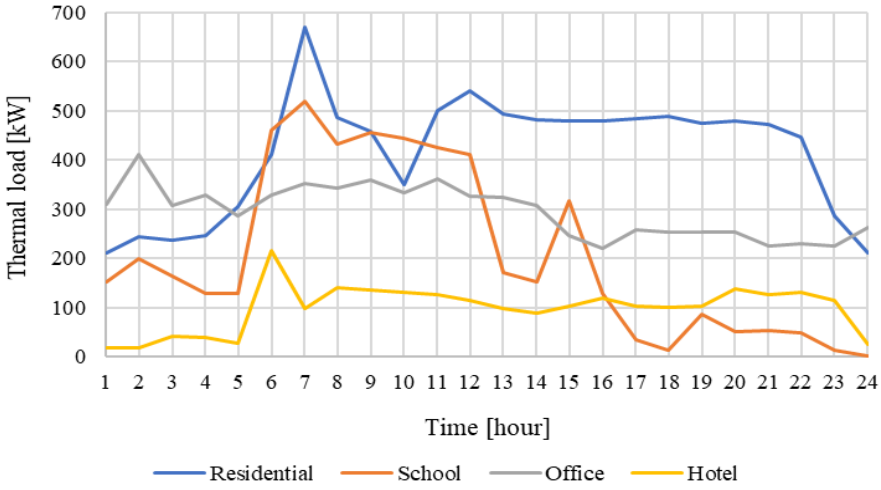

Figure 6.7 Total heat load profiles respectively of all monitored residential, office, school, and hotel substations.

6.2.2.2 Virtual storage tank parameters

Energy Plus simulations were performed respectively for the Condominium Iand the School A, changing the internal temperature setpoint (Ti) schedule in different ways (ADR simulations). As a result, different thermal load profiles were obtained compared to the reference case. Furthermore, the average operative temperature profiles were provided as an output of the ADR simulations. An example of these results for the residential building with upward modulation event is inFigure 6.8.

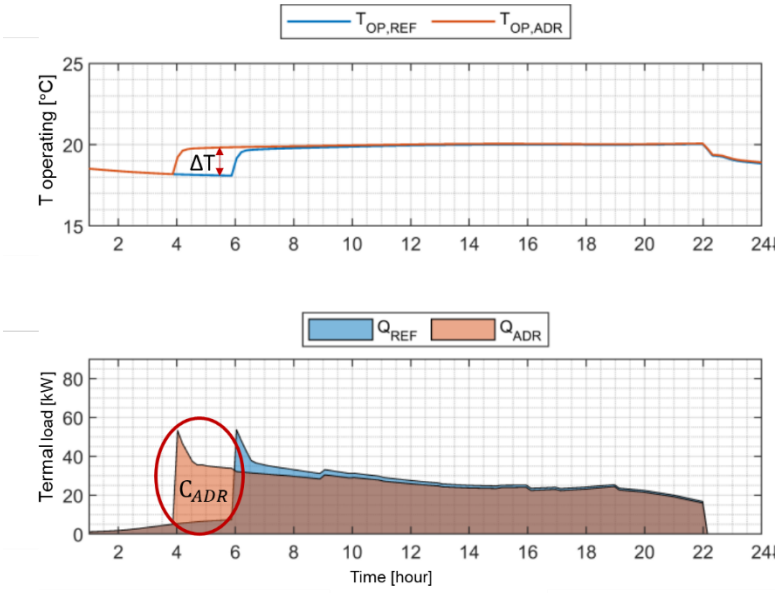

Figure 6.8 Illustration of the difference between the average operative temperatures (ΔT) and the energy moved with the ADR event (C_{ADR}).

Considering the energy moved with the ADR event (C_{ADR}) and the difference between the average operative temperatures (ΔT) resulting respectively in the ADR ($T_{OP,ADR}$) and reference simulation ($T_{OP,REF}$), the Virtual Volume (V) of the corresponding virtual storage tank was calculated in the following way:

$$V = \frac{C_{ADR}}{\rho\, c_p\, \Delta T} \tag{6.21}$$

Where ρ and c_p are respectively the density and the specific heat of the water. While to determine the heat transfer coefficient (U) of the virtual storage tank, the following equation was considered.

$$U = \frac{(1-\eta_{ADR})\, C_{ADR}}{S \int_0^{L_{ADR}} T_{OP,ADR} - T_{EXT}} \tag{6.22}$$

In this equation η_{ADR} is the ADR efficiency, which has been defined in Chapter 5.2; S is the external surface of the considered building; L_{ADR} is the duration of the event.

Considering the V results obtained with Equation 6.21 for the upward and downward ADR simulations at different times during the heating period, the average values respectively for the Condominium I(V_{res}) and the School A ($V_{tertiary}$) were defined. In the same way, the average values of the heat transfer coefficient were determined for the two considered typologies of user substations ($U_{res}, U_{tertiary}$). The following values of the virtual volume and heat transfer coefficient multiplied by the building surface area (UA), reported in Table 6.7, were obtained for the different buildings.

Table 6.7 Virtual Volumes and heat transfer loss coefficients of the considered user substations.

Name	Virtual Volume [m^3]	UA [kW/K]
Condominium A	45.94	0.385
Condominium B	45.94	0.385
Condominium C	12.50	0.105
Condominium D	8.00	0.067
Condominium E	31.12	0.261
Condominium F	30.00	0.252
Condominium G	7.50	0.063
Condominium H	13.43	0.113
Condominium I	14.86	0.125
Office A	56.90	0.93
School A	18.08	0.30
Office B	7.20	0.12
Hotel A	3.08	0.05
Hotel B	16.40	0.27

Condominium A	20.40	0.33
Condominium B	40.00	0.65
Condominium J	117.50	0.985
Condominium K	34.56	0.290
Office D	37.53	0.61
Office E	127.62	2.09
Hotel C	48.00	0.79
Office F	56.40	0.92
Office G	58.80	0.96
Office H	48.00	0.79
Office I	52.80	0.86
Office J	30.26	0.50
Office K	58.80	0.96

6.2.2.3 The optimization problem

The control strategy was based on a *Linear Programming* (LP) optimization problem. In this section, the optimization variables, the constraints, and the cost function to be minimized are resumed. The values of the variables are discretized and considered constant through the time step. Defining m as the number of substations that can be controlled, the problem has 2m "physical" independent variables summarized in Table 6.8. If the time horizon of the optimization (H) is set equal to 24 hours, there is one schedule of 24 values for each "physical" variable. So, considering the 27 user substations selected in the previous chapter as the substations that can be controlled, the problem has 1296 variables.

Table 6.8 Overview of the optimization variables.

Number	**Name**	**Type**	**Description**
1..m	Q_{adr}	real	Heat supplied to the building in active demand response mode
1..m	T_i	real	Average indoor temperature

Regarding the equality constraints, the following equation describes the virtual storage tank energy balance for each considered user substation.

$$\left(\frac{\rho V c_p}{\Delta t} + UA\right) \boldsymbol{T_i}^t - \frac{\rho V c_p}{\Delta t} \boldsymbol{T_i}^{t-1} - \boldsymbol{Q_{adr}}^t = -{Q_{ref}}^t + (UA){T_{out}}^t \quad (6.23)$$

Where Q_{ref} is the thermal energy provided to each building in the reference case; T_{out} is the external temperature. V is the Virtual Volume of water in each virtual storage tank; UA represents the heat loss coefficient of the virtual storage tank.

Finally, there are inequality constraints.

$$\boldsymbol{T_i}^0 - \boldsymbol{T_i}^H \leq 0 \quad (6.24)$$

$$\sum_{t=1}^{H} -\boldsymbol{Q_{adr}}^{t} \leq -\frac{\sum_{t=1}^{H} Q_{ref}{}^{t}}{\eta_{adr}} \quad (6.25)$$

$$19 \leq \boldsymbol{T_i}^{t} \leq 24 \quad (6.26)$$

$$\boldsymbol{Q_{adr}}^{t} \leq Q_{adr,max} \quad (6.27)$$

The first one (6.24) defines that the level of charge of each virtual storage tank at the end of the optimization ($\boldsymbol{T_i}^{H}$) has to be higher or equal to the level of charge at the beginning ($\boldsymbol{T_i}^{0}$). According to the second inequality constraint (6.25), the heat supplied in ADR mode has to take into account the efficiency η_{adr}. The inequality (6.26) constrains the average indoor temperature between 19 and 24 degrees. Finally, the last (6.27) constrains the heat supplied, which has to be equal or lower than the nominal power of the heat exchanger of the considered user substation in each time step. The DHN operator provided the nominal powers of the heat exchangers. The optimal control problem aimed to minimize the operational costs by exploiting the thermal capacitance of the buildings' envelope, and the objective function was the one shown below.

$$f = \sum_{t=1}^{H} (c^{t} * \boldsymbol{Q_{adr,tot}^{t}} * coef_{comfort}{}^{t} * (\boldsymbol{Q_{adr,tot}^{t}} - Q_{ref,tot}^{t})) \quad (6.28)$$

Where $\boldsymbol{Q_{adr,tot}^{t}}$ is the total heat supplied to the user substations in active demand response mode for each time step of the optimization horizon; c^{t} is the cost of the thermal energy; $Q_{ref,tot}^{t}$ is the total heat supplied to the user substations in the reference case; $coef_{comfort}{}^{t}$ is a coefficient that considers the thermal comfort of the user substations. The value of this coefficient can be 0 or 0.001, depending on the time and building considered. Two different $coef_{comfort}{}^{t}$ schedules were considered for the residential and tertiary building, taking into account the presence of people.

6.2.2.4 Main assumptions

The optimizer was run over one day to represent the system behaviour for the winter adequately. The selected day is the 2nd of December. The thermal load ranges between 10 and 37 MW_t with an average of 20 MW_t. It is supplied by the cogeneration plants, which run almost always under full-load, the heat pumps, the heat recovered from the foundry and the gas boilers, which supply the remaining part of the heat load. As said in the inequality constraints, the average indoor temperature (T_i) of each user substation is constrained between 19 and 24 degrees. Furthermore, the initial T_i was supposed equal to 21.5 degrees.

Regarding the forecasts for the external temperature, it was considered the Verona hourly air temperature profile for the 2nd of December 2020, obtained from the weather data of EnergyPlus database.

About the thermal energy cost, two different profiles were considered to perform two different optimizations:

- The real cost profile of the thermal energy (shown in Figure 6.9), knowing the type of generation plants at the supply station and their operation scheduling, to reduce the operative costs.

- A stepwise cost profile of the thermal energy (Figure 6.9), where the step occurs simultaneously with the thermal peak load. This condition was considered to assess the potential for energy flexibility determined by the thermal capacitance of the buildings envelope. The analysis was carried out by considering the peak shaving (Δq_{max}) of the thermal load profile and the *available buildings capacity* ($C_{building}$). The first parameter is the same defined in chapter 5.1.1.2, while $C_{building}$ is the equivalent of the *available network capacity* (C_{net}), considered for evaluating the load shifting results by exploiting the thermal capacitance of the heat carrier fluid inside the network pipelines. The shape of this profile, in which the step starts at the same time as the thermal load peak and last two hours, was thought to obtain an upward modulation event. In fact, the analysis carried out in chapter 5.2 showed that this kind of ADR event, which is characterized by the pre-charge of the buildings envelope, determined the best C_{ADR} results (energy moved).

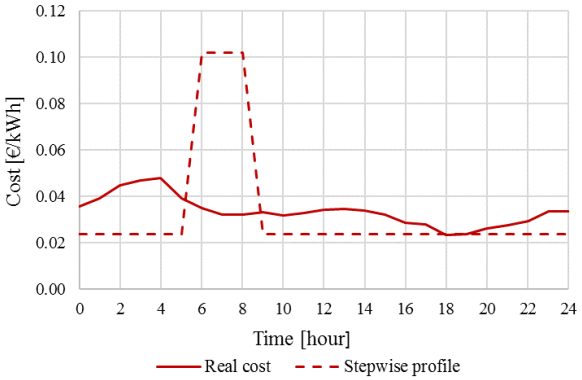

Figure 6.9 Real cost profile and stepwise cost profile of the thermal energy considered for the two different optimizations.

6.2.3 Results

6.2.3.1 Optimization with the real cost profile of the thermal energy

Regarding the results of Demand Side Control, considering the representative winter day and the real cost profile of the thermal energy, in Figure 6.10a, the optimized thermal load profiles respectively of a residential (Condominio Sole Scala A) and tertiary building (Questura di Verona) are shown. The energy was moved compared to the reference cases when the cost of the thermal energy was lower, preloading and discharging the buildings' envelope just like storage tanks. At the same time, the average indoor temperatures were constrained between 19 and 24 degrees (Figure 6.10b), observing the thermal comfort limits.

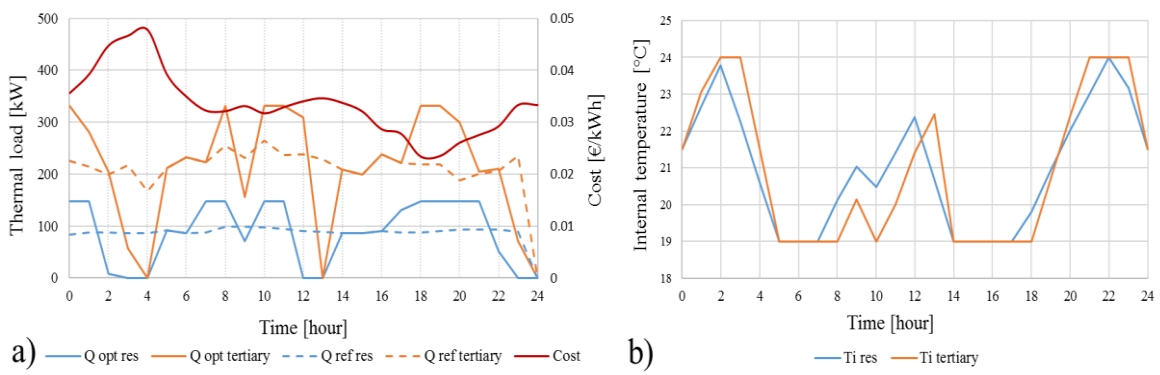

Figure 6.10 The optimized thermal load profiles respectively of a residential and no residential building (a), and the corresponding average indoor temperatures (b).

Finally, the thermal load profiles for the optimized and reference case at the district level for the controlled substations were obtained (Figure 6.11). The optimized one allowed a cost reduction equal to 3.5% compared to the reference case.

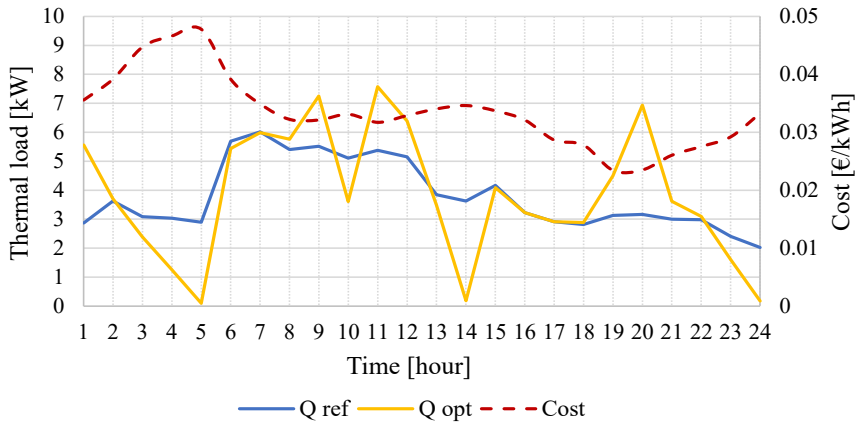

Figure 6.11 Thermal load profiles for the optimized and reference case of the controlled substations at the district level.

6.2.3.2 Optimization with the stepwise cost profile of the thermal energy

Considering the stepwise cost profile of the thermal energy in the representative winter day, the thermal loads of the controlled substations for the optimized (Q_{opt}) and reference case (Q_{ref}) are represented by the orange and blu profiles in Figure 6.12. It can be seen that in the profile resulting from the Demand Side Control (Q_{opt}) the energy was moved before the step of the cost profile by exploiting the thermal capacitance of the buildings envelope. So, considering all the user substations connected to the Verona DHN adding the non controlled buildings, the DSC determined good load shiting and peak shaving results for the optimized thermal load profiles $Q_{tot\ opt}$ compared to the reference case ($Q_{tot\ ref}$).

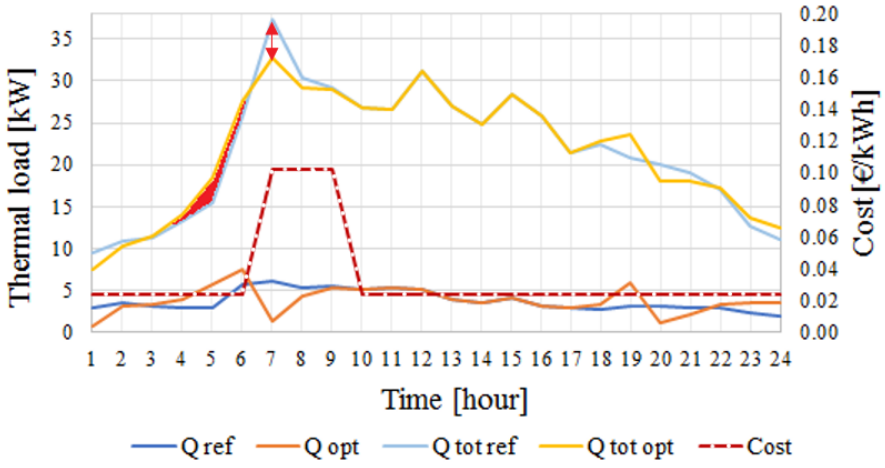

Figure 6.12 Thermal load profiles for the optimized and reference case considering only the controlled buildings or all the substations.

About the load shifting, the $C_{building}$, which is represented by the red area in Figure 6.12, reached a value of 5.2 MWh. As regards peak shaving, the indicator Δq_{max}, which corresponds to the red arrow, resulted in a damping of the maximum thermal load peak equal to 13%.

6.2.4 Comparison of the load shifting results exploiting the thermal capacitance of the network or substations

It is possible to compare the results of load shifting and peak shaving obtained by exploiting the thermal capacitance of the buildings with those obtained with the pumping strategies explained in chapter 5.1 by using the thermal capacitance of the water enclosed in the network pipelines. In both cases, the results of a reference day (2nd of December 2020) were

considered. In the analysis using the thermal capacitance of the network, different pumping strategies were assumed, characterised by different shapes of the modified mass flow profile and different starting times (τ) of the pumping modification before the peak load. The shape of the modified mass flow profile with the best results and τ = 3.5 h was considered. The choice of τ = 3.5 h was made to have the same starting time modification of the thermal load profile in both cases.

On the other hand, in the analysis using the thermal capacitance of the buildings envelope, the stepwise cost profile of the thermal energy was implemented to perform the optimization. Furthermore, three different cases corresponding to three different percentages of the controlled thermal load of all the substations connected to Verona DHN were considered:

- 5% thermal load controlled: in this case, it was looked at the first 16 substations of Table 6.7, corresponding to a Virtual Volume of 371 m^3.
- 10% thermal load controlled: the first 20 substations of Table 6.7 were considered. In this case, total Virtual Volume (688 m^3) is similar to that one of the water enclosed in the DHN pipelines (650 m^3).
- 20% thermal load controlled: all the 27 substations of Table 6.7 were considered, corresponding to a Virtual Volume of 1042 m^3.

In Table 6.9, the load shifting and peak shaving results are shown for the two sources of energy flexibility, considering the different percentages of controlled thermal load for the source represented by the building thermal capacitance.

Table 6.9 Load shifting and peak shaving results, exploiting the network's thermal capacitance or buildings.

	LOAD SHIFTING [MWh]	**PEAK SHAVING [%]**
NETWORK THERMAL CAPACITANCECAPACITANCE	2.21	3.3
BUILDINGS THERMAL CAPACITANCE (5%)	1.34	4
BUILDINGS THERMAL CAPACITANCE (10%)	3.28	7.5
BUILDINGS THERMAL CAPACITANCE (20%)	5.2	13

As a result, compared to the network thermal capacitance, the source of energy flexibility represented by the buildings envelope is always characterised by better peak shaving results,

while the load shifting is lower only in the case with 5% of thermal load controlled. On the other hand, considering the case with a percentage of thermal load controlled (10%), which correspond to a Virtual Volume equal to the total water volume inside the DHN pipelines, showed an increase in the load shifting and peak shaving values respectively of the 33% and 4.2% compared to the results obtained exploiting the network thermal capacitance.

6.3 Conclusions

The current chapter presents two different control strategies developed to exploit the considered sources of energy flexibility: a Supply Station Control and a Demand Side Control.

In Section 6.1 the SSC is described. This is characterized by a MILP optimization problem to schedule the heat supply units of Verona DHN based on heat demand, waste heat availability and electricity price forecasts. Coupling the optimization to the detailed district heating network model, NeMo, allowed repeating the scheduling with a rolling horizon scheme. The objective of the proposed control strategy was to minimize the operational costs for the DH operator using (i) only the thermal capacitance of the water enclosed in the network pipelines and (ii) also using an additional thermal storage tank installed in the main supply station. The results in two reference weeks show that in the optimization problem, the oversimplification of the network thermal behaviour results in an underestimation of the operational cost in comparison to the MPC. This is true especially in the representative middle season week when the cost result of the optimization problem is 8.5% lower than that evaluated by the MPC in the scenario with the storage tank.

Comparing the results of the model predictive control to those of the current control strategy indicates a reduction in the system's operational costs in the middle season and winter weeks of 12.5% and 5.8%, respectively. This is in accordance with the results of Section 5.1, in which it was demonstrated that the flexibility potential of the network is lower in the coldest period. These percentages increase to 20% and 6.3%, respectively, increasing the system's flexibility with an additional heat storage tank connected to the cogeneration units and the heat pumps. This result is related to the case study under consideration. The total installed thermal power of the cogeneration engines and heat pumps connected to the centralized storage tank is limited compared to the peak load during the winter week. In this period, the CHP and HP plants can’t produce more energy than the basic control when the electricity

price is high. So, a small amount of energy is accumulated in the storage tank, and his flexibility potential is not fully exploited.

In Section 6.2 the DSC is presented. This control strategy, which is based on the concept that the substations are virtual storage tanks, aims at determining the optimized energy demand and the average indoor temperature profiles of each considered substation, exploiting the thermal capacitance of their envelopes. A first optimization was performed considering a representative cold day and the real cost profile of the thermal energy and controlling the 20% of the total thermal load of the substations. In the optimized thermal load profiles of the controlled buildings, the energy was moved compared to the reference cases when the cost was lower, preloading and discharging the buildings' envelope just like storage tanks. As a result, the optimization allowed a cost reduction equal to 3.5% compared to the reference case, observing the thermal comfort limits. In a second optimization, a stepwise cost profile of the thermal energy was considered with the cost peak at the same time as the thermal peak. The energy was moved before the step of the cost profile. The result of load shifting reached a value of 5.2 MWh. Regarding peak shaving, the damping of the thermal load peak was equal to 13%.

Finally, a comparison between the load shifting results obtained exploiting the thermal capacitance of the network and the buildings envelope was carried out. Considering the case with the 10% of the total thermal load of the substations controlled by the DSC, which correspond to a Virtual Volume equal to the total water volume inside the DHN pipelines, showed an increase in the load shifting and peak shaving values respectively of the 33% and 4.2% compared to the results obtained exploiting the network thermal capacitance.

CHAPTER 7 INTEGRATION OF RENEWABLE ENERGY SOURCES IN NEW DHN

As a final action to improve the environmental and economic efficiency of the DHN, the integration of renewable energy sources was analyzed. In particular, a novel technical solution for the provision of heating, cooling, domestic hot water and electricity to a small residential district in cold regions was studied. The core of the energy system is an ultra-low temperature district heating network supplied by a high-efficiency ground source heat pump. The source-side of the booster heat pumps installed in the buildings is connected to the district heating network. Furthermore, rooftop photovoltaic thermal panels are installed in the substations.

7.1 Case study

The novel technical system has been applied and simulated for a small residential district composed of 7 buildings, 6 units each. For the simulations, the Test Reference Year (TRY) data from the EnergyPlus database is used: the analysis is carried out for Helsinki, Berlin and Strasbourg. Table 7.1 summarizes the main thermal properties of the envelope of the buildings. The total volume of each building is equal to 2166 m^3, while the heated floor area is equal to 560 m^2.

Table 7.1 Thermal properties of the building envelope for the case study buildings.

	Thickness [cm]	**U-value [W/(m² K)]**
External Wall	42	0.19
Adjacent Wall	12	2.35
On Garage Floor	53	0.28
Intermediate Floor	54	0.44
External Roof	14	0.55
Windows	-	0.82

A scheme of the district heating network under consideration, operating at constant supply temperature and variable flow rate, is shown in Figure 7.1. The network is about 450 m long. The blue dots are the connection nodes between the pipes of the DHN, where water circulates at a temperature of 20°C during the cold season and 25°C during the warm season. The orange dot represents the supply station, characterized by a ground source heat pump. Each of the seven buildings is provided with one heat pump and a PVT field on the roof. The red and light blue dots indicate the HPs when they respectively supply or withdraw heat from

the network. The yellow dots represent the PVT systems, which provide heat to the network when the photovoltaic panels are cooled.

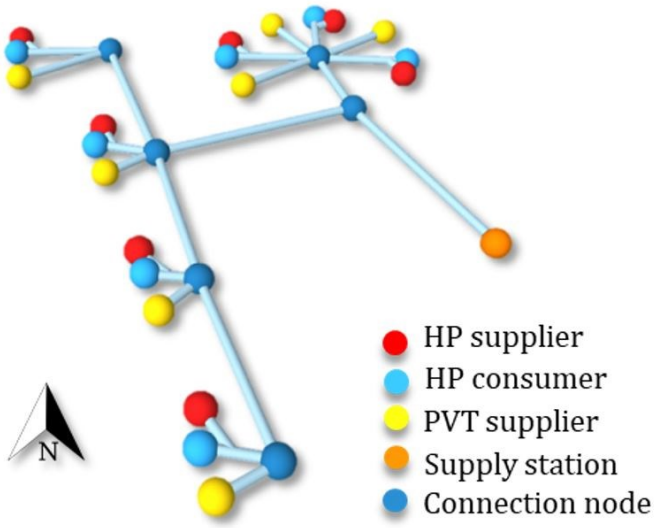

Figure 7.1 Scheme of the considered district heating and cooling network.

7.2 Energy system concept

In this novel energy system, each building is equipped with a rooftop PVT field and a reversible water to water heat pump coupled to the radiant floor on the building side. The solar field produces DHW for the apartments in each building and electricity for the district. Its electrical efficiency is enhanced as the DHN water is used to decrease the temperature of the PVT panels. Moreover, the DHN is employed as the source/sink for the heat pump. The DHN links the substations to the thermal storage in the Supply Station (SS), where GSHP releases heat during the heating season. A direct connection to the BHE field allows rejecting the heat to the ground during the cooling season. Figure 7.2 presents a simplified scheme of the energy system and its energy fluxes (blue, yellow and red arrows).

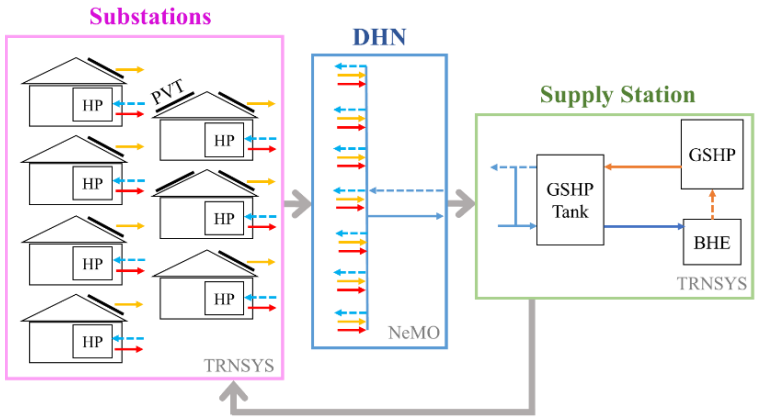

Figure 7.2 Scheme of the energy system and its energy fluxes.

The water flowing in the DHN has a double function: it is used as the heat source/sink for the heat pumps of the substations and the cooling of the PVT panels. In particular, its temperature is chosen as a consequence of a parametric study considering the following aspects:

- the closer the temperatures of the heat source and the heat sink, the higher the efficiency of the reversible heat pumps in the substations: a higher supply temperature leads to higher efficiency during heating operation (space heating and DHW production) a worse performance during the cooling season;
- a lower temperature level of the heat carrier fluid improves the performance of the GSHP in the supply station, which is switched on only during the heating season;
- during the cooling season, a lower network temperature leads to lower efficiency when producing DHW but increases the electricity production due to better cooling of the PVT panels.

An initial parametric analysis based on the considerations above has allowed setting the temperature of the network to 20°C and 25°C during the heating and cooling season, respectively.

A different strategy for enhancing the efficiency of the centralized GSHP was investigated, involving a variation of the DHN water temperature during the heating period: during the coldest months, from November to March, the supply temperature was kept at a constant value of 8°C, while during intermediate seasons, the temperature was set to 20°C.

7.3 Method

7.3.1 Simulation framework for the energy system

The analysis of the whole system, presented in Figure 7.2, involves an iterative simulation of the three main parts: the substations, the thermal network and the supply station (SS). In Figure 7.2, the grey arrows show the steps which are followed for the simulations. First, the detailed models of the 42 housing units, with their plant systems including the PVT fields and the heat pumps, are created. At this level, some boundary conditions are set: the climate conditions of the three investigated localities are used, and the temperature of the water circulating in the DHN is assumed to be constant, differing only for the heating and cooling seasons. Afterwards, the temperatures of the water exiting the source side of the heat pumps and the PVT cooling tank in the substation are given as inputs to the DHN model, where the network's thermal

capacitance and thermal losses are considered. Consequently, the water mass flow rates and temperatures for each time step of the annual simulation are obtained, consisting of the inputs to the third part of the model, the SS. In this last section, the dynamic simulations of the GSHP, the thermal storage and the BHE are carried out, obtaining the values for the DHN inlet temperature. This is kept at the desired value using a tempering valve at the outlet of the thermal storage tank.

For the substations and the DHN, the annual simulations are carried out with a time step of 15 minutes to evaluate the system's dynamic behaviour. The simulations of the SS are instead carried out considering 20 operating years, with a time step of 3 minutes, which allows avoiding convergence problems. The long simulation time is chosen to monitor the thermal drift effect on the ground due to the heating dominant building load profiles, which negatively affects the efficiency of the GSHP.

7.3.2 Detailed building model including substations

The building envelope model is coupled to the plant model of the substations in the Simulation Studio workspace of TRNSYS 18 [84]. The internal gains related to the people occupancy and the use of domestic appliances, the infiltrations and the setpoint temperatures for heating and cooling are defined using the Standards ISO 18523-2:2018 [85] and ISO 7730:2005 [86]. The DHW load profile throughout the year is evaluated employing DHWcalc [87], using default probability distributions and an average DHW consumption of 50 liters/person/day.

Figure 7.3 reports a simplified scheme of the energy plants: dislocated in each building, a high-performance generation system is installed, consisting of a reversible water-to-water heat pump, a PVT field, a DHW tank for the DHW production, the space-heating and cooling radiant system and a PVT tank for the cooling of the PVT panels. Both the heat pump source side and the PVT tank exchange heat with the DHN. A novel TRNSYS Type, described in [88], is used to simulate the operating conditions of the heat pump based on compressor polynomial performance curves. The load-side of the heat pump is connected to the DHW tank and the radiant system for producing DHW at a setpoint temperature of 43°C and for the air-conditioning of the building, which is provided considering a supply temperature of 33°C in heating and 18°C in cooling. The PVT field is installed on the south-facing roof slab for 5 of the 7 buildings, while its area is doubled and distributed on the east and west slabs of the roof for the remaining two buildings. The solar field is employed for the production of DHW

and electricity. The model used for the PVT collector refers to the research carried out by Zarrella et al. [89], and it is implemented by the same research group as a TYPE of TRNSYS software. The heat pump provides heat to the DHW tank when the thermal energy produced by the solar field is not sufficient to reach the setpoint. Whether there is no need for thermal energy production from the PVT field, as the temperature of the water inside the DHW tank is already at the setpoint, and the temperature of the PV surface is above 35°C (with a dead band of 1.5°C), the PVT field is cooled down, exchanging heat with the PVT tank, through a heat exchanger, which is linked to the DHN.

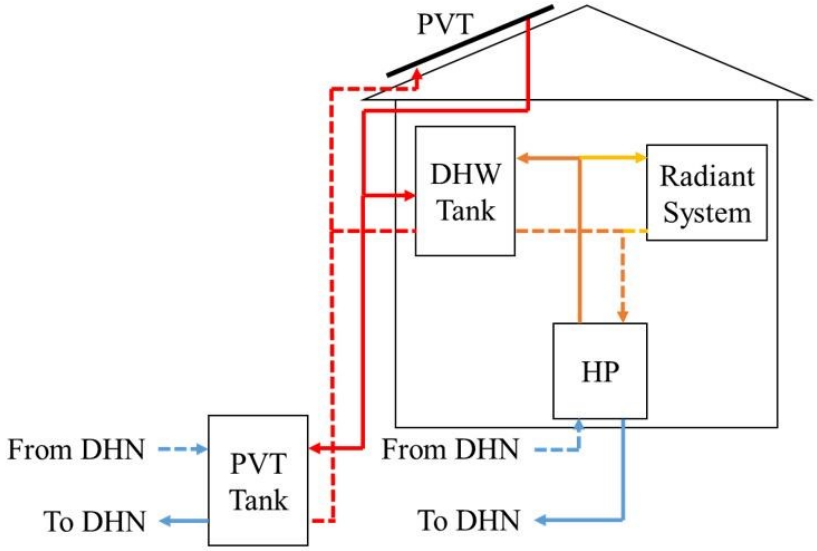

Figure 7.3 Sketch of the energy plant at the substations.

For the heat pump, a size of 36 kW is chosen for the buildings in Helsinki, of 25 kW in Berlin and Strasbourg, on the basis of the thermal loads computed for the analyzed case studies. The tanks have the same volume for the different case studies, equal to 800 liters for the DHW tank and 450 liters for the PVT tank. The PVT field has an overall PV area of 57.6 m^2 and a module area of 66.4 m^2 for the north-oriented buildings, while it is doubled for the buildings whose slabs are east- and west-oriented with a slope of 45°. The thermal efficiency of the PVT panels is expressed as in Equation (7.1) [90].

$$\eta_{th} = \eta_0 - a_1(T_{mean} - T_a)/I - a_2(T_{mean} - T_a)^2/I \quad (7.1)$$

where η_0 is the zero-loss efficiency (set to 0.7), a_1 and a_2 heat loss coefficients (set to 12 W/(m^2 K) and 0 W/(m^2 K^2), respectively), T_{mean} is the mean temperature of the heat transfer fluid, T_a is the ambient temperature, and I (W/m^2) the solar irradiance. The values of the coefficients used in the model are derived from datasheets of commercial panels. The PVT electrical efficiency is a function of the mean temperature of the PV layer, and the electrical energy production is calculated using Equation (7.2) [86]. The value of the coefficient η_{ref-PV} which can usually be found in the datasheet of the PV or PVT module, represents the efficiency of the PV module at the reference temperature $T_{ref-PV} = 25°C$ (standard test conditions). The coefficient b_{PV} is then used to consider the deviation from the reference values and is the area of the PV panels: this coefficient is set to 0.0045 K^{-1}.

$$P_{el} = G \cdot A \cdot \eta_{ref-PV} \cdot [1 - b_{PV}(T_{PV} - T_{ref-PV})] \quad (7.2)$$

7.3.3 Thermal model of the supply station

The model of the SS is simulated in the TRNSYS environment. A scheme of the simulated system can be seen in Figure 7.4, where the configurations used during the heating (a) and cooling (b) seasons are summarized. During the heating season, a stream of water at a temperature of 20°C circulates in the DHN. In order to guarantee the setpoint temperature at the source-side of the heat pumps and the PVT tanks in the substations, a centralized GSHP releases heat to a GSHP tank through an immersed heat exchanger. A tempering valve is used to mix the return DHN stream with the water mass flow rate exiting the GSHP tank port for obtaining the desired outlet temperature.

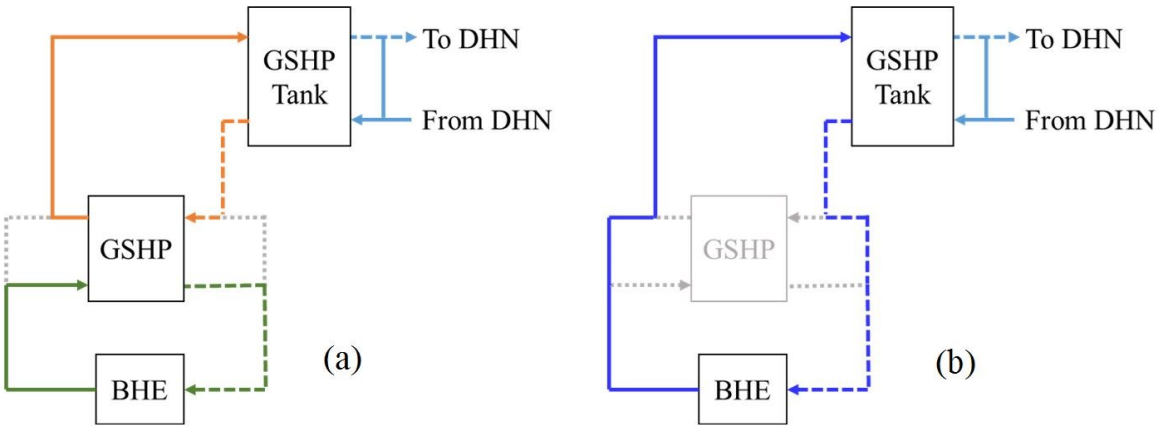

Figure 7.4 Scheme of the centralized GSHP system during the heating (a) and cooling (b) seasons.

The GSHP is modelled using the novel TRNSYS Type mentioned in the previous paragraph, using the compressors' polynomials of machines with a rated heating capacity of 135 kW for the case study of Helsinki, 96 kW for Berlin and Strasbourg. An initial assessment of the borehole heat exchanger (BHE) field size was done using the ASHRAE [91] method. It resulted in a number of BHEs (100 m long each) equal to 98 for Helsinki, 36 for Berlin and 32 for Strasbourg. However, for the analyzed plant configuration, the number of boreholes can be reduced to the values reported in Table 7.2. The BHEs are simulated using TRNSYS Type 557a. The main properties for the borehole field are presented in Table 7.2.

Table 7.2 Main characteristics of the BHE field.

	Helsinki	**Berlin**	**Strasbourg**
Ground			
Specific heat	1000 J/(kg K)		
Density	2500 kg/m^3		
Undisturbed temperature	5.2 °C	9.8 °C	10.2 °C
Thermal conductivity	2.2 W/(m K)		
Thermal gradient	0.03 °C/m		
Specific volume heat capacity	2500 kJ/(m^3 K)		
Pipe			
Length of each borehole	100 m		
Number of Boreholes	75	35	30
Thermal conductivity	0.35 W/(m K)		
Outer/Inner diameter of pipe	32/26 mm		
Center-to-center distance	78 mm		
Distance between BHEs	8 m		
Fluid			
Composition	Water-Glycol (30%)		
Specific heat	3.915 kJ/(kg K)		
Density	1031 kg/m^3		

During the cooling season, as the ground temperature is low enough to cool the GSHP Tank at the desired temperature of 25 °C, the heat pump is bypassed, and the immersed heat exchanger of the GSHP Tank is directly connected to the BHE field (Figure 7.4). This configuration can be employed as the analyzed case studies are characterized by cold climate conditions and, therefore, by low cooling thermal loads of the buildings and low mean temperatures of the ground, which can cool at the set temperature level the water inside the storage tank.

7.3.4 Evaluation of energy system performance

Three performance indicators have been considered to evaluate the energy performance of the novel solution for providing space heating, cooling and domestic hot water to the considered district. One is the Coverage Ratio (CR), which represents the percentage of electrical energy demand ($W_{el,dem}$) covered by the self-generated solar power ($W_{el,PVT}$) using the PVT panels.

$$CR = \frac{W_{el,PVT}}{W_{el,dem}} * 100 \tag{7.3}$$

Similarly, the Self-Use Ratio (SUR) indicates the percentage of the overall electrical energy produced by the PVT field ($W_{el,PVT,tot}$) that is self-consumed by the considered system.

$$SUR = \frac{W_{el,PVT}}{W_{el,PVT,tot}} * 100 \tag{7.4}$$

The last one is the Primary Energy Reduction (PER) indicator, which represents the reduction of primary energy consumption determined by the self-consumption of the electrical energy produced by the PVT systems.

$$PER = W_{el,PVT} * PEF \tag{7.5}$$

Where PEF is the Primary Energy Factor according to Sartori et al. [92]. For Finland (Helsinki) and Germany (Berlin), the PEF values are respectively 1.7 and 3, while for France is 2.58 [93].

7.4 Simulation results

This section presents the results obtained from the simulations at the substations and the supply station levels. Moreover, considerations about the electrical and primary energy at a district level are provided. In conclusion, the results regarding the use of two temperature levels for the DHN water during the heating season are reported.

7.4.1 Results at substations level

The monthly thermal energy demanded by the buildings in heating, cooling, and DHW production is illustrated in Figure 7.5. The thermal loads for all the considered climates are

heating-dominant, with a heating/cooling ratio equal to 4.1 for Helsinki, 2.3 for Berlin and 1.5 for Strasbourg.

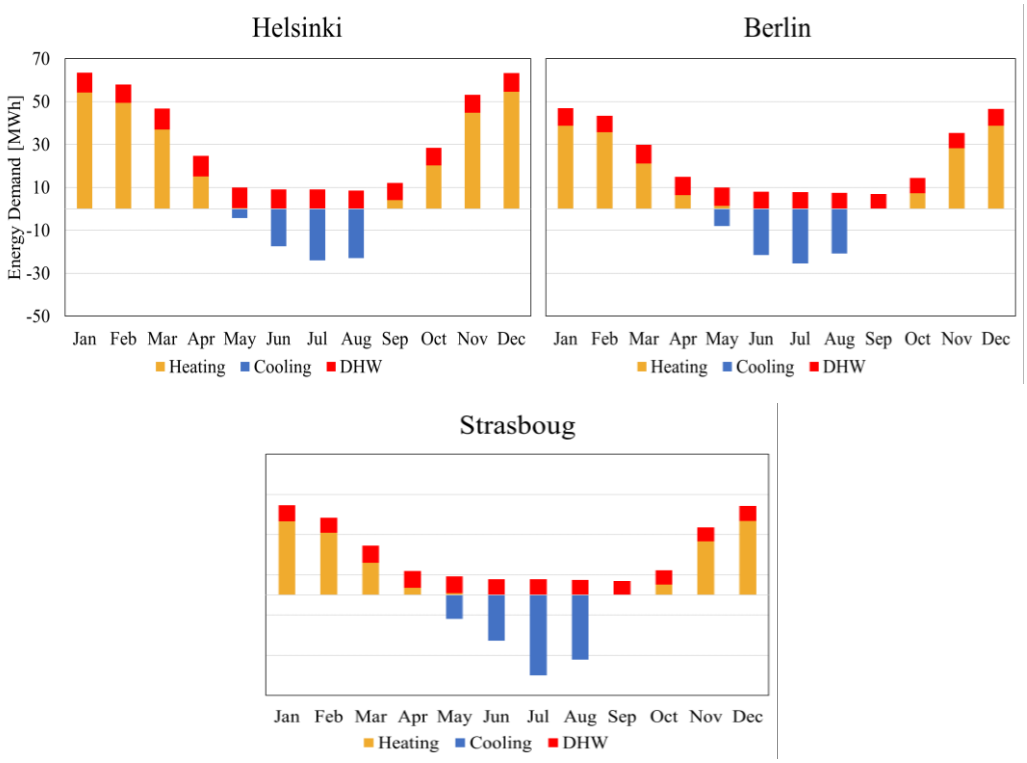

Figure 7.5 Monthly thermal energy demanded by the neighbourhood for heating, cooling and DHW production for the three localities.

Correspondingly, in Table 7.3, the annual and specific (relating to the heated floor area) values for the thermal energy demand of heating, cooling and DHW are shown.

Table 7.3 Annual and specific thermal energy demanded by the neighbourhood for heating, cooling and DHW production for the three localities.

	Heating		**Cooling**		**DHW**	
	[MWh]	[kWh/m^2]	[MWh]	[kWh/m^2]	[MWh]	[kWh/m^2]
Helsinki	279.38	71.3	-68.81	-17.6	106.53	27.2
Berlin	177.57	45.3	-75.96	-19.4	93.57	23.9
Strasbourg	156.34	39.9	-106.94	-27.3	92.44	23.6

The DHW demand is computed considering a setpoint temperature of 43°C and a temperature of the municipality water that differs between the three localities and depends on the mean annual temperature of the external air. In particular, concerning the DHW production, which has priority over the space heating and cooling provision, Table 7.4 reports

the share of thermal energy at the DHW tanks produced by the solar field and by the heat pumps for the three investigated localities. It can be noticed that, as expected, in Helsinki (the coldest locality), the total energy needed is higher than for the other case studies, while the PVT thermal production is lower (up to 34% lower than in Strasbourg). This means that the contribution of the heat pumps is more relevant in Helsinki and, in particular, 28% higher than in Strasbourg.

Table 7.4 Total thermal energy for the DHW production by PVT field and HPs contribution

	PVT		**HP**		**Total**
Helsinki	17.7 MWh	16%	92.9 MWh	84%	110.6 MWh
Berlin	20.0 MWh	21%	77.0 MWh	79%	97.1 MWh
Strasbourg	23.8 MWh	25%	72.0 MWh	75%	95.8 MWh

Table 7.5 presents the electrical energy absorbed by the heat pumps and their performance when operating in cooling mode and in heating mode for space heating and DHW production. The performance is evaluated in terms of seasonal coefficient of performance (SCOP) and seasonal energy efficiency ratio (SEER). The SCOP is the annual thermal energy that is exchanged at the condenser of the heat pump during heating operation, divided for the electrical energy absorbed by the compressor; correspondingly, for cooling operation, the SEER is the annual thermal energy that is extracted from the evaporator at the load side of the heat pump, divided by the electrical energy absorbed by the compressor of the heat pump. Overall, on an annual basis, the electrical energy absorbed by the heat pumps in the substations for the three case studies is around 91 MWh in Helsinki, 71 MWh in Berlin and 73 MWh in Strasbourg. It can be observed that this value is higher for the case of Helsinki, where the thermal load for heating and DHW provision is 46% and 62% higher than for Berlin and Strasbourg, respectively. On the other hand, Berlin presents an electrical consumption that is slightly lower than in Strasbourg due to a cooling load that is 41% higher for this last case study.

Table 7.5 Electrical energy demanded by the heat pump and performances in the substations.

	Electrical Energy Demanded [kWh]			**SCOP/SEER** [kWh/kWh]		
	Heating	**Cooling**	**DHW**	**Heating**	**Cooling**	**DHW**
Helsinki	50303	13947	26967	5.4	4.9	3.7
Berlin	33004	16798	21795	5.2	4.5	3.8
Strasbourg	29096	23529	20404	5.2	4.6	3.8

The heat pumps are very efficient, and their performance values are similar for the different localities, as the temperatures of the heat sources and sinks are constant. In particular, as the same compressor model is chosen for the cases of Berlin and Strasbourg, the values for the SCOPs and SEERs do not change for these two localities, unlike for the case of Helsinki, where different performances characterize the machine. Considering the solar field production, Table 7.6 reports the thermal energy produced by the PVT panels installed in the district and released to the DHW tank or to the DHN. Moreover, it shows the electrical energy production and the overall electrical efficiency of the PVT field.

Table 7.6 Thermal energy produced by the solar field and released to the DHW tank and to the DHN, electrical energy production and electrical efficiency of the PVT field.

	TE to DHW Tank [MWh]	**TE To DHN** [MWh]	**EE** [MWh]	η_{el}
Helsinki	16.81	17.02	112.18	17.9%
Berlin	20.14	18.42	111.35	17.6%
Strasbourg	23.90	21.23	118.98	17.4%

The cooling of the PVT panels allows obtaining higher electrical efficiencies, as the electrical production increases with the reduction in the temperature of the PV cells. Figure 7.6 shows this effect during a representative summer day for a building in Berlin. In the Figure, the temperature of the cells, which is an output of the PVT capacitive TRNSYS type, is reported for the case with and without PVT cooling. When the PVT cooling control is active, the curves for the PV cells' temperatures diverge; correspondingly, the effect of the electrical efficiency rise can be noticed.

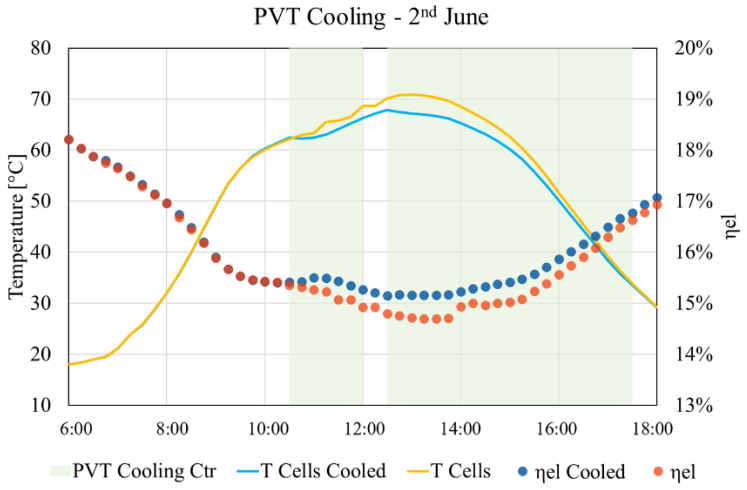

Figure 7.6 Berlin case study: PVT cooling control, PV cells temperatures and electrical efficiencies for the cases with and without PVT cooling.

Table 7.7 presents the annual thermal energy withdrawn from (+) or released to (-) the DHN. In particular, the energy is divided between the contribution related to the HPs operation and the PVT cooling. The PVT field contributes to reducing the thermal energy extracted from the DHN during the cold season, while during the warm season, as the district loads are heating-dominant, it increases the heat fluxes released to the DHN and, consequently, favours the balancing of the thermal load at the ground. For example, when considering the difference between the net thermal energy overall extracted from the DHN during the cold season and the energy released during the warm season, this value amounts to 158.7 MWh in Helsinki, 63.5 MWh in Berlin and 10.4 MWh in Strasbourg. On the other hand, if the PVT contribution is not considered, the net thermal energy to the DHN becomes equal to 176.4 MWh in Helsinki, 83.9 MWh in Berlin and 66.5 MWh in Strasbourg, demonstrating a relevant influence of the PVT field on the thermal load unbalance.

Table 7.7 Thermal energy released to (-) and extracted from (+) the DHN during the cold and the warm seasons.

	Cold Season [MWh]			**Warm Season** [MWh]		
	HP	**PVT**	**HP-PVT**	**HP**	**PVT**	**HP+PVT**
Helsinki	276.8	-3.6	273.2	-101.1	-13.5	-114.6
Berlin	186.6	-5.0	179.2	-102.7	-13.0	-115.7
Strasbourg	167.4	-5.4	159.3	-133.8	-15.2	-149.0

For concluding the evaluation of the substations energy systems, Figure 7.7 shows the intraday effects on the SS return temperature due to the HP sink/source fluctuations and the PVT behaviour at each building for a representative summer day in Berlin. In the Figure, negative values for the thermal power mean that the network supplies heat to the HPs in the substations to produce DHW. On the contrary, positive values stand for space cooling demand or PVT cooling, leading to heat rejection to the network. The PVT contributions are concentrated between 10 am and 8 pm and determine a high increase in SS return temperature, reaching 31°C at 3 pm, whereas the supply temperature is constant at 25°C. On the other hand, the operations of heat pumps are managed differently in the different buildings, resulting in minor variations of SS return temperature.

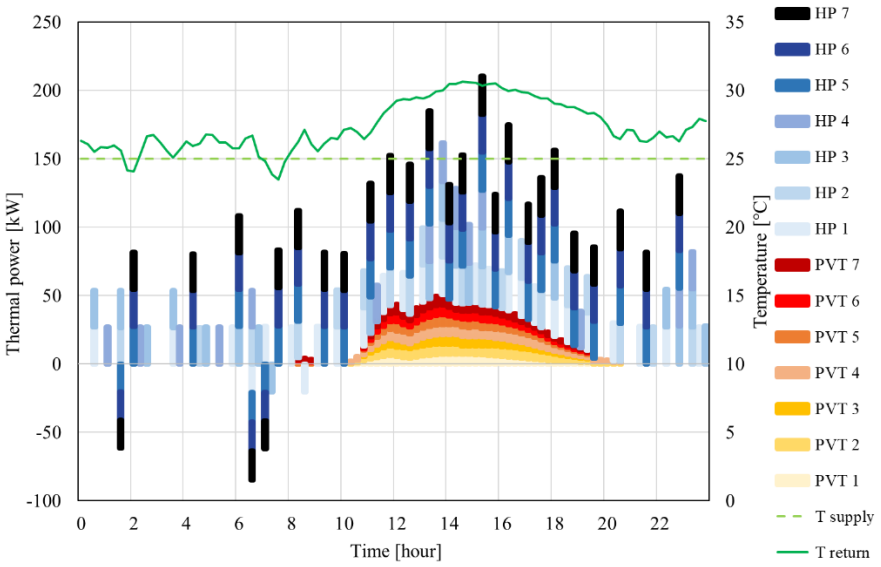

Figure 7.7 Intraday effects on the SS return temperature due to the HP and PVT cooling for a summer day (2nd June).

7.4.2 Results at supply station level

The simulations carried out at the supply station level give information about the behaviour of the GSHP, which is connected to the GSHP Tank and the borehole field. The simulation time was set to 20 years and allowed to monitor the operation of the GSHP. Indeed, the machine's performance might change over time due to the thermal drift effect of the ground, related to the unbalanced thermal load conditions. Figure 7.8 shows the trend along the 20 years of the monthly COP for the three localities, decreasing with a tendency that depends on the BHE outlet temperature drop. Therefore, in the Figure, the annual minimum and maximum temperatures of the heat carrier fluid exiting the BHE field are given as a reference. The SCOP varies from 4.0 for the first year of operation to 3.7 for the 20th year in Helsinki, from 5 to 4.7 in Berlin and from 4.8 to 4.5 in Strasbourg.

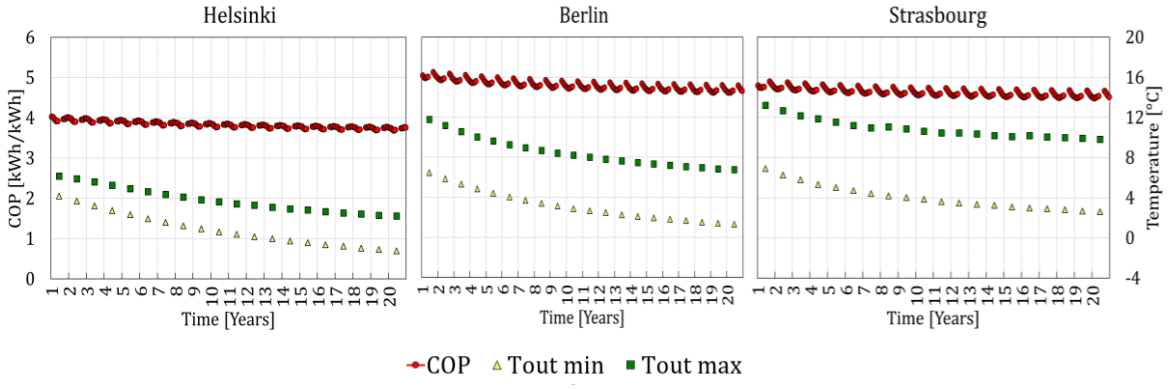

Figure 7.8 Monthly COPs, annual minimum and maximum outlet fluid temperatures at the BHE field.

Concerning the thermal load, Figure 7.9 shows the monthly energy exchanged between the GSHP tank and the DHN. The positive values represent the energy released to the DHN, while the negative values the heat extracted from the DHN.

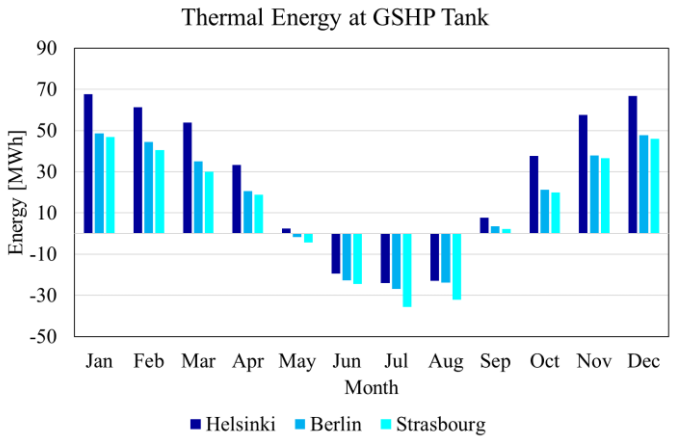

Figure 7.9 Monthly values for thermal energy exchanged between the GSHP Tank and the DHN.

During the first year, the electrical demand of the GSHP is equal to 100.1 MWh in Helsinki, 54.5 MWh in Berlin and 53.4 MWh in Strasbourg. Compared to the case without PVT cooling, in Berlin, between 20th and the 1st year, an energy saving of nearly 200 kWh can be obtained, considering the GSHP consumption solely. Moreover, evaluating the PVT electrical output, during one year an additional difference of 460 kWh in the production can be obtained with the PVT cooling.

7.4.3 Electrical and primary energy considerations at the district level

The electrical production of the PVT field contributes to meeting the electrical energy demand of the plant related to the electrical consumption of the heat pumps in the substations, the consumption of the electrical appliances in the buildings and the GSHP demand. If the electrical production of the solar field installed on the roof of each building was considered for meeting the demand of the same substation (appliances and heat pumps), the CR would be 29% in Helsinki, 30% in Berlin and 32% in Strasbourg. In the same context, the SUR would be around 64% in Berlin and Strasbourg, 66% in Helsinki. On the other hand, it is possible to introduce the concept of energy community, where although the solar field is distributed on the different roofs, it belongs to the whole district. In this way, its production can increase the SUR of the system, which, also considering the GSHP electrical demand, increases to 71% for Helsinki

and Berlin and 70% for Strasbourg. Figure 7.10 shows the electrical energy consumption by use, the production of the whole solar field in the district, the CR and the SUR. In this configuration, the annual electrical energy that must be provided by the grid amounts to 261 MWh for Helsinki, 196 MWh for Berlin and 192 MWh for Strasbourg. On the contrary, the energy produced by the solar field but exceeding the electrical demand of the plant is about 29 MWh for Helsinki and Berlin, 32 MWh for Strasbourg. Finally, in one year, the electrical energy produced by the PVT systems at the district level involves a PER of 212 MWh for Berlin, and it is equal to 122 MWh and 113 MWh respectively for Helsinki and Strasbourg.

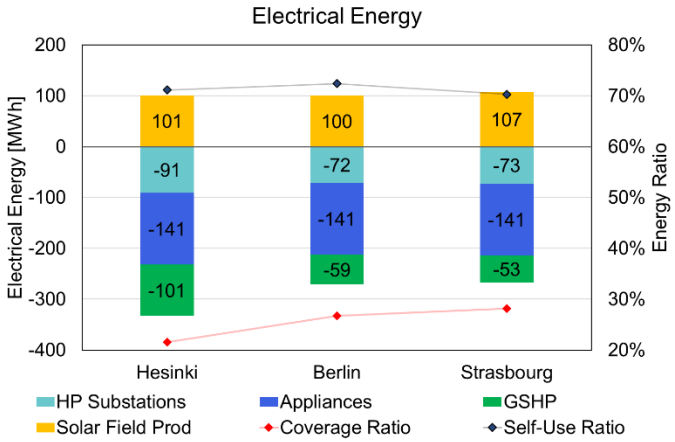

Figure 7.10 Electrical energy consumption by use and coverage and self-use ratio at district level.

7.4.4 Effect of the variation in the DHN water temperature during the heating period

In conclusion, a different strategy for enhancing the efficiency of the centralized GSHP was investigated for Berlin climate, which has been chosen as it is the location characterized by intermediate weather conditions, considering Helsinki and Strasbourg. During the heating period, the supply temperature was kept at a constant value of 8°C from November to March, while during intermediate seasons, the temperature was set to 20°C. For these simulations, the water temperature in the DHN is always at 25°C during summer. The temperature of 8°C was chosen as it is closer to the average temperature of the ground in Berlin and leads to lower energy consumption of the centralized GSHP.

The decrease in the supply temperature during the coldest months, as expected, leads to a decrease in the performance of the substations' heat pumps. Figure 7.11 shows the monthly COP for heating and DHW production, together with the supply temperature level. As it can be

seen from the figure, the performance is higher during the middle seasons' months, when the DHN water temperature is at 20°C.

Overall, the electrical energy consumption related to the operation of the substations' heat pumps for the provision of heating and DHW increases of 8.5% compared to the case with a constant temperature of 20°C during the whole heating period.

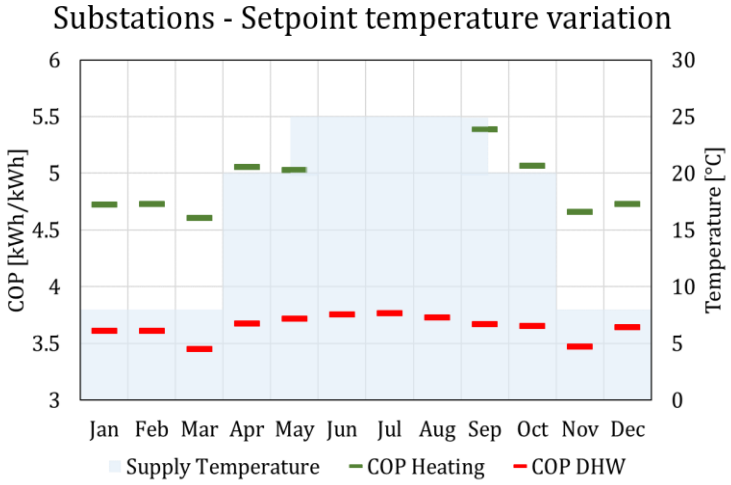

Figure 7.11 Substation heat pumps monthly COP for the provision of space heating and DHW and supply setpoint temperature from the DHN.

On the other hand, during the first year of operation, it is possible to obtain a relevant decrease in the electrical energy demanded by the centralized GSHP, reaching a saving of 21%. This is due to the fact that the lower supply temperature allows a decrease in the temperature of the water contained inside the thermal storage in the supply station, reducing the thermal load to be delivered by the GSHP.

Figure 7.12 shows a comparison between the case with constant DHN water temperature setpoint and variable setpoint is carried out. In particular, the Figure shows the supply water temperature after the mixing with the return temperature from the network, and the monthly values of the GSHP COP, for both the cases with constant heating setpoint temperature and variable heating setpoint temperature. The monthly COP, when the setpoint temperature is equal to 8°C is significantly higher than the case with supply temperature at 20°C.

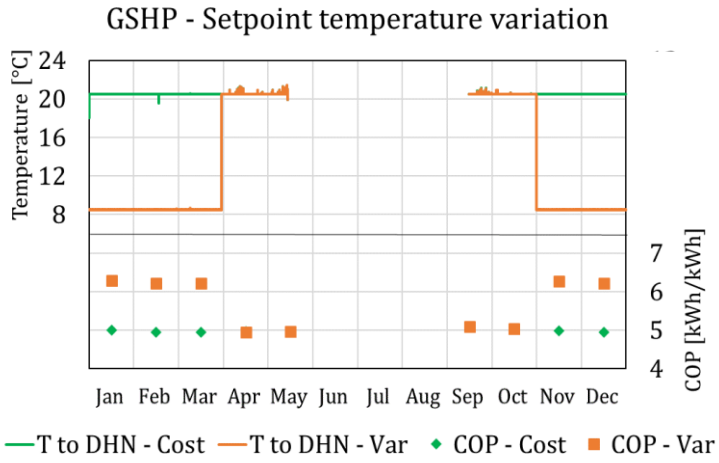

Figure 7.12 GSHP monthly COP and supply water temperature to DHN.

7.5 Conclusions

A technical solution for supplying heating, cooling, domestic hot water and electrical energy to a small residential district is investigated in three locations: Helsinki, Berlin and Strasbourg. The buildings are equipped with rooftop PVT systems and a reversible water-to-water heat pump that can extract/supply heat from/to an ultra-low temperature district heating network. During the heating season, the network is supplied by a high-efficiency ground source heat pump.

The simulations performed at the building level show that in the coldest climate (Helsinki), the PVT covers 16% of the total thermal energy needed for the DHW production. The booster heat pump supplies the remaining part. In Strasbourg, which is characterized by a warmer climate, the PVT contribution for DHW production reaches 25%. The heat pumps show high efficiency in cooling mode (SEER = 4.9) and heating mode for space heating (SCOP = 5.4) and DHW (SCOP = 3.7). As the temperatures of the heat sources and sinks are constant, these values are similar for the different localities.

The simulations of the GSHP coupled to borehole heat exchangers, give information about the long-term performance of the system, considering the thermal drift effect of the ground over 20 years. In Helsinki, the SCOP does not change significantly, i.e. from 4.0 for the first year of operation to 3.7 for the 20th year. This variation is reduced thanks to the PVT panels that help balance the thermal load at the ground, reducing the thermal energy extracted from the DHN during the cold season and increasing the heat fluxes released to the DHN during the warm season. At the same time, the electrical production of the PVT field increases thanks to the

cooling of the PV cells. Finally, the self-consumed electricity is equal to 71% for Helsinki and Berlin and 70% for Strasbourg compared to the overall electricity production from the PVT systems.

A different strategy for enhancing the efficiency of the centralized GSHP was also investigated for the intermediate climate, Berlin. During the heating period, the supply temperature was decreased compared to the reference case, during the coldest months. Despite leading to an overall increase of 8.5% in the electrical demand at the substations' level, this solution allows obtaining a reduction in the centralized GSHP electrical consumption of 21%.

In conclusion, the study presents an overview on the performance of a low-temperature district grid integrated with renewable energy technologies such as PVT systems and borehole heat exchangers. The proposed solution appears attractive for small residential areas in cold climates. In addition, the research highlights how detailed models can be integrated with each other, leading to accurate district-level analysis.

CHAPTER 8 CONCLUSIONS

The research work presented shows the potential of the main sources of energy flexibility that are part of an existing district heating network. In particular, the research shows that by appropriately choosing the mass flow rate circulating through the network, it is possible to shift the thermal load over time, thereby shaving the peak loads. The pre-charge process can achieve significant results in terms of peak shaving, and the amount of thermal energy shifted in time increases linearly with the number of hours between the start of the flow adjustment strategy and the peak load. Furthermore, in the coldest period, the flexibility potential of the network is lower. Considering the case study of the Verona district heating network, to produce the desired change in the mass flow rate, the district heating operator needs to install three or more bypass pipes sufficiently far from the main supply stations, allowing the water flow from the supply to the return pipes.

About the flexibility potential determined by the thermal capacitance of the buildings' envelope, the Active Demand Response (ADR) simulations defined the behaviour of two different buildings (a residential building and a school), considering different boundary conditions. Regarding the comparison between the requalified case and the reference one, it can be said that the efficiency of the ADR events is always higher in the former. This is especially true with the residential building, while in the case of the school, high ventilation loads reduce the gap. In addition, the efficiency of the ADR events is highly dependent on the nominal power of the heating system, with higher efficiency when the system's nominal power is oversized. The discomfort caused by ADR events is always higher in the reference case. Finally, in general, the thermal load shifting capacity is much lower in the requalified case, and this is in line with the results seen in the scientific literature.

In a second step, two control strategies aimed at exploiting the considered sources of energy flexibility were considered. The cost reduction determined by the Supply Station Contol (exploiting the thermal capacitance of the network) compared to the basic control is more relevant in the representative middle season week (-12.5%) than in the winter one (-5.8%). This is in accordance with the results of the analysis on the flexibility potential of the water enclosed in the network's pipelines, in which it was demonstrated that it is lower in the wintertime. Adding a centralized storage tank increases the cost savings in the representative middle season week (20%) compared to winter one (6.3%). The result is related to the case study under consideration. On the other hand, the Demand Side Control, which is based on the

concept that the substations are virtual storage tanks, aims at determining the optimized energy demand and the average indoor temperature profiles of each considered substation, exploiting the thermal capacitance of their envelopes. A first optimization was performed considering a representative cold day and the real cost profile of the thermal energy and controlling the 20% of the total thermal load of the substations. As a result, the optimization allowed a cost reduction equal to 3.5% compared to the reference case, observing the thermal comfort limits. In a second optimization, a stepwise cost profile of the thermal energy was considered with the cost peak at the same time as the thermal peak. The energy was moved before the step of the cost profile. The result of load shifting reached a value of 5.2 MWh. Regarding peak shaving, the damping of the thermal load peak was equal to 13%.

Finally, a comparison between the load shifting results obtained exploiting the thermal capacitance of the network and the buildings envelope was carried out. Considering the case with the 10% of the total thermal load of the substations controlled by the DSC, which correspond to a Virtual Volume (volume of the virtual storage tanks) of the substations equal to the total water volume inside the DHN pipelines, showed an increase in the load shifting and peak shaving values respectively of the 33% and 4.2% compared to the results obtained exploiting the network thermal capacitance.

In conclusion, the study outlined a proposal for an ultra low-temperature district network integrated with renewable energy technologies such as PVT systems and borehole heat exchangers to supply heating, cooling, domestic hot water, and electrical energy to a small residential district.

The rooftop photovoltaic thermal panels partially met the electrical demand of the district. Moreover, they contributed to the production of domestic hot water and, when their thermal energy production exceeded the demand, the heat was injected into the ground to reduce the thermal unbalance, which typically affects the performance of the ground source heat pump systems in cold climates. Using the network heat carrier fluid to decrease the average temperature of the PVT panels further enhanced their electrical efficiency. The proposed multi-energy system reached an electrical self-consumption of 70% in the coldest locality and efficiently combined different renewable energy sources at the district level in cold climates.

Alternative scenarios could pursue an environmental objective instead of an economic one. Future work will concern the simulation of future DHN decarbonization scenarios. In

particular, considering the DHN of Verona, the idea is to integrate a groundwater heat pump into the production mix and optimize the daily production mix through the Supply Station Control (SSC) under various thermal energy demand and CO2 price conditions minimizing operating costs and primary energy consumption. The output of this activity will be the quantification of the gap between these two optimizations in terms of CO2 emitted and cost, and the differences from current operating conditions. Furthermore, future work will try to improve the coupling between the optimization problem and the DH simulation in the SSC. Finally, a detailed model of the thermal storage tank will be introduced.

References

[1] Energy data 2020 edition n.d. https://doi.org/10.2785/68334.

[2] DIRECTIVE (EU) 2018/844 OF THE EUROPEAN PARLIAMENT AND OF THE COUNCIL of 30 May 2018 amending Directive 2010/31/EU on the energy performance of buildings and Directive 2012/27/EU on energy efficiency (Text with EEA relevance).

[3] Lund H, Werner S, Wiltshire R, Svendsen S, Thorsen JE, Hvelplund F, et al. 4th Generation District Heating (4GDH): Integrating smart thermal grids into future sustainable energy systems. Energy 2014;68:1–11. https://doi.org/10.1016/J.ENERGY.2014.02.089.

[4] Buffa S, Cozzini M, D'Antoni M, Baratieri M, Fedrizzi R. 5th generation district heating and cooling systems: A review of existing cases in Europe. Renew Sustain Energy Rev 2019;104:504–22. https://doi.org/10.1016/j.rser.2018.12.059.

[5] Manfren M, Caputo P, Costa G. Paradigm shift in urban energy systems through distributed generation: Methods and models. Appl Energy 2011;88:1032–48. https://doi.org/10.1016/J.APENERGY.2010.10.018.

[6] Frederiksen S, Werner S. District heating and cooling. 2013.

[7] Dalla Rosa A, Boulter R, Church K, Svendsen S. District heating (DH) network design and operation toward a system-wide methodology for optimizing renewable energy solutions (SMORES) in Canada: A case study. Energy 2012;45:960–74. https://doi.org/10.1016/J.ENERGY.2012.06.062.

[8] Werner S. International review of district heating and cooling. Energy 2017;137:617–31. https://doi.org/10.1016/J.ENERGY.2017.04.045.

[9] Magro DF. Waste heat recovery in the steel industry: better internal use or external integration.

[10] Fang H, Xia J, Jiang Y. Key issues and solutions in a district heating system using low-grade industrial waste heat. Energy 2015;86:589–602. https://doi.org/10.1016/J.ENERGY.2015.04.052.

[11] Kensby J, Trüschel A, Dalenbäck JO. Potential of residential buildings as thermal energy storage in district heating systems – Results from a pilot test. Appl Energy 2015;137:773–81. https://doi.org/10.1016/J.APENERGY.2014.07.026.

[12] Brattebø H, Reenaas M. Comparing CO2 and NOX emissions from a district heating

system with mass-burn waste incineration versus likely alternative solutions – City of Trondheim, 1986–2009. Resour Conserv Recycl 2012;60:147–58. https://doi.org/10.1016/J.RESCONREC.2011.11.001.

[13] Caputo P, Ferla G, Ferrari S. Evaluation of environmental and energy effects of biomass district heating by a wide survey based on operational conditions in Italy. Energy 2019;174:1210–8. https://doi.org/10.1016/J.ENERGY.2019.03.073.

[14] Termovalorizzatore di Brescia - Inceneritore rifiuti - A2A n.d. https://www.a2a.eu/it/gruppo/i-nostri-impianti/termoutilizzatori/brescia (accessed January 9, 2022).

[15] Hallgrímsdóttir E, Ballzus C, Hrólfsson I. The geothermal power plant at Hellisheioi, Iceland. Trans - Geotherm Resour Counc 2012;36 2:1067–72. https://www.researchgate.net/publication/286762711_The_Geothermal_Power_Plant_at_Hellisheidi_Iceland (accessed January 9, 2022).

[16] Gunnlaugsson E. 3.5. GEOTHERMAL DISTRICT HEATING IN REYKJAVÍK, ICELAND. Imternational Course Low Enthalpy Geotherm Resour Dev 2004.

[17] Pauschinger T. Solar thermal energy for district heating. Adv Dist Heat Cool Syst 2016:99–120. https://doi.org/10.1016/B978-1-78242-374-4.00005-7.

[18] Tian Z, Zhang S, Deng J, Fan J, Huang J, Kong W, et al. Large-scale solar district heating plants in Danish smart thermal grid: Developments and recent trends. Energy Convers Manag 2019;189:67–80. https://doi.org/10.1016/J.ENCONMAN.2019.03.071.

[19] Palsson H, Forskningscenter Risø., Danmarks tekniske universitet. Methods for planning and operating decentralized combined heat and power plants. Riso National Laboratory; 2000.

[20] Benonysson A, Bøhm B, Ravn HF. Operational optimization in a district heating system. Energy Convers Manag 1995;36:297–314. https://doi.org/10.1016/0196-8904(95)98895-T.

[21] Grosswindhager S, Voigt A, Kozek M. Linear Finite-Difference Schemes for Energy Transport in District Heating Networks. 2011.

[22] Gabrielaitiene I, Sundén B, Kacianauskas R, Bohm B. Dynamic modeling of the thermal performance of district heating pipelines 2003:185–92.

[23] Dénarié A, Aprile M, Motta M. Heat transmission over long pipes: New model for

fast and accurate district heating simulations. Energy 2019;166:267–76. https://doi.org/10.1016/J.ENERGY.2018.09.186.

[24] Duquette J, Rowe A, Wild P. Thermal performance of a steady state physical pipe model for simulating district heating grids with variable flow. Appl Energy 2016;178:383–93. https://doi.org/10.1016/j.apenergy.2016.06.092.

[25] Gabrielaitiene I, Bøhm B, Sunden B. Modelling temperature dynamics of a district heating system in Naestved, Denmark-A case study. Energy Convers Manag 2007;48:78–86. https://doi.org/10.1016/j.enconman.2006.05.011.

[26] Stevanovic VD, Zivkovic B, Prica S, Maslovaric B, Karamarkovic V, Trkulja V. Prediction of thermal transients in district heating systems. Energy Convers Manag 2009;50:2167–73. https://doi.org/10.1016/j.enconman.2009.04.034.

[27] Hassine I Ben, Eicker U. Control aspects of decentralized solar thermal integration into district heating networks. Energy Procedia, vol. 48, Elsevier Ltd; 2014, p. 1055–64. https://doi.org/10.1016/j.egypro.2014.02.120.

[28] Wang Y, You S, Zhang H, Zheng X, Zheng W, Miao Q, et al. Thermal transient prediction of district heating pipeline: Optimal selection of the time and spatial steps for fast and accurate calculation. Appl Energy 2017;206:900–10. https://doi.org/10.1016/j.apenergy.2017.08.061.

[29] Vivian J, De Uribarri PMÁ, Eicker U, Zarrella A. The effect of discretization on the accuracy of two district heating network models based on finite-difference methods. Energy Procedia, vol. 149, Elsevier; 2018, p. 625–34. https://doi.org/10.1016/j.egypro.2018.08.227.

[30] Guelpa E, Barbero G, Sciacovelli A, Verda V. Peak-shaving in district heating systems through optimal management of the thermal request of buildings. Energy 2017;137:706–14. https://doi.org/10.1016/J.ENERGY.2017.06.107.

[31] Guelpa E, Toro C, Sciacovelli A, Melli R, Sciubba E, Verda V. Optimal operation of large district heating networks through fast fluid-dynamic simulation. Energy 2016;102:586–95. https://doi.org/10.1016/J.ENERGY.2016.02.058.

[32] Mugnini A, Comodi G, Salvi D, Arteconi A. Energy flexible CHP-DHN systems: Unlocking the flexibility in a real plant. Energy Convers Manag X 2021;12:100110. https://doi.org/10.1016/J.ECMX.2021.100110.

[33] Bavière R, Vallée M. Optimal Temperature Control of Large Scale District Heating

Networks. Energy Procedia 2018;149:69–78. https://doi.org/10.1016/J.EGYPRO.2018.08.170.

[34] Vesterlund M, Toffolo A, Dahl J. Optimization of multi-source complex district heating network, a case study. Energy 2017;126:53–63. https://doi.org/10.1016/J.ENERGY.2017.03.018.

[35] Fink J, van Leeuwen RP, Hurink JL, Smit GJM. Linear programming control of a group of heat pumps. Energy Sustain Soc 2015;5:1–10. https://doi.org/10.1186/S13705-015-0061-9/FIGURES/4.

[36] Krug R, Mehrmann V, Schmidt M. Nonlinear optimization of district heating networks. Optim Eng 2021;22:783–819. https://doi.org/10.1007/S11081-020-09549-0/FIGURES/8.

[37] Rein M, Mohring J, Damm T, Klar A. Optimal control of district heating networks using a reduced order model. Optim Control Appl Methods 2020;41:1352–70. https://doi.org/10.1002/OCA.2610.

[38] Giraud L, Merabet M, Baviere R, Vallée M. Optimal Control of District Heating Systems using Dynamic Simulation and Mixed Integer Linear Programming n.d. https://doi.org/10.3384/ecp17132141.

[39] Vivian J, Chiodarelli U, Emmi G, Zarrella A. A sensitivity analysis on the heating and cooling energy flexibility of residential buildings. Sustain Cities Soc 2020;52:101815. https://doi.org/10.1016/j.scs.2019.101815.

[40] Vandermeulen A, Reynders G, van der Heijde B, Vanhoudt D, Salenbien R, Saelens D, et al. Sources of energy flexibility in district heating networks: building thermal inertia versus thermal energy storage in the network pipes. Submitt to USIM 2018 - Urban Energy Simul 2018.

[41] Le Dréau J, Heiselberg P. Energy flexibility of residential buildings using short term heat storage in the thermal mass. Energy 2016;111:991–1002. https://doi.org/10.1016/J.ENERGY.2016.05.076.

[42] Reynders G, Nuytten T, Saelens D. Potential of structural thermal mass for demand-side management in dwellings. Build Environ 2013;64:187–99. https://doi.org/10.1016/j.buildenv.2013.03.010.

[43] Van Oevelen T, Vanhoudt D, Johansson C, Smulders E. Testing and performance evaluation of the STORM controller in two demonstration sites. Energy

2020;197:117177. https://doi.org/10.1016/j.energy.2020.117177.

[44] Aoun N, Bavière R, Vallée M, Aurousseau A, Sandou G. Modelling and flexible predictive control of buildings space-heating demand in district heating systems. Energy 2019;188:116042. https://doi.org/10.1016/j.energy.2019.116042.

[45] Olsthoorn D, Haghighat F, Moreau A, Lacroix G. Abilities and limitations of thermal mass activation for thermal comfort, peak shifting and shaving: A review. Build Environ 2017;118:113–27. https://doi.org/10.1016/J.BUILDENV.2017.03.029.

[46] Guelpa E, Verda V. Thermal energy storage in district heating and cooling systems: A review. Appl Energy 2019;252:113474. https://doi.org/10.1016/J.APENERGY.2019.113474.

[47] Alva G, Lin Y, Fang G. An overview of thermal energy storage systems. Energy 2018;144:341–78. https://doi.org/10.1016/J.ENERGY.2017.12.037.

[48] Gadd H, Werner S. Thermal energy storage systems for district heating and cooling. Adv Therm Energy Storage Syst Methods Appl 2015:467–78. https://doi.org/10.1533/9781782420965.4.467.

[49] Thomsen PD, Overbye PM. Energy storage for district energy systems. Adv Dist Heat Cool Syst 2016:145–66. https://doi.org/10.1016/B978-1-78242-374-4.00007-0.

[50] Lottner V, Schulz ME, Hahne E. Solar-Assisted District Heating Plants: Status of the German Programme Solarthermie-2000. Sol Energy 2000;69:449–59. https://doi.org/10.1016/S0038-092X(00)00125-0.

[51] Ochs F, Heidemann W, Müller-Steinhagen H. Seasonal thermal energy storage: A challenging application for geosynthetics 2008.

[52] Ochs F, Heidemann W, Müller-Steinhagen H. Performance of Large-scale seasonal thermal energy stores. J Sol Energy Eng Trans ASME 2009;131:0410051–7. https://doi.org/10.1115/1.3197842/447659.

[53] Dahash A, Ochs F, Janetti MB, Streicher W. Advances in seasonal thermal energy storage for solar district heating applications: A critical review on large-scale hot-water tank and pit thermal energy storage systems. Appl Energy 2019;239:296–315. https://doi.org/10.1016/J.APENERGY.2019.01.189.

[54] Emmi G, Zarrella A, De Carli M, Galgaro A. An analysis of solar assisted ground source heat pumps in cold climates. Energy Convers Manag 2015;106:660–75. https://doi.org/10.1016/j.enconman.2015.10.016.

[55] Emmi G, Zarrella A, De Carli M. A heat pump coupled with photovoltaic thermal hybrid solar collectors: A case study of a multi-source energy system. Energy Convers Manag 2017;151:386–99. https://doi.org/10.1016/j.enconman.2017.08.077.

[56] Sommerfeldt N, Madani H. In-depth techno-economic analysis of PV/Thermal plus ground source heat pump systems for multi-family houses in a heating dominated climate. Sol Energy 2019;190:44–62. https://doi.org/10.1016/j.solener.2019.07.080.

[57] Bellos E, Tzivanidis C, Moschos K, Antonopoulos KA. Energetic and financial evaluation of solar assisted heat pump space heating systems. Energy Convers Manag 2016;120:306–19. https://doi.org/10.1016/j.enconman.2016.05.004.

[58] Calise F, Dentice d'Accadia M, Figaj RD, Vanoli L. Thermoeconomic optimization of a solar-assisted heat pump based on transient simulations and computer Design of Experiments. Energy Convers Manag 2016;125:166–84. https://doi.org/10.1016/j.enconman.2016.03.063.

[59] Dannemand M, Perers B, Furbo S. Performance of a demonstration solar PVT assisted heat pump system with cold buffer storage and domestic hot water storage tanks. Energy Build 2019;188–189:46–57. https://doi.org/10.1016/j.enbuild.2018.12.042.

[60] Connolly D, Lund H, Mathiesen B V, Werner S, Möller B, Persson U, et al. Heat Roadmap Europe: Combining district heating with heat savings to decarbonise the EU energy system 2013. https://doi.org/10.1016/j.enpol.2013.10.035.

[61] Wirtz M, Kivilip L, Remmen P, Müller D. 5th Generation District Heating: A novel design approach based on mathematical optimization. Appl Energy 2020;260. https://doi.org/10.1016/j.apenergy.2019.114158.

[62] Sibbitt B, McClenahan D, Djebbar R, Thornton J, Wong B, Carriere J, et al. The Performance of a High Solar Fraction Seasonal Storage District Heating System – Five Years of Operation. Energy Procedia 2012;30:856–65. https://doi.org/10.1016/J.EGYPRO.2012.11.097.

[63] Østergaard PA, Andersen AN. Booster heat pumps and central heat pumps in district heating. Appl Energy 2016;184:1374–88. https://doi.org/10.1016/j.apenergy.2016.02.144.

[64] Vetterli N, Sulzer M, Menti UP. Energy monitoring of a low temperature heating and cooling district network. Energy Procedia 2017;122:62–7. https://doi.org/10.1016/J.EGYPRO.2017.07.289.

[65] Chen Y, Wang J, Lund PD. Sustainability evaluation and sensitivity analysis of district heating systems coupled to geothermal and solar resources. Energy Convers Manag 2020;220:113084. https://doi.org/10.1016/J.ENCONMAN.2020.113084.

[66] Vivian J, Emmi G, Zarrella A, Jobard X, Pietruschka D, De Carli M. Evaluating the cost of heat for end users in ultra low temperature district heating networks with booster heat pumps. Energy 2018;153:788–800. https://doi.org/10.1016/j.energy.2018.04.081.

[67] Ommen T, Thorsen JE, Brix Markussen W, Elmegaard B. Performance of ultra low temperature district heating systems with utility plant and booster heat pumps 2017. https://doi.org/10.1016/j.energy.2017.05.165.

[68] Behzadi A, Arabkoohsar A. Comparative performance assessment of a novel cogeneration solar-driven building energy system integrating with various district heating designs. Energy Convers Manag 2020;220:113101. https://doi.org/10.1016/j.enconman.2020.113101.

[69] Pardo García N, Zubi G, Pasaoglu G, Dufo-López R. Photovoltaic thermal hybrid solar collector and district heating configurations for a Central European multi-family house. Energy Convers Manag 2017;148:915–24. https://doi.org/10.1016/j.enconman.2017.05.065.

[70] Rosato A, Ciervo A, Ciampi G, Sibilio S. Effects of solar field design on the energy, environmental and economic performance of a solar district heating network serving Italian residential and school buildings. Renew Energy 2019;143:596–610. https://doi.org/10.1016/j.renene.2019.04.151.

[71] Pakere I, Lauka D, Blumberga D. Solar power and heat production via photovoltaic thermal panels for district heating and industrial plant 2018. https://doi.org/10.1016/j.energy.2018.04.138.

[72] Ente italiano di normazione UNI. UNI 10349-1:2016 Riscaldamento e raffrescamento degli edifici - Dati climatici - Parte 1: Medie mensili per la valutzione della prestazione termo-energetica dell'edificio e metodi per ripartire l'irradianza solare nella frazione diretta e diffusa. 2016.

[73] QGIS Development Team. QGIS Geographic Information System 2019.

[74] Vivian JM, De C, Zarrella DA. Direct Use of Low Temperature Heat in District Heating Networks with Booster Heat Pumps.

[75] Vivian J, Quaggiotto D, Zarrella A. Increasing the energy flexibility of existing district heating networks through flow rate variations. Appl Energy 2020;275:115411. https://doi.org/10.1016/j.apenergy.2020.115411.

[76] Shampine LF, Reichelt MW. THE MATLAB ODE SUITE.

[77] Patankar S., Spalding D. A calculation procedure for heat, mass and momentum transfer in three-dimensional parabolic flows. Int J Heat Mass Transf 1972;15:1787–806. https://doi.org/10.1016/0017-9310(72)90054-3.

[78] Shampine LF, Reichelt MW, Sci Comput SJ. THE MATLAB ODE SUITE *. Soc Ind Appl Math 1997;18:1–22.

[79] Ente italiano di normazione UNI. UNI 10339:1995 Impianti aeraulici a fini di benessere - Generalità, classificazione e requisiti 1995.

[80] Ente italiano di normazione UNI. UNI EN 16798-1:2019 - Prestazione energetica degli edifici - Ventilazione per gli edifici 2019.

[81] Ferguson SC, Harrold RM, Garrigus J, Mehl M, Chair V, Glazer J, et al. ASHRAE Standing Standard Project Committee 90.1 Cognizant TC: TC 7.6, Systems Energy Utilization SPLS Liaison: Doug Reindl ASHRAE Staff Liaison 2009.

[82] van der Heijde B, Vandermeulen A, Salenbien R, Helsen L. Representative days selection for district energy system optimisation: a solar district heating system with seasonal storage. Appl Energy 2019;248:79–94. https://doi.org/10.1016/J.APENERGY.2019.04.030.

[83] Quaggiotto D, Vivian J, Zarrella A. Management of a district heating network using model predictive control with and without thermal storage. Optim Eng 2021;22:1897–919. https://doi.org/10.1007/S11081-021-09644-W/TABLES/5.

[84] EnergyPlus n.d. https://energyplus.net/weather/sources (accessed January 9, 2022).

[85] ISO 18523-2:2018(en), Energy performance of buildings — Schedule and condition of building, zone and space usage for energy calculation — Part 2: Residential buildings n.d. https://www.iso.org/obp/ui/#iso:std:iso:18523:-2:ed-1:v1:en (accessed April 29, 2021).

[86] ISO 7730:2005(en), Ergonomics of the thermal environment — Analytical determination and interpretation of thermal comfort using calculation of the PMV and PPD indices and local thermal comfort criteria. https://www.iso.org/obp/ui/#iso:std:iso:7730:ed-3:v1:en (accessed April 29, 2021).

[87] Jordan U, Vajen K. DHWcalc: PROGRAM TO GENERATE DOMESTIC HOT WATER PROFILES WITH STATISTICAL MEANS FOR USER DEFINED CONDITIONS.

[88] Bordignon S, Emmi G, Zarrella A, De Carli M. Energy analysis of different configurations for a reversible ground source heat pump using a new flexible TRNSYS Type. Appl Therm Eng 2021;197:117413. https://doi.org/10.1016/J.APPLTHERMALENG.2021.117413.

[89] Zarrella A, Emmi G, Vivian J, Croci L, Besagni G. The validation of a novel lumped parameter model for photovoltaic thermal hybrid solar collectors: a new TRNSYS type. Energy Convers Manag 2019;188:414–28. https://doi.org/10.1016/j.enconman.2019.03.030.

[90] EN 12975-2:2006 - Thermal solar systems and components - Solar collectors - Part 2: Test methods n.d. https://standards.iteh.ai/catalog/standards/cen/3ae62ba7-404b-4c89-852d-2124d280eb40/en-12975-2-2006 (accessed December 20, 2021).

[91] ASHRAE. Geothermal Energy. Heat. Vent. Air-Cond. Appl. SI Ed Am Soc Heating, Refrig Air-Conditioning Eng 2011;34.

[92] Sartori I, Napolitano A, Voss K. Net zero energy buildings: A consistent definition framework. Energy Build 2012;48:220–32. https://doi.org/10.1016/j.enbuild.2012.01.032.

[93] NOTE FROM THE FRENCH AUTHORITIES Subject: Implementation of Directive 2012/27/EU on energy efficiency-Communication from the French authorities of their Annual Report (Article 24 of the Directive).